Numerical Investigation of Unintended Yaw for Helicopter Accident Mitigation

Marc Vives Massana

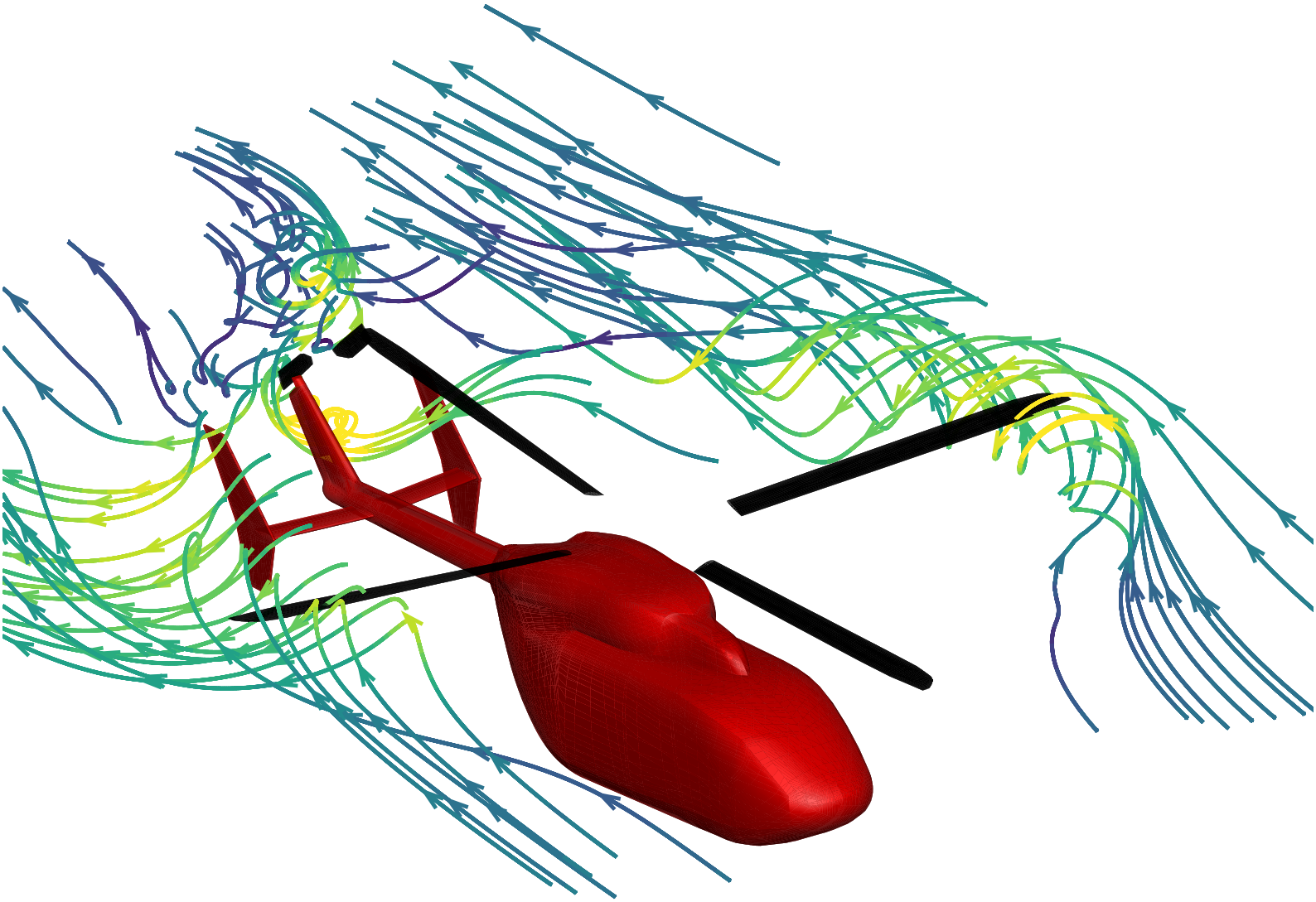

TU Delft

AIRBUS

Numerical Investigation of Unintended Yaw for Helicopter Accident Mitigation

by

Marc Vives Massana

in partial fulfilment of the requirements for the degree of

Master of Science
in Aerospace Engineering

at the Delft University of Technology,
to be defended publicly on the 25th of June 2024

Student number:	5859328	
Supervisors:	Dr. T. Sinnige	TU Delft
	Dr. T. Gogel	Airbus Helicopters
	Dr. T. Ries	Airbus Helicopters
	Dr. P. Zanella	Concepts Beyond, FAA Contractor
Thesis committee:	Dr. ir. T. Sinnige	TU Delft
	Dr. A. H. van Zuijlen	TU Delft, chairman
	Dr. M. D. Pavel	TU Delft
	Dr. T. Gogel	Airbus Helicopters
Project Duration:	September 2023 - May 2024	

TU Delft AIRBUS

Preface

This thesis will put an end to the master program in aerospace engineering which has been a truly exciting period of my career. I have met incredible people throughout this journey which started in Delft, Netherlands and ended in Donauwörth, Germany.

I would like to thank the experts Thomas Gogel, from the Aviation Safety department, Tobias Ries and German Roth, from the aeromechanics department and Paola Zanella, as an FAA contractor, who have been carefully supervised me during my stay in Airbus Helicopters to carry this master thesis. Needless to say the great help from the colleagues in accident investigation, flight mechanics and aerodynamics departments.

Marc Vives Massana
Delft, May 2024

Summary

An unintended yaw is a type of accident characterised by an unexpected helicopter rotation around the yaw axis without the pilot's intention and any technical malfunctions. Unintended yaw accidents are one of the top operational causes of helicopter accidents, causing serious damages and fatalities each year. Literature provides documents from the FAA or helicopter manufacturers with a limited description of unintended yaw. These documents already move a step forward in the characterisation of unintended yaw but either provide confusing explanations or are not generally applicable.

This thesis does a numerical investigation of unintended yaw to provide a characterisation of the phenomena for different helicopter configurations with an open tail rotor and find an optimal recovery method. The research questions involved are formulated to find uncontrollable unintended yaw accidents, the necessity of the numerical tools used for the thesis, the impact of tail rotor vortex ring state and main rotor wake interference in unintended yaw, how the physical effects affect the handling qualities of the helicopter and how to recover in case of an unintended yaw accident. The research approach to answer the research questions is based on the coupled workflow between a flight mechanics code, Gensim, and an aerodynamics code, UPM, which uses combined panel and particle methods. Trimmed flight simulations are run to find possible flight states where uncontrollable unintended yaw appears for the different helicopter configurations considered; these simulations are also used to answer the following research questions. Specific attention is placed on the tail rotor aerodynamics and operative characteristics. Also, time domain simulations are run to test optimal recovery methods for different situations where the helicopter started an unintended yaw.

The results illustrate that the helicopter can achieve a trim state for all flight cases and helicopter configurations considered since the pedal required to maintain the trim is within the pedal range, and the pilot still has sufficient control margin. Therefore, showing that there is not an uncontrollable uninteneded yaw case. Additionally, the numerical coupling used for the simulations is essential to capture the important aerodynamics and performance of the tail rotor. The tail rotor vortex ring state reduces the tail rotor thrust for flight states where the freestream velocity opposes the tail rotor wake, requiring more left pedal by the pilot. On the other hand, main rotor wake interference increases the tail rotor thrust for top aft rotating tail rotors. A high position is a beneficial configuration compared to a top forward rotating tail rotor, which is equally beneficial if a low tail rotor location is used. Furthermore, the handling qualities of the helicopter are affected by the tail rotor vortex ring state since, for a specific range of wind speeds and azimuths; more left pedal is required when not expected. The influence of the main rotor wake interference is to reduce the control margin for top forward rotating tail rotors at a high position. Finally, the time domain simulations of a recreation of an unintended yaw accident during an approach to landing are used to test different recovery techniques. For instance, the results show that applying a maximum opposite pedal to the yaw rotation is always sufficient to stop a developed yaw rate due to an unintended yaw.

Contents

List of Figures

List of Tables

Nomenclature

Acronyms

Acronym	Definition
LTE	Loss of Tail rotor Effectiveness
UY	Unintended/Unanticipated Yaw
T/R	Tail Rotor
M/R	Main Rotor
VRS	Vortex Ring State
HOST	Helicopter Overall Simulation Tool
OGE	Out of Ground Effect
IGE	In Ground Effect
UPM	Unsteady Panel Method

Symbols

Symbol	Definition	Unit
V_{eff}	Effective velocity from the blade's section reference frame	[m/s]
α_{eff}	Effective angle of attack at the blade's section	[deg]

1

Introduction

Helicopters, with their unparalleled versatility and capability to access remote areas, have become indispensable assets in various sectors, including military operations, emergency medical services, and aerial transportation. However, amidst their utility, helicopters have faced a persistent operational threat since their invention. The underlying phenomenon, referred to as unintended yaw, characterised by an unexpected rotation around the yaw axis, poses significant safety risks and remains one of the most frequent causes of accidents in helicopter operations. In the event of an accident attributed to an unintended yaw, the helicopter may appear to yaw autonomously, typically in a direction contrary to the rotation of the main rotor blades and in defiance of the pilot's intentions, despite the absence of any technical malfunction. The helicopter impacts the ground with a high yaw rate, which usually results in significant damage to the aircraft and, too often, in fatalities or injuries. Since several complex physical effects contribute to this phenomenon, many opinion-driven explanations exist which are confusing for pilots. This frequently leads to the pilot's inability to execute corrective control inputs based on this vague characterisation and inadequate comprehension of unintended yaw.

Therefore, due to their potentially catastrophic consequences, unintended yaw incidents have garnered substantial attention from aviation authorities, researchers, and industry stakeholders. A series of accidents due to losses of yaw control occurred in the US Army during the 1980s [26] and the British Army [1, 14]. Overall, the worldwide helicopter fleet has also experienced a high amount of accidents attributed to unintended yaw. These led to the publication of technical and safety documents for pilots, such as the FAA Advisory Circular [4] in 1995 and, more recently, the Airbus Helicopter safety notices [21, 23]. These documents contain recommended actions for pilots to be carried out to prevent and recover unintended yaw accidents. The information from Administration [4] was at that time based on state-of-the-art investigations; however, the conclusions led to confusing terms since some of the effects were not clearly explained, and the recovery methods were not described adequately. In Helicopters [23], the analysis is now updated. Still, the results need more research since the explanations are based on a flight mechanics code with simplified aerodynamics that cannot capture important tail rotor aerodynamics.

The literature shows that there is still a lack of research on unintended yaw since the investigations have neither captured the rotor aerodynamics with enough fidelity required by the nature of the phenomena, nor used full-body simulations, nor evaluated different tail rotor configurations or not provided a detailed physical explanation for the cause. Therefore, this thesis aims to investigate unintended yaw with mid-fidelity numerical tools to characterise the phenomenon for helicopters with different open tail rotor configurations and test recovery methods to provide a complete and detailed overview of the characteristics involved in unintended yaw. This detailed description of unintended yaw will help raise pilots' awareness while comprehensively explaining the contributing causes to these accidents and clarifying an optimal recovery method. Consequently, this will improve pilot training and thus reduce related accidents, which is highly interesting to aviation authorities such as the FAA and EASA.

Following this paragraph, a short introduction to helicopter basics, such as design and controls, is presented to familiarise the reader with helicopter technology. The thesis's second chapter, chapter 2, describes the literature related to unintended yaw accidents and flight physics, together with the research proposal for the thesis where the research questions are formulated. Then, the third chapter, chapter 3, shows the methodology followed during the

thesis. The numerical tools are explained in detail, a verification of the coupling between the flight mechanics code and the aerodynamics code is provided for low-speed forward flights, and the helicopter models used in the aerodynamics code are depicted, followed by the approach used to answer the research questions. The results are presented and discussed in the third chapter, chapter 4. Finally, in the last chapter, chapter 5, the conclusions of the thesis are stated and recommendations for future work are given.

1.1. Helicopter Design

It is essential to know the components of the helicopter to understand its flight capabilities. In this section, only the exterior parts of single main rotor helicopters, the most frequent helicopter configuration, are described as being the most relevant regarding aerodynamic loads. The helicopter consists of seven parts: main rotor, fuselage, tail rotor, tail boom, landing gear, horizontal stabiliser and vertical stabiliser or fin. These parts are illustrated in Figure 1.1a.

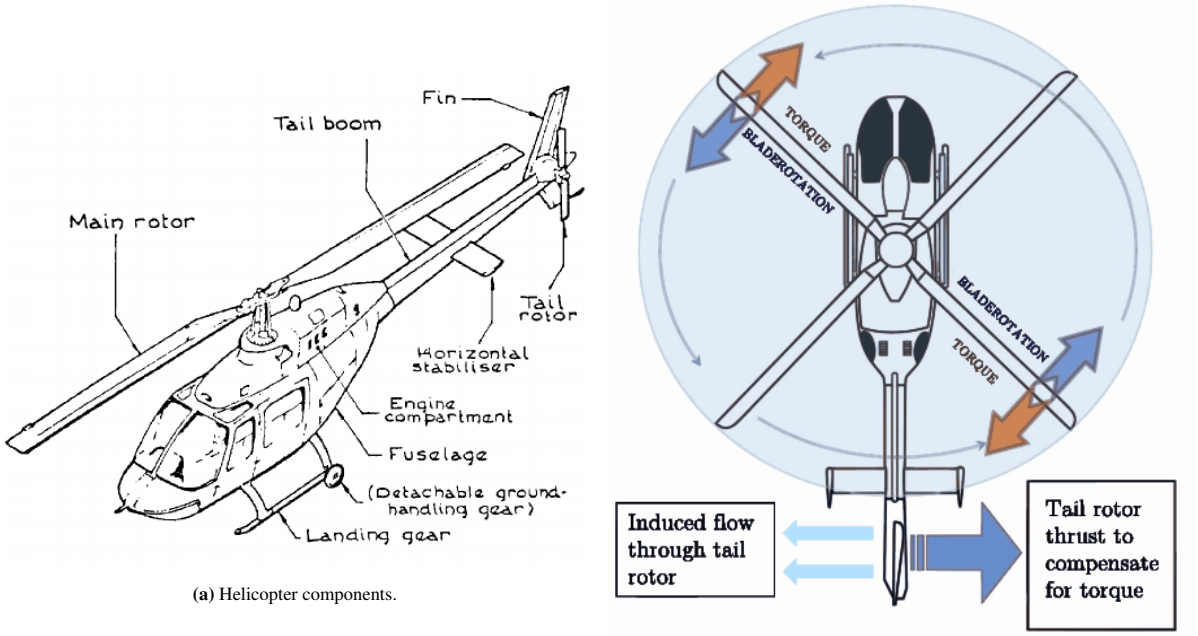

(a) Helicopter components.

(b) Loads on main rotor and tail rotor.

Figure 1.1: Helicopter design components.

Source: Cavalcante et al. [12]

The main rotor consists of several blades attached to the hub, where the mast is located. Each blade has a variable chord and twist distribution and can have variable airfoil geometry along the span. The main rotor provides a thrust resulting from the integrated aerodynamic loads acting on each blade section; additionally, a torque transmitted to the mast appears due to the lift, which is less critical, and drag, the main contributor, from the blades. The same configuration is used for the tail rotor but is tilted such that the axis of rotation is located horizontally. The main purpose of the tail rotor is to provide an anti-torque to compensate for the main rotor torque. The tail rotor thrust and wake directions are shown in Figure 1.2 for a counterclockwise rotating main rotor. Two types of tail rotor exist: the classical tail rotor, which is the one used for this investigation, and the so-called Fenestron, which is a product of Airbus Helicopters, that has a shroud surrounding the tail rotor system and integrates the vertical stabiliser.

The vertical stabiliser or fin is an aerodynamic surface which produces a lift component that provides yaw stability to the helicopter for sufficient high forward velocities. The horizontal stabiliser provides a lift that can help the main rotor provide pitch stability but does not contribute to the yaw moments on the helicopter reference frame. The fuselage includes the cockpit and the engines, having a negligible impact on the yaw moments of the

helicopter. The landing gear consists either of landing skids or wheel landing gear. Finally, the tail boom is the component that carries the tail rotor, horizontal stabiliser and vertical stabiliser.

(a) Classic tail rotor.

(b) Fenestron.

Figure 1.2: Helicopter classic tail rotor and Fenestron.

Source: Wikipedia [44]

1.2. Helicopter Controls

The pilot operates the helicopter through the flight controls. These consist of the collective, often with an integrated throttle, the cyclic and the anti-torque pedals. Before precisely defining each flight control, presenting another essential element, the swash-plate illustrated in Figure 1.3 is beneficial. It consists of a mechanical device responsible for changing the pitch angle for the rotor blades. This is done by changing the orientation of two disks located in the hub. One is attached to the mast, and the other is fixed. The disk attached to the mast is also attached to the blade's trailing edge with rods. Furthermore, if the disk is tilted, it can produce a variable pitch angle depending on the azimuth location.

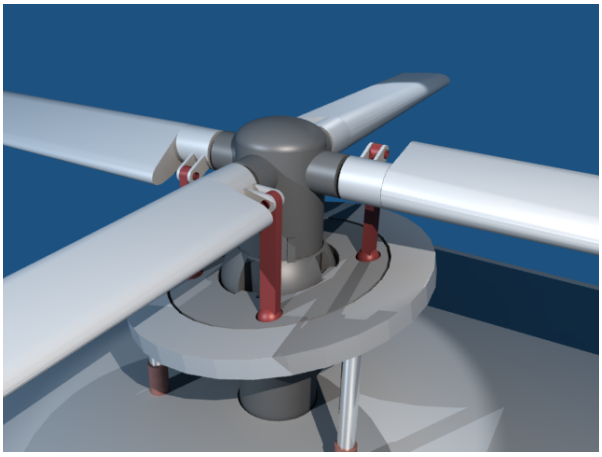

Figure 1.3: Helicopter swashplate.

Source: Wikipedia [43]

The controls that the pilot can change are now explained in detail:

- **Collective:** the collective changes the pitch angle of all blades simultaneously. This occurs because the swashplate is increased or decreased in the same amount vertically. An increase in collective will cause an increase in the pitch angle, which will cause a higher angle of attack, and if a stall does not occur, the rotor thrust will increase. If the collective decreases, the rotor thrust will decrease following the same logic.
- **Cyclic:** the cyclic changes the pitch angle depending on the azimuth location. This is obtained thanks to the tilting of the swashplate; when the mast rotates, the rods following the trajectory of the disk are raised or lowered depending on the location, producing a local change in pitch angle. This difference in pitch angle along the azimuth location also makes a difference in lift, which results in a moment that tilts the rotor plane. This allows the helicopter to initiate a lateral or forward/backward movement.
- **Anti-torque pedals:** to counteract the moment created by the spinning main rotor and to control the yaw orientation of the helicopter, most helicopters have a tail rotor orientated vertically at the end of the tail boom. The purpose of this rotor is to create enough moments to control the helicopter's yaw. The anti-torque pedals control the collective of the tail rotor blades, generating more or less thrust depending on the moment needed. Other methods to control the yaw exist in helicopter configurations, such as jet air exhausted from the tail boom or more complex configurations with two main co-rotating rotors. Since the present investigation is strongly related to the tail rotor performance, the focus lies on the tail rotor collective and, consequently, the anti-torque pedal position.
- **Throttle:** most rotors are designed to operate a given specific rotation speed. Depending on the flight manoeuvre, the moment the rotor drag changes, the engine must supply different power to maintain rotation speed. This is controlled with the throttle. Modern helicopters have the throttle control automatically integrated into the collective control.

2

Literature Study

For a helicopter to perform a trimmed flight, some kind of anti-torque system must be used to counteract the main rotor torque. These systems can be the tail rotor, which provides a thrust in the lateral direction to produce a counter-torque; the vertical fin, which can create a lateral aerodynamic force if enough wind speed is provided; or more advanced methods, such as ram-air exhaust in the tail boom. These systems must provide enough anti-torque but also satisfy the other helicopter manoeuvrability performance. This means that depending on the flight condition, there is a strong interaction between all helicopter aerodynamic surfaces, which can create not apparent effects.

The unintended yaw is an accident caused when the helicopter is flying in a trimmed condition and loses the yaw stability, meaning that the yaw rate starts developing. This situation causes a potential loss of helicopter control, leading to severe consequences if the pilot is not experienced enough. This loss of yaw stability is a product of numerous aerodynamic interactions between the helicopter exterior components and flight operation conditions such as power demand, flying height and weight. Furthermore, these types of accidents usually occur while close to the ground, leading to a potential fatal crash. The name of unintended yaw is given since the start of yawing is not something intended, and it was established from a previous work on this topic in Airbus Helicopter; in the rest of this section, other wordings are explained and also potential wording confusions.

This section introduces the fundamental concepts for developing the thesis through a literature review. A historical background is first given, followed by a summary of accident databases found in the literature. Afterwards, the most important safety information notices published for pilots currently available are explained. Then, concepts referring to the different flight characteristics are presented together with investigations from the literature that study such phenomena if found. Eventually, the research proposal can be formulated with the research questions.

2.1. Historical Background

The first explicit mention of a phenomenon involving an apparent loss of tail rotor effectiveness can be found in the US Army Aviation Digest journal [26], reporting in 1977 a series of accidents on OH-58 helicopters that were not due to maintenance error, material failure or exceeding an aircraft limitation. Although flights were planned and conducted according to Army aviation procedures, conditions were encountered where pedal inputs could not stop the right yaw rate. The proposed explanation is that the full left pedal, in combination with the left wind component induced at the tail rotor by the right yaw rate, generates a high blade angle of attack leading to tail rotor stall; being the title of a reprint made about one year later [40].

In 1980, another paper from the US Army was written by a British exchange officer assigned to the US Army Aviation Center of Fort Rucker [25]. It provides a theory developed in the Empire Test Pilot School of Boscombe Down about this phenomenon named “tail rotor breakaway”. Therefore, The issue had already been found on other helicopters in Great Britain; tail rotor stall is also considered the cause. Four factors are necessary to enter

into the problem: a high power, a decelerate attitude, slow airspeed and relative wind coming from the left.

In 1982 the “Loss of Tail rotor Effectiveness” designation appears [29], but “tail rotor spin” is also used [32]. At that time, the US Army recorded 18 OH-58 accidents caused by that phenomenon since 1973, with an increasing rate (already 5 accidents in the current fiscal year). The tail rotor of the Kiowa helicopter is acknowledged as being marginal according to US Army criteria and this is seen as a contributing factor. The limited experience of the involved pilots is also pointed out but the difficulty of the mission of the OH-58, most often flown by a single pilot, shall not be underestimated.

Investigations were carried and the first results were published in 1983 in a Bell Operations Safety Notice sent to Bell 206 operators [3], with also a complementary information letter issued the following year. The phenomenon is designated as unanticipated yaw and the first graphs showing in which wind azimuth conditions it may occur are provided, as well as a recommended recovery technique associating full opposite pedal, forward cyclic and if altitude permits, power reduction. The information letter clearly utters that the tail rotor is not stalled and that the corrective pedal input shall always be opposite to the turn direction [14].

The US Army is not the only helicopter operator facing the unanticipated yaw problem. In the 80s, British Gazelles suffer from a high accident rate due to losses of control in yaw [14]. When hovering with wind, unanticipated left yaw occurs (or yaw rate rapidly increases during left turns) that pilots do not succeed to stop which often ends with substantial damage to the helicopter. This looks quite similar to the problems encountered by the US Army with the OH-58, but on the left-hand side because of the French sense of rotation of the Gazelle main rotor (clockwise). The issue was raised to the manufacturer, at that time Aerospatiale Helicopter Division which would later merge with the Helicopter Division of MBB into Eurocopter, now Airbus Helicopters. The strange point is that almost only the British Gazelles suffer from that problem. One or two accidents in the French Army present similar features, which is nothing compared to the number of accidents in the United Kingdom. An AAIB accident analysis reports 15 losses of yaw control accidents or incidents in the UK Armed Forces [1].

A tale was born that the Fenestron stalled when a full pedal was applied. The official procedure at that time, in case of unanticipated left yaw, can still be found in a CAA analysis of tail rotor failures [10]: "Recommended procedures for military operators following Fenestron stall have included reducing right yaw pedal application until Fenestron effectiveness is restored and then reapplying right pedal, attempting to shut down the engine, and lowering the collective lever and accepting a heavy landing." It is quite similar to what the US Army recommended some years earlier.

The unanticipated yaw phenomenon was investigated at Eurocopter and the tests were performed to demonstrate a successful recovery procedure. The British Navy lent one of their Gazelle fitted with a test installation. Flight tests were carried out, in different wind conditions, where yaw rates as high as 165 degrees per second were achieved. Applying the full pedal in the opposite direction of the yaw rotation still helps recover from those extreme spot turns.

The results are presented to the British Army. Any reference to the Fenestron stall is removed from documentation and a full pedal application is requested in case of unanticipated yaw (designated as yaw divergence in the Royal Navy). The Ministry of Defence issued the Advance Information Leaflet 1/93, including the following information reported [2]: "In light wind conditions, an extremely rapid build-up of yaw rate can follow a relatively small left pedal application during low-speed flight or in the hover. In this event, immediate and positive application of the right pedal, up to the maximum, should be applied and maintained to arrest the rate of yaw. Recovery action may be ineffective if the pedals are returned only to the hover position, and the yaw rate may initially continue to increase before deceleration and an eventual steady hover are established. Furthermore, if the pedals are not returned as far as the original hover position, a steady hover will never be achieved and the aircraft will stabilize at a particular rate of yaw which may be very high. Pilots may misinterpret this as a loss of yaw control. Be warned that any delay in applying corrective action will require progressively larger right pedal inputs to achieve a steady state hover and may lead the pilot to believe that he has lost control. Yaw rates of up to 165° per second to the left can rapidly be arrested by applying full right pedal without any discernable loss of fenestron performance."

Unanticipated yaw is not exclusively encountered during military missions. The civil usage of helicopters increasing, and NTSB investigations identify that it is a contributing factor in several civil helicopter accidents. FAA issues then AC 90-95 [4]. It provides most of the material of the Bell Information Letter, including the

recommendations about recovery actions. AC 90-95 is still today the main source of information about what is called LTE. Many accident investigation boards, after an event involving LTE, urge their Operational Authorities to make pilots aware of the content of the AC. More than twenty years later, having observed that unanticipated yaw accidents still occur (55 identified between 2004 and 2014), NTSB issues a Safety Alert [31] to remind pilots of the issue, provide them with recommendations and give them some FAA references for further information, including AC 90-95.

Finally, it has been recently that Airbus Helicopters has released a safety information notice [23] which gives a more accurate explanation of unintended yaw. This document focuses on analysing the yaw stability through the pedal curve and identifying the most critical regions and manoeuvres.

2.2. Accidents Databases

Unintended yaw accident databases have been explored from different sources found in the literature and inside Airbus Helicopters. When an accident takes place, the local authorities are the first organisation to attend the location for the first investigation of the potential cause of the accident. All accidents related to a helicopter from Airbus Helicopters are reported to the accident investigation department, where they are stored in a database with a description of the accidents. For some accidents, it is required that an Airbus expert also investigates the accident. Then a more detailed description of the accident is provided.

In Airbus Helicopters, it is possible to obtain data on accidents involving the company's helicopters during the past ten years. The database is from January 2013 until July 2023 and includes all types of aircraft in Airbus Helicopters. This was facilitated by the accident investigation department. The database is classified in the type of accident by the accident investigator who was responsible for the investigation of the accident in particular. The investigator also added useful information such as aircraft model, date of the accident, location, a small description of the accident made by the investigator and sometimes a description by the local authorities was also available. Additionally, information on the number of fatalities was also accessible. Overall, it can already be found that about 9.3% of all the accidents happening to Airbus helicopters can be quantified as unintended yaw.

The next step is to sub-classify the accidents related to unanticipated yaw to a more detailed nature of the accident because this type of accident appears in different flight manoeuvres and flight states. Furthermore, the exact specific cause is also added if it can be identified from the accident description. The classification can follow as:

- **UY hover/slow flight:** flights where the unintended yaw developed while hovering or flying slowly.
- **UY hover/slow flight (EFSTU):** flights where the unintended yaw developed while hovering or flying slowly. It is clear from the accident description that they are related to EFSTU (entry from stable to unstable). EFSTU refers to entering the unstable region about the yaw axis coming from a stable position.
- **Dynamic approach to land:** unintended yaw appears while manoeuvring for an approach to land, slowing down and increasing collective.
- **UY after lift-off:** unintended yaw appears when lifting off after an increase in collective.
- **UY undefined:** could not determine the exact situation in which unintended yaw developed.
- **UY go around:** unintended yaw develops after a decision of go around.
- **UY wind gust very low hover:** unintended yaw develops in a situation with wind gust and very low hover.
- **UY after touch down:** unintended yaw appears during landing just after touch down.

The classified accidents are shown in Figure 2.1, where it is found that the most frequent are accidents which appeared while the helicopter was hovering or in a slow flight condition, representing a 46.67%. From these flights, a small part of 10.67% could be attributed to EFSTU. The second most frequent accidents appeared during a dynamic approach to landing, where the collective is increased and the helicopter starts to flare. The third most frequent accident was during a lift-off, which also involves an increase in collective with 14.67%. The fact that most of the accidents were related to hover/slow flight is not a big surprise because it is a flight in which the pilot does not have a clear awareness of the surrounding freestream velocity which might change without notice until unanticipated yaw is already developed. Furthermore, this category includes a wide number of possible

situations but the specific one could not be extracted from the accident investigators' descriptions. The next two most important categories, the dynamic approach to landing and after lift-off, are also important contributors because they normally involve a sudden increase in collective which increases the torque of the main rotor so the helicopter loses the yaw stability if enough pedal to counteract is not provided.

On top of that, the accidents usually appeared with light to medium aircraft. This means that the accidents due to a loss of yaw control might be also related to the inertia about the yaw axis and the disc loading. The fatality of unintended yaw represents 2.5% of the global fatality of all accidents and from all the unintended yaw accidents, 8% are fatal.

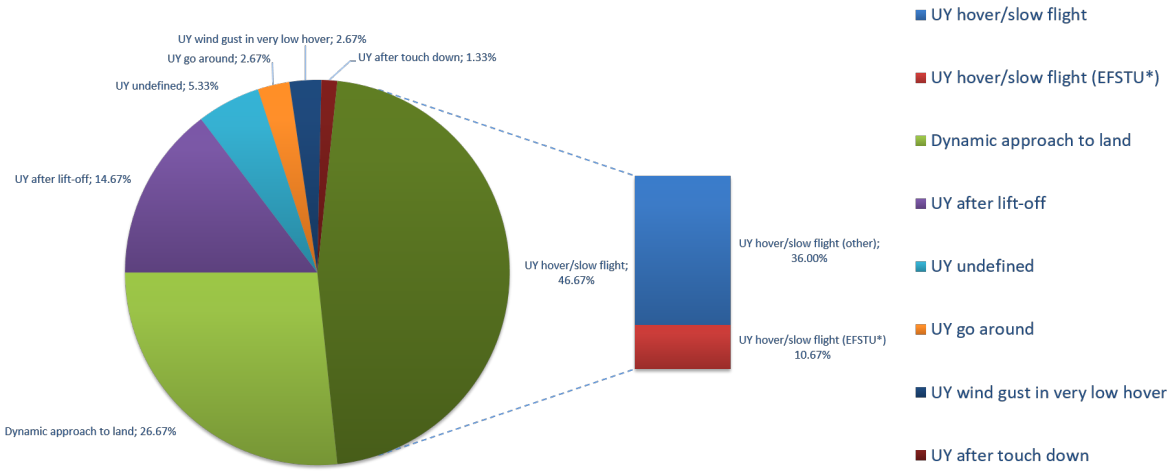

Figure 2.1: Situations in which unanticipated yaw accidents appeared.

In Dequin [14] and Ferullo [16], more accident data can be found. Their search has been limited to the 2000-2016 period. In these 17 years, as many as 310 events have been found. This makes a bit more than 18 events per year expected to be not comprehensive. This only concerns civil events that were investigated and reported in the relevant databases. About 90% of the unanticipated yaw accidents took place in the opposite direction of the torque (rightwards with US rotors, leftwards with French rotors) and only 3% in the direction of the torque. The status is quite different for the accidents classified as "others", with 52% opposite to the torque direction and 35% in the torque direction. Summing both values does not lead to 100% as the spinning direction is not explicitly provided in some cases or is contradictory reported. 35 of the 310 accidents (1 out of 9 accidents) resulted in at least one fatality, with an average of 1.7 fatalities per fatal accident. 77 accidents (1 out of 4 accidents) resulted in at least one serious injury, with an average of 1.6 serious injuries per accident. Losses of yaw control occur in the low-speed range, usually close to the ground. The helicopter is in most cases destroyed or otherwise badly damaged. The usual end to an unanticipated yaw accident is a helicopter lying on its side. Minor damages are recorded for only very few cases. It was summarized that each year many unanticipated yaw accidents are recorded, everywhere in the world, on many single-rotor helicopters, without any trend towards reduction; light helicopters with low-experience pilots are the preferred victims; in 3 out of 4 accidents, the recovery recommended in AC90-95, the reference publication on unanticipated yaw, is not applicable due to the very low altitude where the event starts.

2.3. Technical and Safety Advisories for Pilots

From the need to investigate this type of accident, the FAA in 1995 released a first advisory circular [4] which referred to the phenomena of unintended yaw as loss of tail rotor effectiveness. In the advisory circular, it is stated that the LTE is related to manoeuvres which require high power, and low speed with a left crosswind or tailwind condition. Furthermore, it is also stated that there is a greater susceptibility for LTE in right turns with special attention on not letting the yaw rate develop too much before it is unrecoverable. The specific characteristics of this phenomenon were evaluated through flight and wind tunnel tests by aircraft manufacturers. Four azimuth relative

wind azimuth regions which could lead to LTE were identified. These regions although specifically identified, can overlap and produce more pronounced thrust variations in these overlapping. Furthermore, an increase in pilot workload was identified for low-speed flights. In particular, these characteristics appear for velocities lower than 30 knots.

For a counterclockwise rotating helicopter, the first identified region classified as main rotor disc vortex interference, is related to wind azimuth angles of 285° to 315°, in Figure 2.2. Low-speed winds from these azimuth directions will redirect the main rotor wake to interfere with the tail rotor wake and cause turbulent conditions. When the main rotor wake can interfere with the tail rotor from both left or right sides, this interaction will produce an increase or decrease in thrust depending on the tail rotor rotation direction which can lead to pilot confusion.

The second region is referred to weathercock stability which is most intense in the region 120° to 240° wind azimuths. The tailwinds can increase the pilot pedal workload to maintain trim conditions and they can develop the yaw rate very fast. Therefore, if the pilot allows a yaw rate to develop and enters this region, the effort to stop the yaw rate increases. The third identified region is the winds with azimuth from 210° to 330°, i.e. left crosswinds, these can cause a tail rotor vortex ring state because they oppose the tail rotor induced velocities direction. The vortex ring state is explained in more detail in the following sections of the literature study but the main effect is that it can reduce the rotor thrust, leading to more pilot workload. Finally, the last region is the so-called loss of translational lift which relates to operating near the operational limits. Then, the helicopter might lose heading due to a lack of tail rotor power.

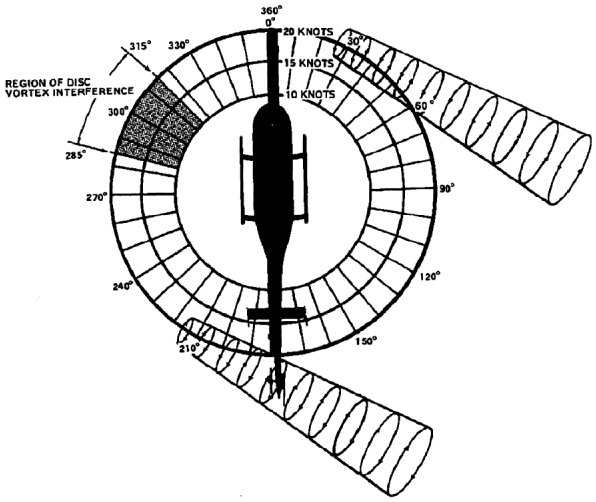

Figure 2.2: Wind azimuth angles and main rotor interference.

Source: Administration [4]

The advisory circular gave a correct explanation according to the state of the art when it was published, however, if the current state of the art is considered, it provides a limited explanation of unintended yaw, which is referred to as LTE in their study. Firstly, many of the identified characteristics were associated with a loss of tail rotor effectiveness but the wording can lead to confusion because the tail rotor is not losing its effectiveness. Additionally, some of the identified regions were explained physically in a vague way. These confusions led to a revision of the topic in the Airbus safety notice [23]. In this document, the unanticipated yaw is explained and it is related to some of the causes already stated in the FAA advisory circular. However, it is clearly stated that a loss of tail rotor effectiveness doesn't occur because the rotor still can generate thrust. Therefore, the problem derives from the capacity of the pilot to react in time and give sufficient pedal input to maintain trimmed flight. As additional information, Airbus Helicopters also released a second safety notice [21] where a special investigation of the characteristics of the helicopter with a Fenestron is held. It is explained how the Fenestron allows less tail rotor thrust in cruise due to the fin help to anti-torque and how it changes to the hover case, where the tail rotor thrust is the same thrust needed as for a conventional tail rotor as there is no freestream velocity.

In the Airbus safety notice [23] the phenomenon is now called unanticipated yaw. Furthermore, the development of the safety notice is done from a simplified flight mechanics code which lacks aerodynamic accuracy. In this safety notice, the explanation for unanticipated yaw can be found in a diagram/curve which charts pedal

position according to helicopter heading relative to true wind direction (while at trim and in hover). Such a curve exists for each combination of weight, altitude, temperature and wind speed. In Figure 2.3a the pedal input curve for a hover flight is illustrated. Now, as an example, let us imagine that the pilot applies the right pedal, and then, the pedal position moves upwards in the pedal input curve as observed in Figure 2.3b depicted in black. This shift in pedal position implies a right yawing until the trim is reached again. However, if the helicopter is flying with a sideslip, imagine at around 70 degrees, it could happen that when the pilot applies the right pedal the helicopter starts yawing without reaching a trimmed state at all. This refers to the case depicted in red in Figure 2.3b.

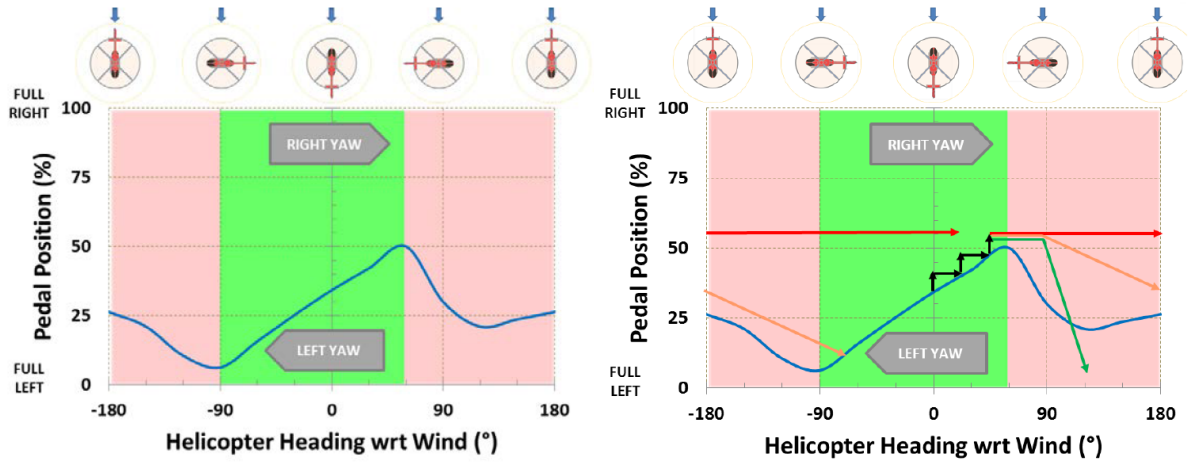

(a) Hover pedal position curve.

(b) Change in yaw stability with pedal position change.

Figure 2.3: Pedal position curve provided in the Airbus safety notice.

Source: Helicopters [23]

If the yawing rate develops, to stop the yawing, a quick and large opposite pedal input must be applied to reach the trim curve again. These cases are depicted in green and yellow in Figure 2.3b. Therefore, it is observed that unanticipated yaw can be anticipated and stopped if correct actions are taken. However, when the pilot is flying, the reaction of the helicopter to a pedal input might not be directly noticeable because depending on the flight speed the pedal curve is flattened, and a small change of pedal might not have a big effect. Additionally, in some azimuthal flight directions, the needed pedal input might not converge to a fixed value because strong wake interactions might appear.

2.4. Flight Physics Investigations

There have been several studies which focused on investigating the cause of unintended yaw accidents. The unintended yaw accident is better understood if it is broken down into different regions with particular characteristics. Hence, most of the studies focus on investigating the phenomena by specifically analyzing different regions which affect the yaw stability depending on the wind azimuth direction. For example, three main affected azimuth regions can be identified. These are the weathervaning region, tail rotor vortex ring state region, and quartering flight regions. However, there are also other studies which combine all these effects into the so-called pedal curve. This section presents the numerical and experimental studies related to explaining unintended yaw and explanation of its characteristics.

From studies that focus on investigating unintended yaw, it is possible to distinguish that in Cuzieux et al. [13], the main purpose is to introduce a simple flight mechanics modelling of the different phenomena characteristic of each region with HOST. In Ragazzi et al. [34], the simulation work was done to define the rotorcraft flight emergency procedure for loss of tail rotor effectiveness for the AW169 helicopter. Additionally, in Roh et al. [36] numerical analyses are conducted to investigate the LTE characteristics of the ducted fan tail rotor. The complete helicopter configuration (main rotor, ducted fan tail rotor, fuselage, and tail boom) is simulated to obtain the mechanism of wake interaction for a range of whole crosswind angles, from 0º to 360º. Srinivas and Chopra [37] presents an investigation of the effectiveness of yaw control in low-speed flight at different headings. The SH-2 servo-flap controlled helicopter is modelled and the predicted trim results are correlated with flight test data. In

Stanislawski [38], the paper presents the results of the simulation tests on the performance of the tail rotor in the directional manoeuvre of the helicopter due to changes in the flow of the tail rotor blades. In Dequin [14] and Ferullo [16], an investigation based on flight tests is presented with a theoretical discussion about the unanticipated yaw phenomena based on the pedal curve and with further recommendations for recovery methods. The flight tests were conducted with an H130. Furthermore, in RAAF [33] an analysis of flight tests is also performed where it is interesting to observe how the unintended yaw appears in other helicopter configurations, in this case, a Bell 206B-1 helicopter. These studies are the most relevant when it comes to the specific topic of unintended yaw; however, the purpose of this section is to explain the different effects that have an impact on the yaw stability of a helicopter as found in the literature.

2.4.1. Weathervaning Stability

The weathervaning region refers to the region approximately enclosing the wind azimuth directions from 120º to 240º which represent tailwinds, see Figure 2.4. This region is greatly influenced by the vertical fin, fuselage and tail boom which tend to weathervane the nose of the aircraft. If the helicopter enters such a relative rear wind condition, it will make a slow uncommanded turn either to the right or left, depending on the exact wind direction, unless a resisting pedal input is made. If the pilot allows a yaw rate to develop, because inattentive for some reason, it may increase. If this happens in the opposite direction of the main rotor rotation, the pedal margin can quickly become insufficient to counteract the yaw [13]. The wind magnitude and wind azimuth are important variables that may heavily impact the weathervaning stability of an aircraft. The prediction of weathervaning stability is not of much difficulty as there is a strong validation availability for this flight configuration which is influenced mostly by a wing surface [49]. Additionally, the effect of the weathervaning stability is to require large pedal inputs from the pilot.

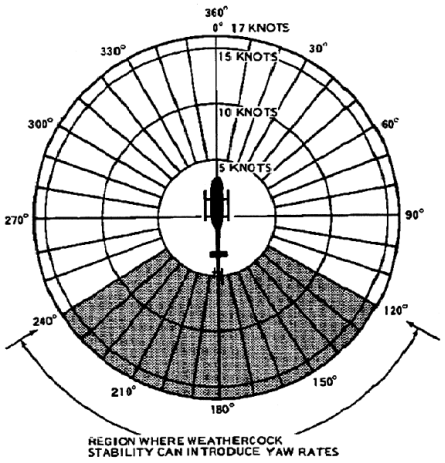

Figure 2.4: Weathervaning region.

Source: Administration [4]

2.4.2. Tail Rotor Vortex Ring State

The flights where the wind azimuth is which has the contrary direction of the sidewash of the tail rotor wake can lead to the tail rotor vortex ring state. VRS has been extensively investigated for main rotors as it is an important accident cause. The phenomena happening at the tail rotor are not exactly as it is in the main rotor due to the interactions between both wakes from the main rotor and the tail rotor.

To understand VRS it is best to consider first the main rotor. During a low forward speed flight, when a helicopter's descent rate approaches the downward speed of its wake, the blade tip vortices organise in recirculating patterns beneath the rotor. A stable, ring-like wake structure emerges. A vortex ring state is detected when the toroidal wake formation enters a buildup phase where organised vorticity accumulates more rapidly than it dissipates. The highly organised VRS wake dominates the descending rotor's inflow field, reducing the blade

angle of attack and creating thrust loss. The main event, observed in piloted rotorcraft during VRS, occurs when the ring makes a single transition through the rotor plane from below. Steady-speed wind tunnel tests do not appropriately simulate VRS because thrust loss does not lead to higher descent rates in a wind tunnel. A vortex ring can only propel itself in a single direction. Thus, before transition, a curved flight trajectory, or manoeuvre, will tend to preclude or suppress VRS [9].

To understand how the wake develops in a helicopter flying with a rate of descent, it must be realised that the wake in reality does not have a smoothly contracting cylindrical wake as expected from momentum theory. In fact, due to local interactions, released vortices start interacting with each other merging and co-rotating. When the rotor is descending, the inflow starts to decrease meaning that the wake starts to compress as discussed before and as observed in Figure 2.5a. This compression not only increases the influence of the wake on the main rotor but also distorts the wake pattern. When the rate of descent is higher, the vortices start to be so close to each other that the vortex sheet starts to roll up due to the self-induced velocities, see Figure 2.5b.

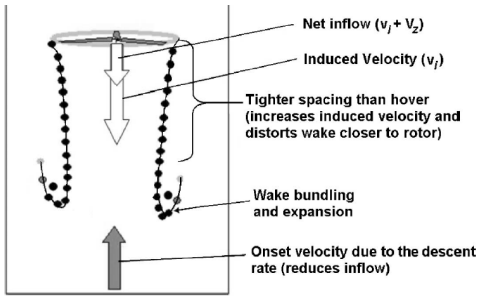

(a) Wake pattern for low rates of descent.

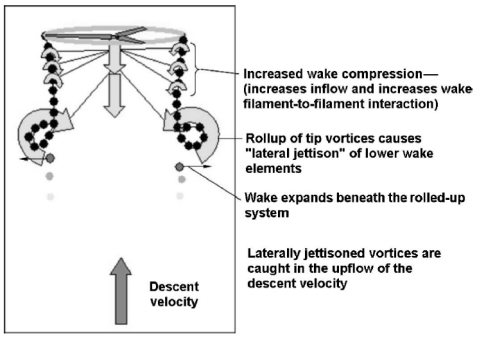

(b) Wake pattern when VRS starts to develop.

Figure 2.5: VRS wake explanation.

Source: Brand et al. [9]

Eventually, the vortex ring state is reached, meaning that a circulating flow generates a big vortex flow around the tips of the blade which increases the inflow in the rotor. The effects of this vortex ring state can be observed in Figure 2.6b, where it is observed that the inflow decreases for an increase in the rate of descent up to a certain speed. Then the inflow starts to increase. The effect of the inflow can be better understood from the velocity field around an airfoil which is part of the blade as illustrated in Figure 2.6a. If the inflow is increased, the effective angle of attack is decreased which implies a lower thrust. If the inflow is decreased, the opposite effect appears. Therefore, this means that when the helicopter starts descending it first has a damping effect because the rotor thrust increases due to a decrease in inflow. However, when the vortex ring state starts to develop, the inflow is increased resulting in a negative damping which causes an acceleration of the rate of descent. Hence, the helicopter falls faster until it reaches a certain speed where the rotor has travelled through the vortex ring state and the wake is above the rotor. Then, the inflow drops and the thrust increases again.

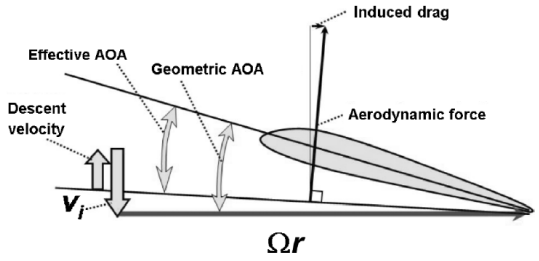

(a) Velocity field around a section of the rotor blade.

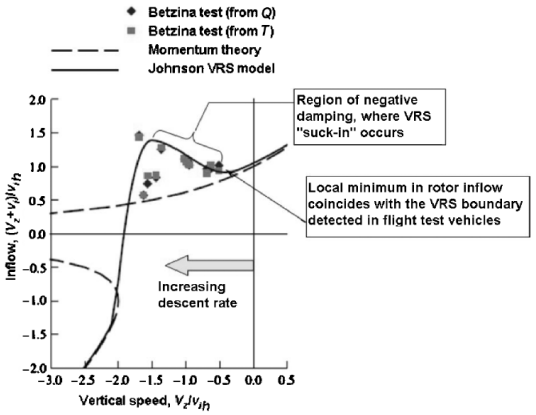

(b) Induced inflow as a function of descend speed.

Figure 2.6: Effects of VRS on the blade inflow.

Source: Brand et al. [9]

Therefore, if the helicopter is flying in a flight configuration where the tail rotor might see a relative velocity in the opposite direction of its wake, this can cause the rotor to operate under VRS conditions, see Figure 2.7. However, note that the VRS only appears for certain values of descending rates in the case of the main rotor so for certain values of side velocity in the case of the tail rotor, which could be the case for certain side flight velocities or yaw rates that could only worse the situation.

In RAAF [33], the tail rotor vortex ring state in more detail. Considering the manoeuvres in which the tail rotor vortex ring state can appear, for a counterclockwise rotating main rotor, a right turn or a left crosswind can create a vortex ring state at the tail rotor. For example, to produce a right turn in a hover, the tail rotor thrust is decreased by reducing its collective pitch with more right pedal and the overall positive yaw moment in the helicopter reference frame forces to yaw the helicopter. For a slow right turn started with a small pedal displacement, the tail rotor is placed in a condition corresponding to a main rotor in a low rate of descent. As the turn rate increases, tail rotor thrust also increases to a point where it again balances the main rotor torque and the helicopter settles on a constant yaw rate indicative of a positively damped (stable) system.

For a larger right pedal step input, the higher yaw rate may put the tail rotor into the vortex ring state where the collective pitch required to maintain a constant thrust is increasing rather than decreasing. Conversely, for collective pitch held constant after the step, the tail rotor thrust decreases rather than increases and the yaw rate suddenly increases. This is indicative of a negatively damped (unstable) system. In an attempt to control the sudden increase in the right yaw rate, the pilot may apply the left pedal, but the initial response could be to deepen the vortex ring state, and the yaw rate might still increase.

The tail rotor vortex ring state may also manifest itself as an inability to maintain heading in left sideward flight or while hovering over a spot with wind from the left. The critical left speed range for tail rotors of most current helicopters is 10 knots to 30 knots as it is stated in the certification specifications CS-27. Flight tests of several main rotor/ tail rotor configured helicopters have demonstrated difficulty in establishing pedal trim position in left sideward flight. The pedal position/relative-airspeed gradient appears to be flat or with a slight reversal.

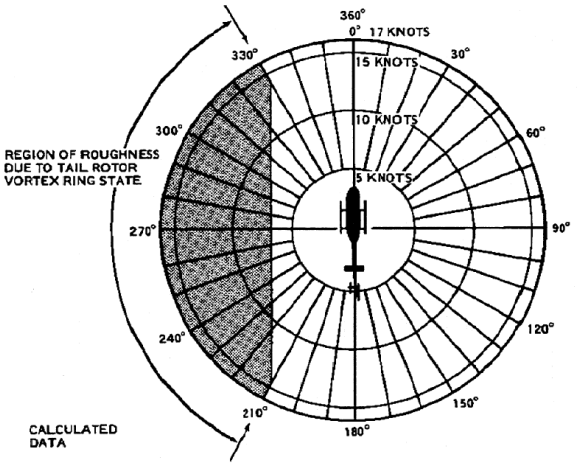

Figure 2.7: Regions where tail rotor vortex ring state can appear.

Source: Administration [4]

2.4.3. Tail Rotor Interactions

The tail rotor is the most important component to provide enough anti-torque and guarantee yaw control. However, due to its location, the tail rotor is strongly interacting with the wake of almost all aerodynamic surfaces of the helicopter. Therefore, it is of key importance to investigate how the tail rotor is affected by either the main rotor wake or the horizontal stabiliser wake. Compared to an isolated rotor, the main rotor's aerodynamic performance is reduced by the presence of the airframe, tail rotor and tail boom in its wake. Reciprocally, tail boom aerodynamic isolated design efficiency is generally not achieved on a full aircraft. Horizontal and vertical tails operate in the wake of the main and tail rotors, respectively, and therefore they do not operate in the free stream condition. Helicopter fuselage vertical drag component is increased in magnitude by the wake impingement (so-called "downwash" generating a "download" on the airframe). In Figure 2.8 the wakes for a hover flight and a forward flight are illustrated. Indeed, in forward flight, blade circulation results in two large vortices that are shed aft and down by the free stream, forming a skewed wake that impinges the airframe, tail boom and tail rotor. As the helicopter transitions from hover to low-speed forward fight, the wake impingement on the tail rotor significantly changes its aerodynamic environment. The tail rotor itself can also introduce distortions in the flow field. Moreover, the anti-torque operates in the complex aerodynamic environment that results from the wakes of the fuselage, and tailboom. The interactions of the wakes of the rotors in addition to other disturbances due to fuselage and tailboom, or external perturbations (e.g. gusts, ship turbulent airwake) generate strong loads on geometrically distant parts of the aircraft. Any unsteadiness in these loads can strongly affect the stability and performance of the vehicle. Those aerodynamic interactions have been investigated thoroughly. Nonetheless, reliable design tools to account for these phenomena are still lacking [8].

In conventional helicopter flight dynamic simulations, main rotor wake interference effects on the fuselage, tail boom and tail rotor are typically roughly estimated using tabulated data, derived either from empirical models or experimental measurements, as a function of airspeed and wake skew angle. Those tables evaluate local changes in dynamic pressure and downwash which are also contingent on the positioning of the component concerning the main rotor hub [20].

Experimental and numerical investigations of those mechanisms have been performed to first optimise helicopter design and performance and, lately, to assess pilot workload. A few examples of those works are presented here. Wiesner and Kohler [42] conducted a series of wind tunnel tests of an idealised rotorcraft: this is the simple association of the main rotor and tail rotor, without tail boom or tail rotor. The wind tunnel tests investigated tail rotor aerodynamic operating conditions and performance for various main rotor/tail rotor/fin relative positions and tail rotor direction of rotation. Several flight conditions were also reproduced in the wind tunnel, such as various wind conditions or aircraft operating Out-of-Ground Effect (OGE) and In-Ground Effect (IGE). Two other groups of researchers, Menger et al. [28] and Balch et al. [7], performed a similar survey for hovering flight, with the addition of fuselage and tail boom using a scaled model of a helicopter. It was found

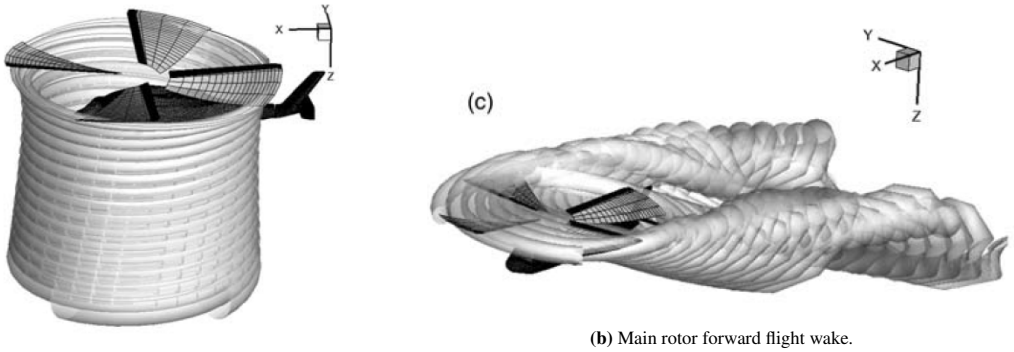

(a) Main rotor hover flight wake.

(b) Main rotor forward flight wake.

Figure 2.8: Main rotor wakes in different flight configurations.

Source: Cao et al. [11]

hover performance could be reduced by 6.7% OGE and 4.4% IGE. Additionally, penalties on tail rotor power due to fin blockage ranged up to 10% for pusher, and up to 50% for tractor configurations. Even so, tail rotor efficiency can significantly be improved by further aft placement, canting angle and pusher configuration: those solutions help to reduce fin blockage and move the anti-torque device out of the main rotor downwash in hover. The main rotor wake effects were secondary to the tail rotor/fin interference. It was also observed that when the main rotor trailing tip vortex interferes with the tail rotor blade, it causes spanwise and azimuth-wise impulsive loading which exacerbates tail rotor harmonic and broadband noise. This was corroborated in Balch et al. [7] where the authors found that in low-speed quartering flight and forward flight IGE, the strong main rotor wingtip vortices directly impinge the tail rotor. Those experimental studies agreed that for a counter-rotating main rotor, the preferred combination is a pusher tail rotor, with a top aft direction of rotation. Later, Balch and Lombardi [6] focused on the influence of main rotor tip geometry on main rotor performance with and without tail rotor. They found that the benefits from the advanced main rotor tip configuration tested are not substantially different when operating in the presence of a tail rotor. Numerical analyses of helicopter aerodynamics also became more widespread with the advancements in computing technologies. Numerous authors have endeavoured to model and analyse main rotor wake statics or dynamics, and to carry out numerical experiments. An example of research focused on tail rotor/main rotor interaction can be found in Reddy and Truong [35]: in this paper, the authors combined a vortex-lattice method for both rotor inboard vortex sheets. They applied a free wake method to the main rotor and a prescribed wake model for the tail rotor. They concluded that depending on the tail rotor location to the main rotor, the wake either opposes or adds to the tail-induced velocity, by generating an additional velocity component in the sideward direction. Their results showed that power requirements could vary from a 20% reduction to a 35% increase compared to an isolated rotor, which was consistent with the experimental results of Refs. [6, 7, 28].

Aside from the complexity of the flow arising from wake impingement on the tail rotor, main rotor/tail rotor interactions were also identified by the Federal Aviation Administration (FAA) as a potential hazard during hovering, takeoff, and landing operations. The FAA Circulatory [4] points out tailwind orientations within the range 210° to 330° for an aircraft with a counter-clockwise rotating rotor; and between 30° to 45° for European (clockwise rotation) vehicles, as favourable conditions for the tail rotor to enter into the influence of the main rotor shed vortices. In those conditions, the main rotor blade tip vortices are pushed into the tail rotor by the wind, creating a highly turbulent environment. Hence the pilot needs to make a lot of adjustments in pedal control to stabilize the aircraft.

Several research works have attempted to model this critical flight condition. For instance, Cuzieux et al. [13] appended a semi-empirical model to ONERA helicopter flight mechanics simulation tool HOST to account for LTE. The model consisted of three parts: firstly, the fin blockage effects on its performance in the vertical tail/tail rotor pusher configuration were condensed in the fin aspiration ratio. Secondly, a vortex ring state model, developed in earlier works, was applied for both rotors. Lastly, the main rotor disk vortex wake contraction was estimated with empirical factors, whereas the tail rotor-induced velocity calculation used the standard Biot-Savart law approach. The model was validated by comparing different configurations and directions of rotation to tune the corrective coefficients. The authors found that for the top/forward rotation of the tail rotor, the direction of rotation is the same as the oncoming main rotor vortex. Therefore, this may accentuate the mutual interaction of

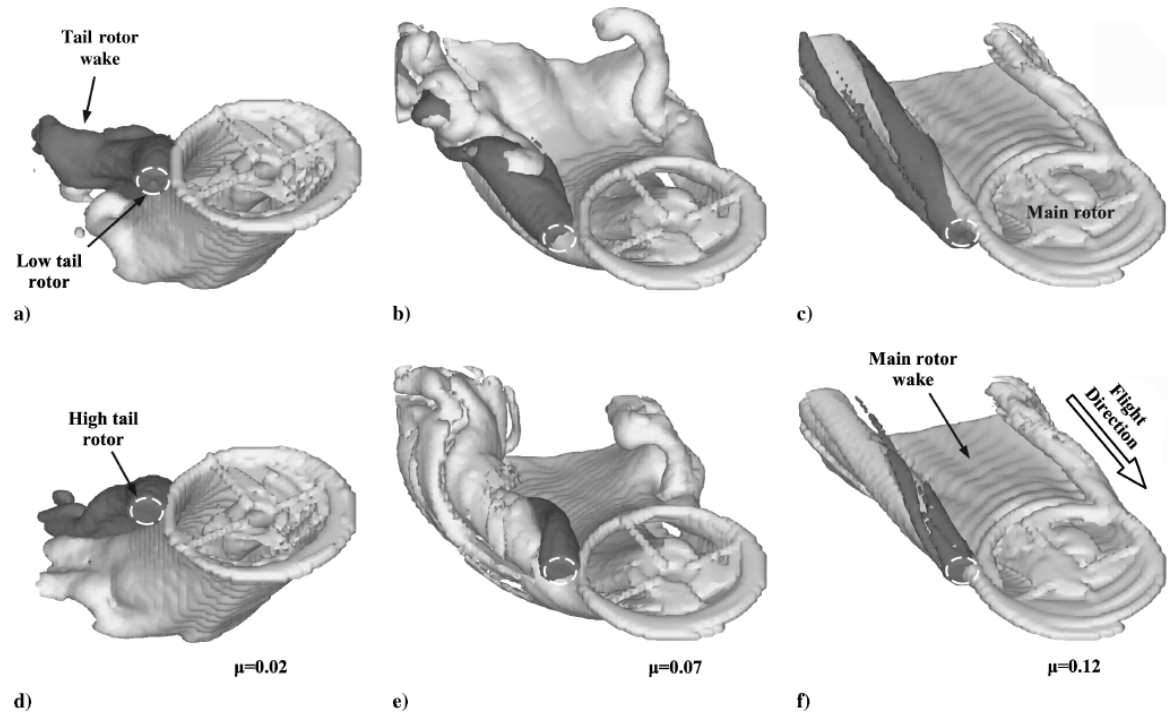

Figure 2.9: Instantaneous snapshots of the main rotor and tail rotor wakes that represent the interaction between the rotors at three pertinent advance ratios. MR–TR systems with low and high tail rotors are shown at the top and bottom, respectively.

Source: Fletcher and Brown [17]

the rotors. Other numerical studies were set with a focus on dynamic loads and control responses to tail rotor/main rotor interference. In Fletcher and Brown [18], numerical simulations using Brown's vorticity transport model, of the aerodynamic interaction between the main and tail rotors of a helicopter are presented for a range of forward and lateral flight trajectories simulations. The results show distinct differences in the behaviour of the system in left sideward and right sideward flight that are consistent with flight experience that the greatest fluctuations in loading or control input are required in left sideways flight (for a counterclockwise rotating main rotor) and are generally more extreme for a system with tail rotor rotating top-forward than top-aft. The simulations also expose distinct differences in the character of the lateral excitation of the system as forward flight speed is varied, and suggest the existence of an intermediate flight speed at which the lateral dynamics of the system are most strongly affected by fluctuations in the loads on the system. Traces of very low-frequency periodicity in the simulated results at low forward speed may be evidence that main rotor–tail rotor interaction might be partially responsible for such practically encountered lateral oscillations such as tail shake or lateral snaking. To extend their work, Fletcher and Brown [17], coupled a vorticity-velocity based CFD simulation of an idealised helicopter with the classic Blade Element Method (BEM). First-order control laws for the main rotor collective and cyclic controls, and tail rotor pitch were also implemented. The investigation studies different tail rotor vertical locations and rotation directions with varying advance ratios, see Figure 2.9 and Figure 2.10. Their analysis showed that the tail rotor wake and yaw moment exhibited increased unsteadiness, that needed to be neutralised with appropriate anti-torque collective control input. This mechanism was found to be dominant in stationary and low-speed flight.

Those results were corroborated in Cao et al. [11] who examined the tail rotor induced unsteady and impulsive loading fluctuations at the main rotor in hovering flight. They implemented a vortex particle method for the wakes, combined with a vortex lattice approach for the rotor blades. The aircraft was also reduced to an idealised helicopter without a fuselage. Only the collective controls were used in this analysis. The group of researchers noticed that the tail rotor wake was dragged into the main rotor wake inner region, resulting in an increased unsteadiness of the main rotor wake. More specifically, for low main rotor/tail rotor separation, the helical structure of the wake was broken by the tail rotor, and the tip vortex trajectory was distorted and irregular.

Ellin [15] have also investigated the effect of the main rotor wake interaction on the tail rotor with a theoretical

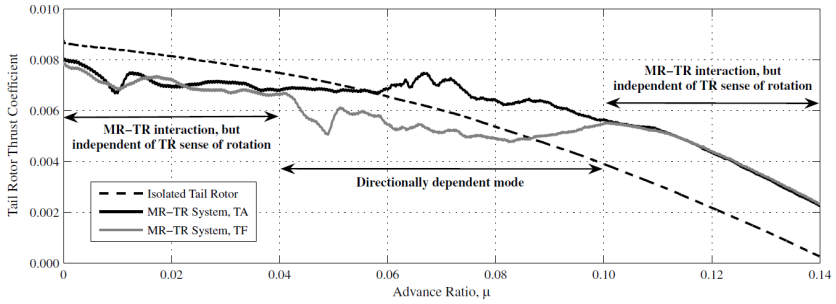

(a) Low tail rotor.

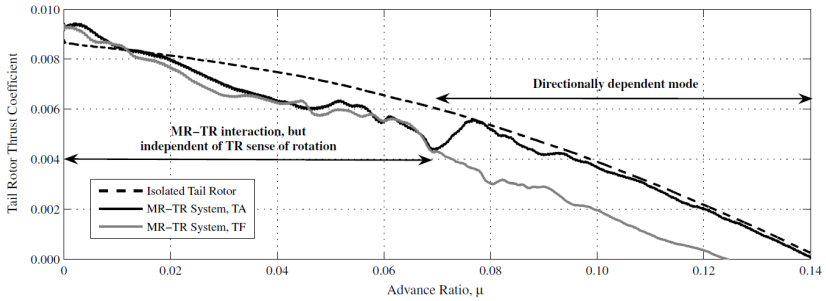

(b) High tail rotor.

Figure 2.10: Variation in the thrust coefficient developed by the tail rotor as the MR–TR system accelerates gradually along a 60[a] sideslip trajectory (TA: top-aft tail rotor, TF: top-forward tail rotor).

Source: Fletcher and Brown [17]

approach by data analysis of flight tests. It was concluded that in quartering flight the tail rotor can be immersed in the roll-up of the main rotor blade tip vortices trailed behind the edge of the disk. For a tail rotor rotating top-blade-forward, this results in a large net reduction in the dynamic pressure at the blade giving rise to a reduction in control margin. This is the most significant interaction influencing the tail rotor and its effect should be included in any helicopter model. Close to the hover, the main rotor wake passes just forward of the leading edge of the tail rotor disc distorting the tail rotor trailing vortex wake. This results in a localised reduction in tail rotor loading. In low-speed forward flight, the main rotor blade tip vortices can interact with the tail rotor tip vortices and, where the distance between the two vortices is small, they each impose a strain field on the other which can cause vortex disintegration with a resultant reduction on the tip loading peak on the following tail rotor blade. In low-speed forward flight, the main rotor blade tip vortex can interact with the section of the tail rotor blade inboard of the lading peak producing changes in the local chordwise velocity and incidence at the blade with consequent variations in blade loading. In rearward flight the tail rotor can experience small loading variations at main rotor induced frequencies possibly due to main rotor wake effects on the fuselage causing sideways movement of the tail rotor gearbox and hub. The research group from Wang et al. [41] also did some experiments and CFD simulations to investigate main rotor wake effects on tail rotor thrust in crosswind. Results confirmed the previous results found in the literature and indicated that the MR disc vortex has a remarkable interference effect on the tail rotor aerodynamic performance characteristic and that the effect is sensitive to wind speed, wind direction, and MR disc loading. The observed yaw instability is considered to be related to the lesser inflow introduced by the MR disc vortex due to the change in the relative position of the disc vortex filament and tail rotor with the wind azimuth. The increase in tail rotor thrust at moderate wind speeds is due to the increase in leading-edge dynamic pressure caused by the opposite swirl direction of the disc vortex contrasted to the tail rotor. The MR disc loading affects the tail rotor thrust due to the change of disc vortex strength and position.

Finally, the investigations from Roh et al. [36] are also of great importance in the field of full helicopter simulations using CFD to analyse the appearance of LTE in helicopters with Fenestron. Numerical analyses were conducted to investigate the LTE characteristics of the ducted fan tail rotor. The complete helicopter configuration (main rotor, ducted fan tail rotor, fuselage, and tail boom) is simulated to obtain the mechanism of wake interaction for a range of whole crosswind angles. It is confirmed that both the main rotor wake and port wing wake are immersed within the tail rotor disk by the suction force of the tail rotor. The main rotor wake rotates in the opposite direction to the tail rotor, and it contributes to the improvement of thrust. The port wing wake works oppositely.

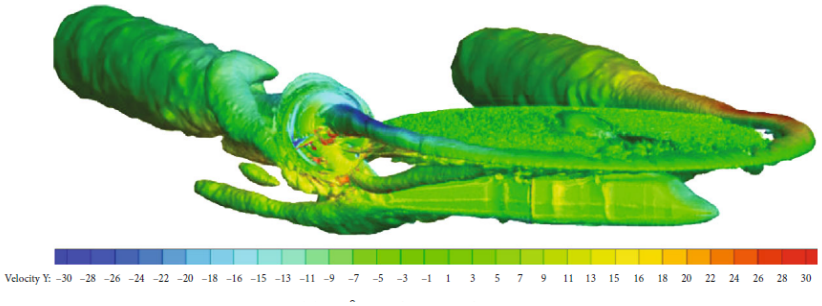

Figure 2.11: Q-criterion (250) of rotor wake colored by velocity in the transverse direction (V = 22 m/s) and 50º wind azimuth case.

Source: Wang et al. [41]

These behaviours can be observed in Figure 2.12. As the flow enters from the front side, both the magnitude and vibration of the thrust are increased due to the broad influence of the main rotor wake. Nevertheless, direct impingement of wakes is prohibited by the structures of the tail rotor system, and also substantial wake of the tail rotor prevents re-entering of the tip vortex. Consequently, the ducted fan tail rotor maintains acceptable thrust variation in comparison with the open-type tail rotor.

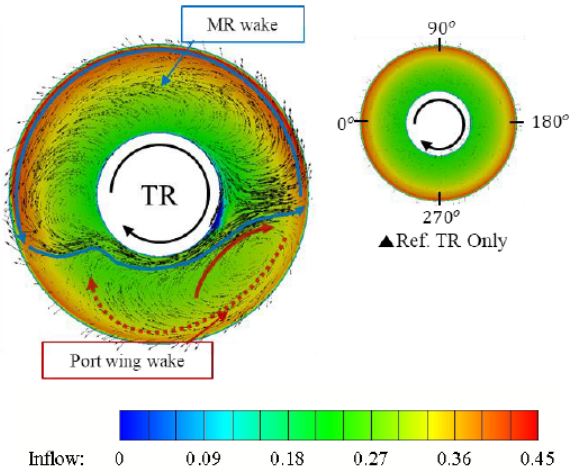

Figure 2.12: Inflow and velocity vector in hover flight. Solid line is counter direction and dashed line is same direction.

Source: Roh et al. [36]

2.5. Yaw Stability Analysis

The yaw stability of a helicopter can also be understood from the perspective of the pedal curve, which is often more intuitive for pilots. The pedal curve is a curve which gives the pedal position that the pilots need to apply to maintain heading. Hence, this pedal curve will include all the previously documented effects superposed. A pedal curve exists for each combination of weight, altitude and temperature conditions. It is beneficial to take a look into the pedal curve as it gives a good understanding of the dynamic behaviour during unintended yaw.

In Dequin [14] and Ferullo [16], they based their explanation of unanticipated yaw on the pedal curve. The results from the flight test of a Bell 206B-1 from the RAAF [33] were used to give a theoretical explanation of the phenomena of unanticipated yaw. Then, the results of the flight test with an H130 were also performed to confirm the approach discussed in the paper and the efficiency of the recovery method. An example of a pedal curve was already given in Figure 2.3a, Dequin [14] and Ferullo [16], base their studies in the pedal curve shown in Figure 2.13b. The pedal curve is a kind of sinusoid with a minimum when the wind comes from the right-hand side (critical azimuth) and a maximum when the wind comes from the left-hand side. As a first approximation

it can be stated that, for a given wind speed, the main rotor torque is almost constant. Neglecting the airframe yawing moment, a constant anti-torque force, oriented to the right, must be delivered by the tail rotor. A right wind component induces some inflow through the tail rotor that reduces the angle of attack on the blade and thus the tail rotor thrust. Maintaining the anti-torque level therefore asks for additional tail rotor collective pitch, i.e. more left pedal. The opposite occurs in a left wind condition where more right pedal is needed. The pedal curve therefore indicates the thrust variations with heading.

Furthermore, an increase in velocity makes the amplitude of this curve increase as shown in Figure 2.13a. At some time the tail rotor performance limit may be reached. It can be seen in Figure 7 that in the considered WAT conditions 40 kt is beyond this limit, the available tail rotor pitch being insufficient in right wind.

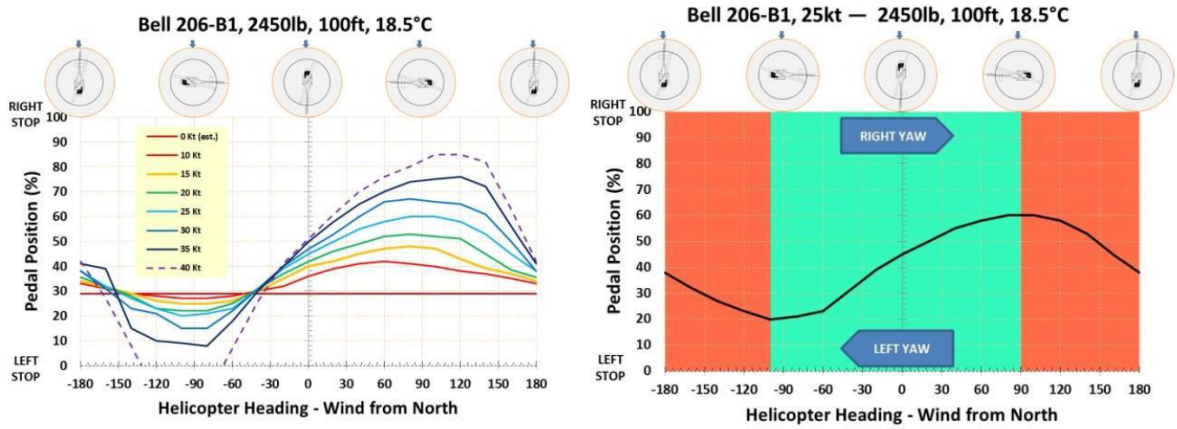

(a) Pedal curves for different velocities.

(b) Pedal curve used in Ferullo [16] paper to explain approach.

Figure 2.13: Pedal position curves from a BELL 206-B1.

Source: Ferullo [16]

As was discussed in the Airbus safety notice, if a right pedal step is made, the helicopter configuration is now in a position above the black line in Figure 2.13b. This means that the helicopter will start yawing to the right so will do in the pedal curve, until it reaches the trim curve. Then, the helicopter will be stable again and in level flight. However, if the pilot makes a too-large right step, it might position himself above the maximum of the pedal curve. This means that the helicopter will start to spin without stopping if no input is made. The same behaviour appears if a too-large left pedal step is made, leading to a left spin.

In Ferullo [16], the author states that the most common accident of unintended yaw is to the right. To explain why is it more frequent to the right than to the left, the pilot logic must be understood. For instance, the pilot usually flies in a comfortable position with a pedal position of around 50 to 60%, this means that when the pilot is pushing the left pedal close to the limits of around 5 to 10%, the pilot is carefully controlling the heading of the aircraft because of the physical awareness of the pedal being close to the limit. Secondly, an unintended yaw to the right might be wrongly perceived as a complete loss of tail rotor thrust, which would also lead to similar symptoms, a right yaw. Eventually counteracting a right yaw asks for increasing the tail rotor pitch and boosts the power consumption. The pilot might be somewhat reluctant to do that, especially in performance-limited conditions, and try to limit his pedal input. A large pedal input on the opposite side has no detrimental consequence and should not be seen as a problem by the pilot.

The idea that not being able to provide enough anti-torque, also called running out of pedal, can initiate unintended yaw is also investigated. For instance, let us imagine that the pilot is flying with right crosswind wind which is demanding the most left pedal. Then, the collective could be increased and make the pedal position above the pedal curve resulting in a right yaw. If the pedal input is not changed, the pedal curve will be reached at some point with a heading closer to 0 degrees, therefore, the helicopter will be in equilibrium again and the right yaw will be stopped. Hence, running out of pedal cannot produce unintended right yaw. However, a collective decrease will lead to unintended left yaw.

In the paper from Ferullo [16], flight tests with the H130 are performed to confirm the theory. In Figure 2.14 different pedal curves for different wind velocities are shown. Note that the H130 main rotor spins clockwise,

therefore, to compare the results with the BELL, a symmetry from the 0 heading must be made. The results show that indeed the helicopter behaviour is consistent with the analysis done using the pedal curve.

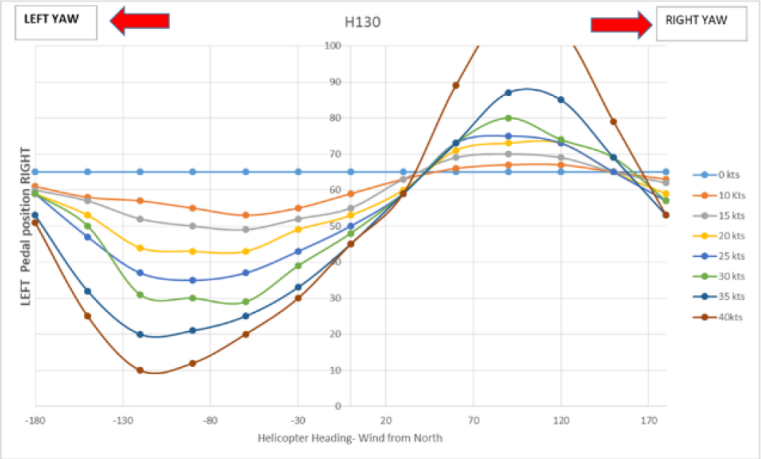

Figure 2.14: Pedal curve from flight tests of the H130.

Source: Ferullo [16]

The flight tests performed by the Royal Australian Air Force [33] show the required pedal position for different wind azimuths and a range of freestream velocities inside the operational limits of the helicopter. The results show that the required pedal position to maintain trim flattens or slightly reverses for wind azimuths close to 270º as can be observed in Figure 2.15a, the plot is interpreted more easily if a fixed velocity is followed. In their study, the handling qualities were also assessed employing the Handling Quality Regions (HQR) where a low HQR indicates low handling difficulties and a high HQR high handling difficulties. These regions are defined in terms of pilot workload, low remaining control travel, unacceptable control excursions about trim or aircraft reaching operational limits such as torque. These HQRs are shown in Figure 2.15b. The highest handling quality region is observed to be located for wind speed of around 15-20 knots and wind azimuths of around 270º. Additionally, the results for the pedal position for a wind azimuth of 270º, see Figure 2.15c, show that the velocities ranging from 15 to 25 knots have a high pedal movement about trim, indicating high handling difficulties.

2.6. Recovery Methods

The advisory circular Administration [4], the safety notice from Airbus Helicopters Helicopters [23], the paper from Ferullo [16] and Dequin [14] are the only documents which have proposed a recovery method for unintended yaw. However, the methods proposed in Helicopters [23] are derived from the studies of Ferullo [16] and Dequin [14], therefore, these will be presented as a whole. Hence there are two recovery methods in total. The methods proposed in Administration [4] recommend the following actions:

1. If a sudden unanticipated right yaw occurs the pilot should apply full left pedal and simultaneously move cyclic forward to increase speed. Additionally, if altitude allows, reduce power. Then, after recovery, adjust the controls to level flight.
2. Decrease collective pitch angle to reduce torque and help bring yaw rate back to zero. Also, any large increase in collective to prevent ground or obstacles may further increase the yaw rate and decrease rpm.
3. The amount of collective pitch reduction should be based on the height above obstructions or surface, the gross weight of the aircraft, and the existing atmospheric conditions.
4. If the rotation cannot be stopped and ground contact is imminent, an autorotation may be the best course of action. The pilot should maintain the full left pedal until rotation stops, then adjust to maintain the heading.

On the other hand, the method proposed in Airbus Helicopters from Helicopters [23], Ferullo [16] and Dequin [14] are based on the pedal curve which can be easily explained from a consideration of the pedal input during

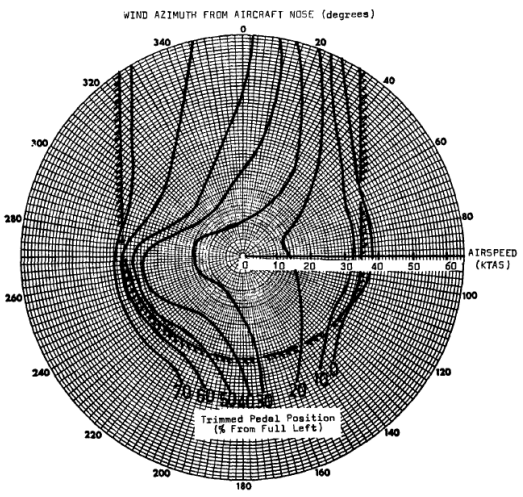

(a) Pedal position for trim.

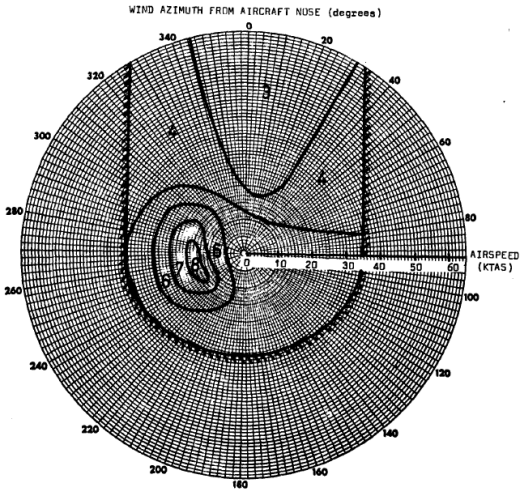

(b) Handling qualities regions.

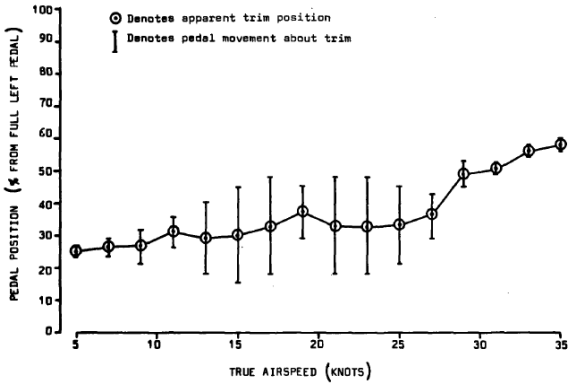

(c) Pedal position for trim at a wind azimuth of 270º for different freestream velocities.

Figure 2.15: Results of the flight tests for a BELL 206B-1 from the Royal Australian Air Force. Helicopter weight is 3200 lb (1451.5 kg).

Source: RAAF [33]

the recovery technique. As an example, different recovery methods are shown in Figure 2.16 and discussed. For instance, it is shown that if no input is changed, the yawing cannot stop. If a large and slow input is held, it can stop the yaw rate but at a very late stage when the helicopter has already yawed a large amount. Then, if a large and rapid input is done the yaw stops quickly but the trim is found close to the unstable tailwind range, susceptible to weathervaning. Considering the analysis of these different recovery situations and the performance limitations, Airbus Helicopters proposes the following method:

1. Take particular care when the wind comes from the left side or forward-left quadrant. Do not fly unnecessarily in those conditions.
2. Prefer, as much as possible, yaw manoeuvres to the left, especially in performance-limited conditions. It is easier to monitor the torque demand at the start of the manoeuvre than when responding to an abrupt unanticipated yaw.
3. To make a yaw manoeuvre, apply a low angular rate of turn and closely monitor it. Yaw acceleration will be more obvious than during an aggressive manoeuvre.
4. If unanticipated yaw occurs, react immediately and with large amplitude opposite pedal input. Be ready to use the full pedal, if necessary. Do not limit yourself to what you feel is sufficient, your feeling can be wrong. Never bring the pedal back to neutral before the yaw is stopped.

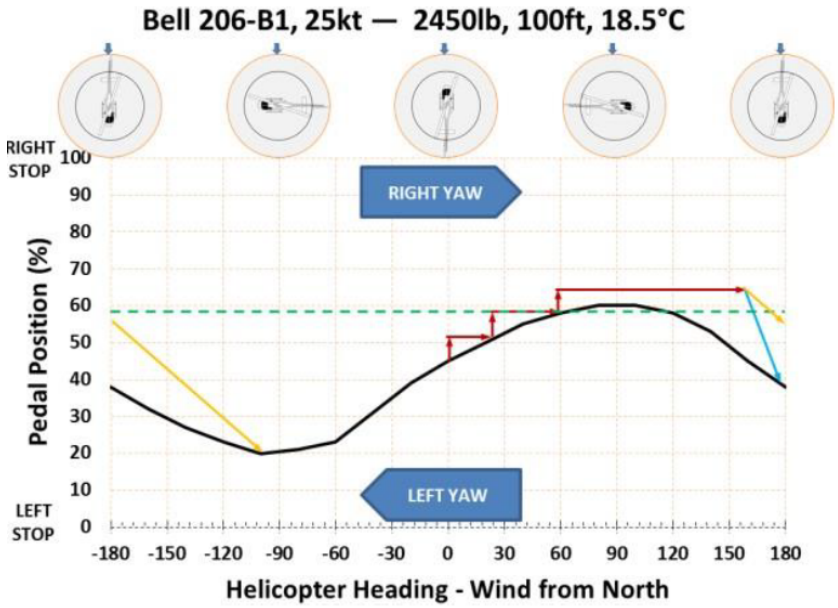

Figure 2.16: Examples of different recovery methods using the pedal curve from a BELL 206-B1.

Source: Ferullo [16]

2.7. Research Proposal

Literature has been provided with investigations related to explicitly unintended yaw or tail-rotor interactions. Many studies are based on flight tests or numerical simulations. Some of these studies are limited to specific case analyses where the helicopter is not flying in a realistic flight state. Although these studies give a better understanding of the helicopter behaviour in such specific cases, the topic of unintended yaw has not been studied in sufficient detail to provide physical explanations of the tail rotor requisites for yaw trim and different speeds, wind azimuths and other tail rotor configurations. Moreover, multiple proposals for recovery methods have not been proposed as a result of previous studies and the most efficient and practical method has to be identified and validated for different classic tail rotor configurations. In fact, until now, the studies about unintended yaw have been studied either with simplified aerodynamics, with isolated academic cases, without realistic flight conditions or with flight tests which lack a detailed physics explanation and are only applied to a specific helicopter model. Additionally, tail rotor vortex ring state has not been studied in detailed tail rotor aerodynamics but it's identified as a prime effect. For these reasons, it is necessary to study unintended yaw through numerical simulations to provide more detailed oriented answers to the helicopter demands in yaw stability and control so as to give an overview of the characteristics of unintended yaw. Furthermore, it is known from the contacts of Airbus Helicopters experts that it is still believed among part of the pilot community that the unintended yaw is a catastrophic scenario which is unrecoverable when fully developed. Airbus accident investigators also confirm that in some accidents, the pilot has not been able to apply a correct recovery method due to a poor understanding of the phenomena and the current overwhelming recommendations which can confuse the pilots. On top of that, it is also necessary to assess the handling qualities of the aircraft to prevent the start of unintended yaw and test recovery methods to gain control again when unintended yaw has started.

The results from the thesis should be valid as generally as possible. Hence, different tail rotor and helicopter configurations have to be investigated to make it representative of all helicopter types with a classical tail rotor. The different configurations include the tail rotor rotating in the opposite direction, the top forward, the tail rotor centre of rotation located at the tail boom height and low-weight helicopters' typical tail rotor configuration by lowering the disk loading of the main rotor. Therefore, the first objective of the thesis is to prove that the evolution of an uncontrollable unintended yaw is excluded from the operational envelope of the helicopter. This is important to overcome the wrong perception that still persists in parts of the pilot community that there are some conditions which could lead to an unstoppable unintended yaw. If no such cases are found, it is necessary to explain how unintended yaw can start in such cases. This results in the first research question:

RQ1: "Is there a flight condition that causes uncontrollable unintended yaw?"

the answer to this question is found with the help of some sub-questions which at the same time will provide a detailed explanation of the reasons for the needed tail rotor performance:

- How much anti-torque and tail rotor thrust is needed for different low speeds and wind azimuths?
- How much collective and pedal is needed to generate the desired thrust and are these values within the operation limits?
- How can the helicopter lose the yaw trim and start an unintended yaw?

The second objective of this work is related to the necessity to have more accuracy of the helicopter performance in the numerical simulations thanks to a coupling between a flight mechanics code with an aerodynamics code to investigate unintended yaw. Formulated in the next question,

RQ2: "Is a coupling between a flight mechanics code and an aerodynamics code needed to study unintended yaw?“

whose answer finding will be helped by these sub-questions:

- How do standalone Gensim tail rotor collective and anti-torque demands compare to the coupled results with the aerodynamics code?
- Which flight states need the more accurate rotor aerodynamics feedback the most?

From the pursuit of a detailed oriented study of the helicopter yaw demands, the tail rotor aerodynamics must be assessed in detailed research. For instance, the third objective of this study is to assess how the tail rotor aerodynamics is affected by the main rotor wake interactions or a possible vortex ring state developing at the tail rotor and how this relates to unintended yaw. Even though studies investigating main rotor wake interactions with the tail rotor have been found, they have shown limited results due to the analysis of limited wind azimuths only and the application of simplified helicopter and aerodynamic models. Similarly, the vortex ring state has been exhaustively studied for the main rotor, as found in the literature, but not for the tail rotor and its implication in unintended yaw. This results in the following research question:

RQ3: "How do main rotor wake interactions and tail rotor vortex ring state affect tail rotor aerodynamics and are they important for starting unintended yaw?"

following the answer to this research question, these sub-questions will also be tackled to provide a more robust answer:

- Is a vortex ring state appearing at the tail rotor?
- How does a potential vortex ring state at the tail rotor affect the needed tail rotor thrust and collective to maintain yaw trim?
- Are the main rotor wake interactions with the tail rotor providing a detrimental tail rotor performance?

The handling qualities of the helicopter dictate whether the pilot will have difficulties maintaining the helicopter's heading in certain flying states. The start of unintended yaw could be related to regions with difficult handling capabilities. Therefore, a research objective is also to assess if there are flying states that are difficult to handle by the pilot. The research question that follows this investigation is:

RQ4: "How do the physical effects related to unintended yaw affect the handling characteristics?"

Finally, the last objective of this thesis is to study if once unintended yaw has developed to a high yaw rate, the pilot can perform a recovery procedure to gain yaw trim control again and stabilise the helicopter, giving place to the next research question:

RQ5: "Is unintended yaw recoverable and what pilot control inputs are needed"

furthermore, the sub-questions to this research question are:

- How is unintended yaw starting while manoeuvring?
- How much pedal and how fast does the pilot need to apply to recover a started unintended yaw?

3

Methodology

This chapter walks through the methodology used to carry out the present investigation. The study is performed using numerical simulations thanks to the availability of detailed descriptions of the helicopter components' loads and flow field, which is especially important for rotor aerodynamics. On top of that, it is also possible to make changes to the simulated flight conditions in a short period. Therefore, this chapter is organised with a detailed explanation of the numerical tools used first, together with the main assumptions and limitations of the method. Then, the helicopter used to perform the simulation is described, followed by a verification of the numerical simulations with flight test data of this helicopter model. Finally, the simulation setups for the investigation are presented.

3.1. Gensim

Gensim was Eurocopter's in-house helicopter simulation tool for global steady and unsteady performance, flight mechanics, and loads calculations, and it is still used in what is now Airbus Helicopters. The code allows for computing a nonlinear flight model with six degrees of freedom in stationary and transient motions for various simulation types; however, for this thesis, only the trimmed and manoeuvring simulations are of interest.

To run a simulation in Gensim, it is first necessary to define the helicopter model. This model consists of a file where all the parameters specific to the helicopter and the simulation type are defined. Firstly, the polar of the airfoils used in the aerodynamic surfaces are defined for a range of Mach numbers. These will later be used to compute the aerodynamic loads in the solution loop. Following the polars, the Gensim parameters are defined. In Gensim 1845, parameters can be defined depending on the simulation type. However, the most critical parameters are the ones that are commonly used throughout all kinds of simulations, which are helicopter-specific. These include the geometry: fuselage location, main rotor, tail rotor, tail boom, horizontal stabiliser, vertical stabiliser, end-plates locations or landing gear location. The rotor characteristics, such as the airfoils used and their locations, chord distribution, twist distribution or inertia of the blade, are also specified. Also, it is essential to define the location of the centre of gravity. The rest of the parameters are also important, but some are either very specific to each component geometry, interfere between them or are numerically related to the solver.

Gensim can use analytical models or tuned models from flight tests to model the forces acting on the aerodynamic surfaces and the forces acting on the aerodynamic surfaces, depending on the component. The tuned models from flight tests can predict the forces of the rotors, fins, fuselage and interference between the aerodynamic surfaces with reasonable accuracy. However, these are not useful for prediction capabilities. Therefore, if analytical models are used, they can predict helicopter performance without flight tests. For example, to model the rotors, Gensim models the blade as a rigid blade with 4 degrees of freedom: flapping, lead/lag, blade and control torsion. The aerodynamics are based on the blade element theory; this theory assumes that the rotor blade can be discretised as several spanwise sections contributing to the total aerodynamic forces. If the velocity field around the blade is known, the effective angle of attack of the section can be found; therefore, the

aerodynamic forces and moments can also be computed from the airfoil 2D polar. The most critical part is to obtain a good prediction of the inflow over the rotor; to do so, Gensim uses the Pitt and Peters dynamic inflow model. To account for the interactions of the rotors with the rest of the helicopter components, Gensim uses empirical correction factors that depend on the main rotor down-wash for the cases of the fuselage, tail boom or horizontal stabiliser and on the tail rotor downwash for the vertical stabiliser.

The limitations of Gensim when used without tunning are the assumption of an inflow model for the velocity flow field at the rotors, which assumes a linearly distributed inflow over the rotor depending on the forward speed, for example. Therefore, it doesn't allow for considering a limited number of blades as the model is derived considering an infinite number of blades. Additionally, the polar from which the lift, drag, and moment coefficients are interpolated must account for compressibility effects and be accurate enough to perform decent Gensim computations. This also assumes that the rotors' thrust is the contribution of each local section's smaller contributions, which are considered 2D. On top of that, the interference of the wake from the aerodynamic surfaces of the helicopter with the rest of the components is complicated to predict. Gensim uses correction factors, which are limited to normal flight conditions but not for low-speed flights where VRS could appear on the tail rotor.

3.1.1. Trimmed Flight Simulation

The trim simulation finds a solution that satisfies equilibrium on all six force and moment directions through a Newton-Raphson update iteration. To perform a trimmed flight simulation in Gensim, the number of degrees of freedom must be specified first. Typically, the main rotor collective, the lateral and longitudinal cyclic, the tail rotor collective, the pitch attitude and the roll attitude are set as degrees of freedom. This means that the heading or yaw rate can be a specified value. Therefore, specifying case-specific parameters like weight, temperature, flight altitude, and translational velocity on all three axes. Hence, the trimmed simulation inputs the case-specific parameters and outputs a trim state.

3.1.2. Time Domain Simulations

Gensim can also perform time domain simulations where the helicopter can be simulated to follow a specified manoeuvre. This is thanks to the autopilot implemented in Gensim. We must select an initial state often taken from a trim simulation for a time domain simulation. Then, the autopilot is activated depending on the objective manoeuvre. For example, if the helicopter needs to maintain the same initial state over time, it is possible to just set control over the heading, bank, and pitch angles. However, more options exist, such as maintaining a certain height, vertical speed or overall speed. If no further inputs are provided, the autopilot will keep the same initial flight state concerning the autopilot controls. Thus, the interesting part is specifying how the flight parameters should change over time, allowing us to simulate a manoeuvre.

3.2. UPM

The aerodynamics code used throughout this thesis is the free-wake panel method code from DLR Institute of Aerodynamics and Flow Technology called UPM (Unsteady Panel Method). This code is based on numerical schemes to solve potential flow problems and can treat flows about complex three-dimensional (3-D) configurations in combination with a non-linear 3-D unsteady free wake. In general, this code was developed for rotorcraft purposes. It can be used for rotorcraft main/tail rotor interaction, including rotor thrust and hub moment trimming. Still, the applications can also be applied to the propeller and the wings.

3.2.1. Free Wake - Panel Method

Panel methods are numerical schemes for solving potential flow problems and can treat flows about complex three-dimensional (3-D) configurations [19, 24, 39]. Based on a non-linear 3-D unsteady free wake panel method developed to simulate aerodynamic characteristics of isolated rotors with arbitrary blade geometry and motion [5, 46, 48], the prediction of wake configuration and pressure distribution on the closely interfering main and tail rotor configuration was derived [47]. The current aerodynamic model of DLR's 3D unsteady free wake panel code

(UPM) can treat two simultaneously turning multi-blade rotors each with a (full-span) free wake in any arbitrary motion. The effects of main/tail rotor interaction or interference have been included in the following manner:

1. Satisfying boundary condition of no flow through the main rotor blade surface or flow tangency condition at every instant time, including the effects of tail rotor singularity and it's free wake.
2. Satisfying boundary condition of no flow through the tail rotor blade surface or flow tangency condition at every instant time, including the effects of main rotor singularity and its free wake.
3. Calculating induced velocity on each corner points of either main rotor or tail rotor wake surface, including effects of main and tail rotor.

The model of a lifting rotor blade or wing consists of the following elements, refer to Figure 3.1a:

a) A source/sink distribution on the surface to simulate the displacement effect of the wing/blade.
b) A surface with bound vorticity inside the wing/blade for modelling the lift of the wing/blade. For numerical stability, the circulation increases from zero at the leading edge to full circulation at the trailing edge using some weighting function.
c) A short zero-thickness elongation of the trailing edge along its bisector (Kutta panel) to satisfy the Kutta condition which is a tangential flow at the training edge. The flow tangency condition on the Kutta panel fixes the total strength of the circulation of the blade section.

Remark: In UPM an iterative scheme is used to fulfil the Kutta condition: At first, the tangential flow condition is satisfied as described previously. The resulting equation is linear and is easy to solve. However, it was found that the Kutta condition does not ensure identical pressures on the upper and lower panels at the trailing edge of an airfoil especially in unsteady flow. Therefore, in a second step, a non-linear equation is solved iteratively to get matching pressures. This method is called "pressure Kutta condition".

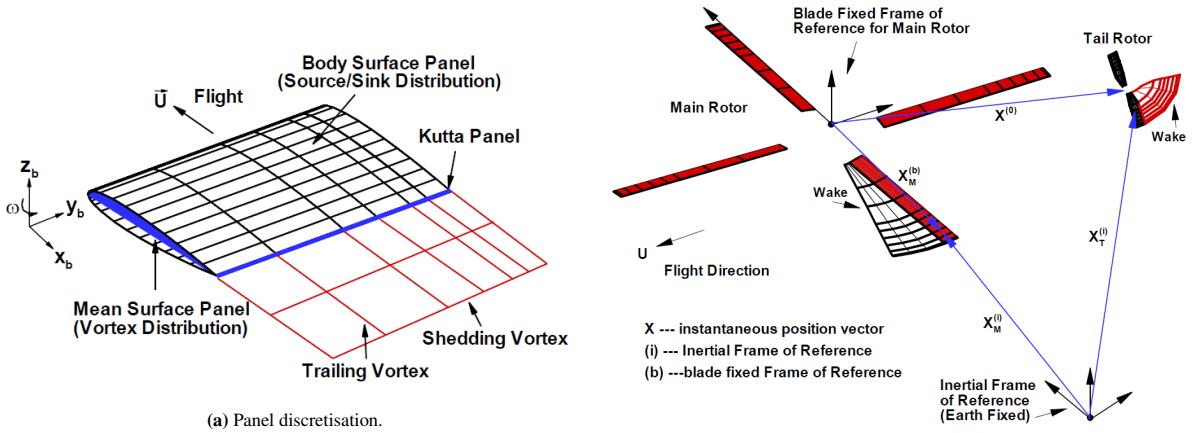

(a) Panel discretisation.

(b) Blade fixed and inertial frame of reference.

Figure 3.1: UPM discretization details.

The problem formulation is based on a reference frame fixed to the ground, see Figure 3.1b. All the blade or wing motions and positions are referred to this frame of reference. For the application of the wings, the rotational speed is zero as default value. The relationship between the ground fixed and a blade-fixed frame of reference can be expressed with the help of the transformation matrices. The details of these matrices are given in [47, 48]. The blade (or wing) and its mean surface are first partitioned into small planar surface elements (panels) which carry a source/sink or doublet distribution of unknown strength, σ_j, μ_j respectively. After the boundary condition of flow tangency imposed on the blade or wing surface is satisfied with full consideration of the mutual interaction between the blades or wings and their free wakes, a system of linear algebraic equations can be written as:

$$\sum_{j=1}^{m_s} A_{ij}\sigma_j + \sum_{j=1}^{n+m_s} B_{ij}\mu_j = R - \sum_{j=1}^{p} C_{ij}Z_j \tag{3.1}$$

where $i = 1 \ldots m_s + m_k$ and whose solution gives the strength of singularities (source/sink or doublet) on all collocation points ($m_s + m_k$) of blades or wings after each computation (time) step. Hereby m_s is the total number of panels on the blade or wing surface, n the total number of panels on the blade or wing mean surface, and m_k the total number Kutta panels. The number of surface panels plus the number of Kutta panels remains constant. The number of wake panels p , however, increases as the computation progresses. The above system of equations is solved iteratively for each time step. A_{ij} , B_{ij} and C_{ij} are the mutual "influence coefficients" of the (surface and wake) panels. Z_j are the known panel strength shedded in the wake. Since the relative position of the blades or wings and their wakes changes after each time step, these influence coefficients need to be updated after each computation step. The pressure on the blade surface is calculated using the unsteady Bernoulli equation. The free wake is generated with the following steps:

a) At the start of a computation no wake is present.
b) At the beginning of a time step, all rotor blades or wings move to their new positions.
c) While repositioning a blade a new wake row is released from the Kutta panels and is added to the existing wake.
d) Figure 3.1a shows the wake after some time steps. The spanwise distribution of circulation on a new row of wake panels is the same as the bound circulation of the blade. The circulation distribution on the wake row will remain unchanged throughout the whole computations which is an assumption to be valid for high Reynolds numbers.
e) Now the linear system in Equation 3.1 is set-up and solved.
f) At the end of the time step the self-induced velocities of the wake are computed (=the velocity induced by each wake filament onto each wake filament) and the wake positions are advanced in time. Thus, the whole wake surfaces is freely deformed according to the locally induced velocities.

A full-span free wake is generated in this manner step by step behind the blades or wings as the computation proceeds. Please note that the wake behind a wing or rotor blade is a continuous layer of vorticity. In freewake methods this vortex sheet is discretized by a finite number of vortex filaments, where the continuous distribution of vorticity is lumped into individual vortices. Thus, the individual filaments do not have a certain physical meaning.

The evolution of the wake in time is computed from the wake positioning at the previous time step and the velocities acting on the wake elements. In UPM so called multistep-methods are used to integrate the positioning of the free-wake and the particle wake in time. The basic approach is to apply explicit Adams-Bashforth-methods. These calculate the new wake position from the wake position at the previous time step and the induced velocities acting on the vortex filaments on a range of previous time steps. For example, the two step Adams-Bashforthmethod is given by

$$\vec{x}_t = \vec{x}_{t-1} + \frac{\Delta t}{2}\left(3\vec{v}_{t-1} - \vec{v}_{t-2}\right) \tag{3.2}$$

where $\vec{x}$ denotes the coordinates of a point on the wake, t denotes the time, Δt is the size of the time step and $\vec{v} = f(t,\vec{x})$ are the induced velocities acting on the wake point. In UPM, the Adams-Bashforth method is implemented up to third order temporal accuracy. The leading term of the truncation error of the Adams-Bashforth method using a third order scheme is given by $3/8 v''' \Delta t^3$. In the table the variable Δt denotes the size of the time-step and v', v'', v''' denote the first, second and third spatial derivative of the local velocity. It can be seen that increasing the accuracy order reduces the truncation error. However, increasing the accuracy order leads to a decrease of stability of the Adams-Bashforth method. Reducing the time-step size increases both, accuracy and stability.

Overall, the limitations of using such aerodynamic modelling are strongly related to the fact that the formulation is inviscid and incompressible. This inviscid formulation will not predict the drag due to skin friction, which is considered to be of low order magnitude, and the incompressible formulation will mainly affect the main rotor tip blade sections loads prediction since the Mach number is expected to be high, leading to a different blade pressure prediction but only to limited regions. Nevertheless, since the helicopter loads are significantly driven by the pressure forces, the unsteady panel method is expected to provide a good compromise between accuracy and computational time. Higher fidelity methods such as CFD could be used, however, for the purpose of this thesis, many different full helicopter simulations will need to be investigated so it would be prohibitive to use CFD.

3.2.2. Particle Solver

The previous section the wake is represented by a vortex lattice model, where the points are connected by straight line vortex filaments. An alternative approach is to model the wake by using vortex particles, called vortex blobs. The vortex blob model solves the vorticity transport equation, written in a Lagrangian frame like,

$$\frac{D\omega}{Dt} = (\omega \cdot \nabla) u + \nu \nabla^2 \omega \tag{3.3}$$

where ω is the vorticity of a fluid particle, u is the velocity of the particle and ν is the kinematic viscosity. The first term on the right side describes the stretching of vorticity due to a velocity gradient, whereas the second term on the right side describes the diffusion of vorticity due to viscous effects. The vorticity equation can be derived from the incompressible Navier-Stokes equations without any simplifications. The vortex blob method models all terms of the vorticity transport equation. When using a very high number of vortex blobs, the approach correctly represents viscous flow. Comparing the vortice lattice and the (inviscid) vortex blob model, the vortex filaments with strength γ and length $\vec{l}$ are replaced by point vortices with strength $\vec{\omega} = \gamma\vec{l}$. A comparison of a panel wake and a particle wake used in UPM is shown in Figure 3.2.

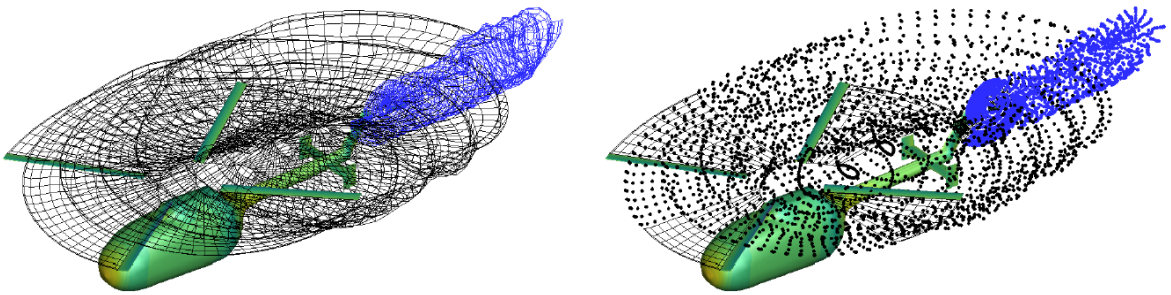

Figure 3.2: Vortex lattice wake and a particle wake used in UPM.

The particle wake method promises an improved simulation robustness for cases where straight line vortex filaments would cross solid body surfaces. Furthermore, viscous effects are taken into account. As an additional advantage for future applications the vortex particle method allows for placing particles at arbitrary positions into the flow without considering any connections with neighbouring vortices. A drawback of the vortex blob model compared to using vortex filaments is a lower accuracy near vortex lines, since the vortex line is discretized by a limited number of vortex blobs. As an additional drawback it is difficult to analyze larger scale vortical structures because the vortex particles are not connected with neighboring particles as in the vortex lattice method.

UPM is linked to a particle solver originally coded for the DUST-panel method. DUST is being developed by the Politecnico di Milano [30]. The underlying equations are given in Winckelmans and Leonard [45]. In the DUST approach all vortex particles have the same vortex core radius. No vortex core aging is applied. The velocity distribution inside the vortex core is given by the Scully-model. The computational domain for the particles is defined by a bounding box. Any particles leaving the box are removed from the simulation. The computational effort can be reduced by applying a Fast Multipole Method (FMM). The FMM uses multipole expansions to calculate the velocities induced by particle ensembles and an octree-data structure to reduce the number of operations needed to predict particle-particle interactions from O(N2) to O(N), where N is the total number of particles In UPM the first wake rows behind a wing/rotor blade are modelled by the panel-wake. At the last wake row the particles are emitted into the field.

3.3. Coupling Gensim with UPM

The flight mechanics code has been briefly explained in general and the aerodynamics code has been explained more thoroughly. In Airbus Helicopters, an interface has been developed to take the best of each code to perform more accurate full helicopter simulations. For instance, this interface consists of a coupling between the aerodynamics code and the flight mechanics code. The coupling has successfully been implemented and showed impressive results in Kunze and Ries [27] where both trimmed and time domain simulations were performed.

The coupling is based on the fact that the flight mechanics code can perform trim and manoeuvring simulations but makes use of low-fidelity aerodynamics which are not sufficient for prediction capabilities. Therefore, as the aerodynamics code can obtain more accurate predictions of the vehicle's aerodynamics and flow behaviour but is not able to perform flight mechanics simulations, the loads and induced velocities of the aerodynamic surfaces can be transferred to the flight mechanics code to improve results. As an additional note, although in the present coupling interface, the aerodynamics code consists of a free-wake panel method and particle method, this is similarly done with CFD finite volume method codes.

Before going into the detail of how a trimmed flight simulation or a time domain simulation is performed, the exchange of information between the codes must be explained. The process is illustrated in Figure 3.3. The coupling consists of a weak coupling, meaning that the information is exchanged separately after having simulated each code. Instead, if it were a tight coupling, the information would be exchanged every inner iteration when advancing one time step. To run a UPM simulation, the motion which was obtained in a previous Gensim simulation is used as input. This includes position and velocity of the centre of gravity; pitch, roll and bank attitudes; flapping, lead-lag, control and mount modes of the main rotor blades; collective and rotation velocity for both main and tail rotor; longitudinal and lateral cyclic for the main rotor. Therefore, the loads and flow velocities are obtained for the same case which was obtained from the flight mechanics code. After the aerodynamic simulation finishes, the loads of the main rotor, tail rotor, fuselage, and vertical and horizontal stabilisers can be obtained as an average of a given number of main rotor revolutions. These loads are then processed to obtain the difference in loads between the loads from the aerodynamics code and the loads obtained from the Gensim simulation from which the motion for the aerodynamics code was taken, thus, the previous Gensim simulation. These delta loads can be formulated as:

$$\Delta Loads^{i} = Loads^{i}_{UPM} - Loads^{i-1}_{Gensim} \tag{3.4}$$

where i refers to the coupling iteration. In addition, the local averaged induced velocities over the main rotor are also obtained for the same averaged period. Then, the next Gensim simulation can be executed. However, the difference with the first Gensim simulation is that now the difference in loads and the new induced velocities for the main rotor are introduced. A small limitation of Gensim is that additional loads can only be applied either at the fuselage, the vertical stabiliser or the horizontal stabiliser. This means that the difference in loads for the main and tail rotors needs to be applied to the fuselage through a coordinate transformation. Therefore, when checking the Gensim results, the additional loads will be seen to be applied at the fuselage and the main and tail rotor loads from the output will be missing the additional loads. However, this is not a problem since the rotors will change the controls according to an additional load seen in the fuselage which is effectively the same. For the locally induced velocities over the main rotor plane, the following formulation is used in Gensim:

$$v^{0}_{i} = \frac{1}{2}\left(v_{i_{UPM}} + v^{0}_{i_{Gensim}}\right) \tag{3.5}$$

$$v^{n}_{i} = v^{n}_{i_{Gensim}} + \left(v_{i_{UPM}} - v^{n-1}_{i_{Gensim}}\right) \tag{3.6}$$

where n represents an inner iteration inside Gensim, v_i refers to the induced velocities that will be used for the final computation in Gensim, $v_{i_{UPM}}$ refers to the induced velocities from the UPM simulation and $v_{i_{Gensim}}$ the induced velocities from the Gensim model. One could think about replacing the induced velocities directly, however, this would have convergence problems for the overall Gensim simulation. Instead, this formulation allows for the convergence of the Gensim simulation to be smoother as the changes in the blade controls will affect the induced velocities.

3.3.1. Trimmed Flight Simulation

To run a coupled simulation of a trimmed flight, the procedure is simple. A first Gensim simulation is run with the settings for running trimmed simulations as discussed in the previous section. Then, the coupling starts with a UPM simulation which is followed by a Gensim simulation that has feedback on the aerodynamics from the UPM simulation. Although the UPM is also a time domain simulation itself, the time steps can be thought of as steady time steps to achieve a converged UPM result. This is repeated until convergence of parameters of interest is established, which is also equivalent to achieving convergence for the value to exchange in loads. Note that three iteration types exist: first, the inner Gensim iteration to achieve a trim state; second, the inner UPM time step; and the coupled iteration.

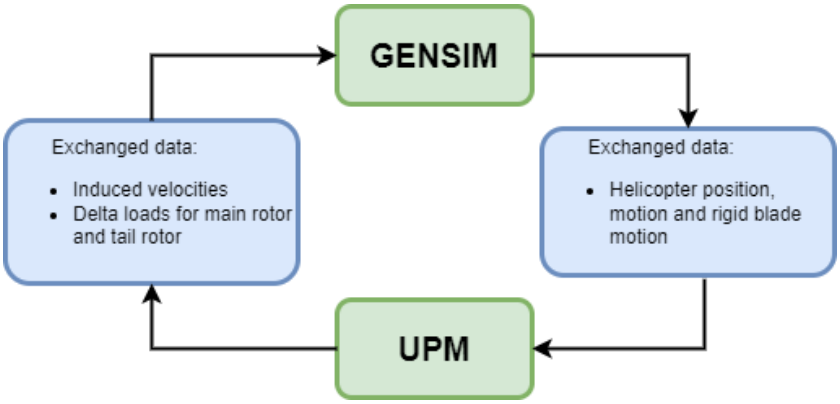

Figure 3.3: Work flow of the coupling.

3.3.2. Time domain Simulation

Running time domain simulations with the coupling is slightly more complex, but it is possible to get accurate time response manoeuvres that react to the autopilot from Gensim and the control inputs. For a coupled time domain simulation, a coupled trimmed simulation is run to get an initial flight state that represents the trim as accurately as possible. Then, at this point, the intervals for the coupled time domain simulation start.

The first interval has the controls for the converged coupled trim state obtained from the last trimmed Gensim simulation together with the delta loads and the induced velocities that were obtained on the last trim UPM simulation. Therefore, the first time domain Gensim simulation for the first interval has the controls and loads corresponding to the results for the trimmed coupled simulation. Then, the Gensim simulation is run for a minimum of one main rotor revolution with the settings for the time domain simulation. The minimum time for the time domain Gensim simulation is one main rotor revolution as by default, Gensim starts a simulation with the first blade aligned with the tailboom. After running the first Gensim simulation, similarly to the trimmed flights, a UPM simulation follows with a motion that recreates the same from the Gensim simulation and for the same time. Hence, in this UPM simulation, the time does not represent a steady state iteration anymore, but rather a real-time one. After this UPM simulation, the Gensim simulation is run again with the new feedback on loads and induced velocities. A limitation exists on the number of coupled steps Within one interval, as only one coupled step shall be performed. This is because since time-domain simulations are being performed, the helicopter is accelerating, which is not possible to simulate a helicopter accelerating in UPM. Therefore, the exchange of loads can start to diverge.

For the next intervals, the process is the same except that the initial conditions for the first Gensim simulation in each interval are taken as the flight state at the last time step from the last Gensim simulation from the previous interval and the time for the control inputs file is updated so the control parameters at the initial time in the next Gensim simulation are the parameters at the actual time of the interval. This results in a time domain simulation where the feedback from the aerodynamics code is performed, and a schematic representation of the process is illustrated in Figure 3.4.

3.3.3. Main Assumptions and Limitations

The principal assumptions and limitations of the coupling can be summarised as follows:

- Inherent assumptions from UPM when it comes to aerodynamic modelling which were discussed in the previous section
- The induced velocities that are exchanged during the coupling are only transferred to the main rotor. This means that if not all components are modelled when running the aerodynamics simulation, the interactions will be modelled from the Gensim implementation which sometimes relies on the induced velocities from other helicopter components.
- The weak coupling can miss high-frequency oscillations which are higher than one main rotor revolution, so the helicopter controls provided by Gensim won't capture high-frequency inputs. This is because for

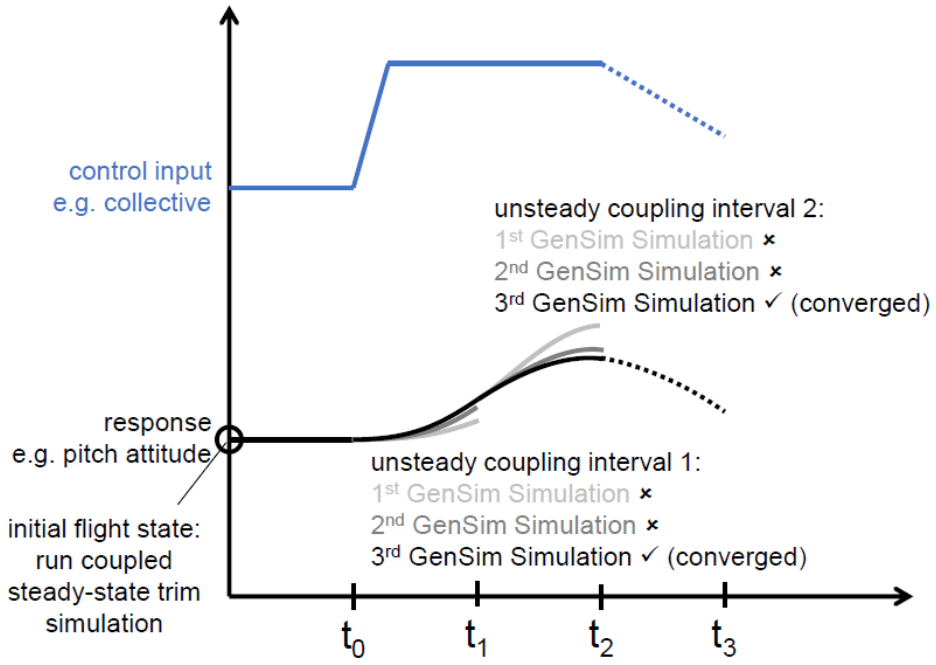

Figure 3.4: Time domain coupling process.

the weak coupling, the loads and induced velocities are averaged over one main rotor revolution, therefore, fluctuations happening within a main rotor revolution are missed. This is not the case if a tight coupling is done.

- The time domain simulations can be performed using one main rotor revolution time step as the lowest. This limitation is due to how Gensim is coded since a simulation in Gensim always starts with the first blade aligned with the tail boom.

3.4. Helicopter Model

The helicopter model used for the simulations is the BK117-C2, which was jointly developed and manufactured by Messerschmitt-Bölkow-Blohm (MBB), from Germany, and Kawasaki, from Japan. This helicopter is the old version of today's H145, in particular, it is the last version with a classical tail rotor. The most important aspects of the BK117-C2 rotor technical information are detailed in Table 3.1 and the technical drawings are illustrated in Figure 3.5. The BK117-C2 is chosen since it is a representative helicopter of its class with an open tail rotor.

The models that are used in Gensim and UPM are exactly the same except that the end plates are not modelled. The end plates are removed from the models since the results must be as generalised as possible, thus, the end plates of the BK117-C2 are very exceptional and could lead to very specific results for this particular helicopter. To avoid the computation of the end plates, in Gensim it is as simple as deactivating the component calculation. In UPM, the helicopter model of the BK117-C2 is simplified and only contains three main parts. The main rotor, the tail rotor and the other parts as a whole component that includes the fuselage, tail boom, horizontal stabilisers, vertical stabilisers and end plates. During the computation, the main rotor and tail rotor are modelled as lifting surfaces while the other components, englobed as a whole, are modelled as bluff bodies. Hence, since the end plates are only obstructing the flow field of potential flow and not creating any loads, they are expected to not influence the loads obtained at the rotor, which at the end of the day is the information transferred back to Gensim.

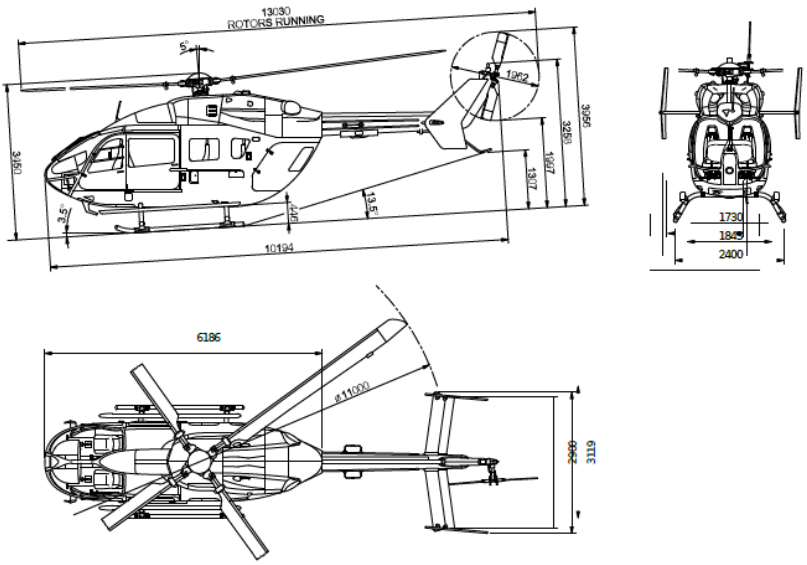

Figure 3.5: Technical drawing of the BK117-C2.

Source: Helicopters [22]

Table 3.1: Main rotor design parameters for the BK117-C2.

	Diameter	**Number of blades**	**Mean chord**	**Ratio of RPM**
Main Rotor	11 m	4	0.3235 m	-
Tail Rotor	1.962 m	2	0.2 m	5.658

During the thesis, two models are used in UPM, the normal BK117-C2 model which has been presented previously and the model used to investigate the tail rotor position lowered at the tail boom height. Both models consist of a blade discretisation for the main and tail rotors with structured panels whose density is higher towards the tips of the blade and the leading and trailing edges of the airfoils. The fuselage, tail boom, horizontal stabiliser, vertical stabiliser and end plates are also modelled with structured panels. The only difference between the original model and the modified model is that in the modified model, the tail rotor centre of rotation is moved 1.025 m down in the z-direction, closer to the tail boom. This is done both in Gensim and UPM. Additionally, for the modified model, the end plates are removed to avoid possible modifications of the flow field at the tail rotor since they are now quite close. The model's top view is shown in Figure 3.7 and the lateral viewpoint in Figure 3.8. As an additional verification, the effect of removing the end plates from the original configuration was tested with a 20 knot wind from an azimuth of -90º, which is the condition where the end plates could be affected the most. The results in Figure 3.6 show that it is not affecting the loads at the main and tail rotors.

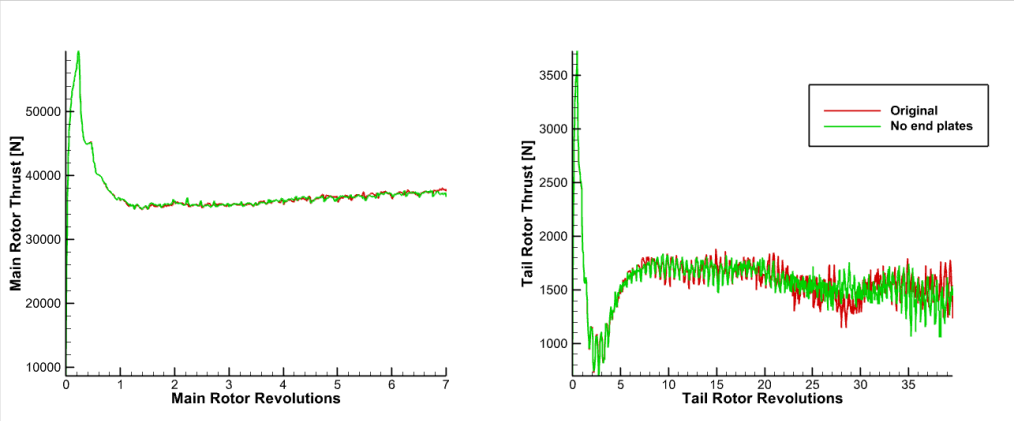

Figure 3.6: Main rotor and tail rotor thrust effect of not including the end-plates as bluff bodies. Wind speed of 20 knots and azimuth of -90º.

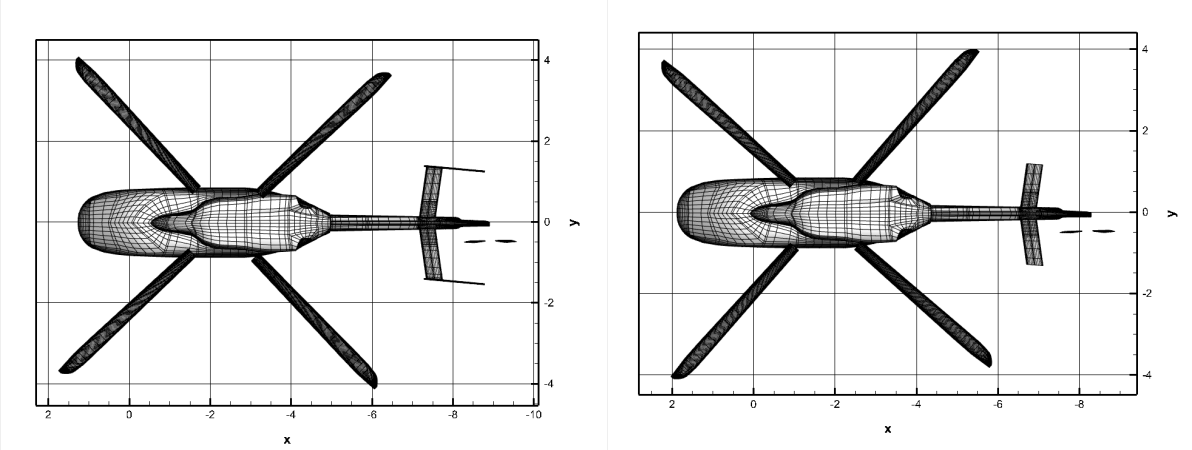

(a) Original model.

(b) Modified model.

Figure 3.7: Top view of the helicopter models used in UPM.

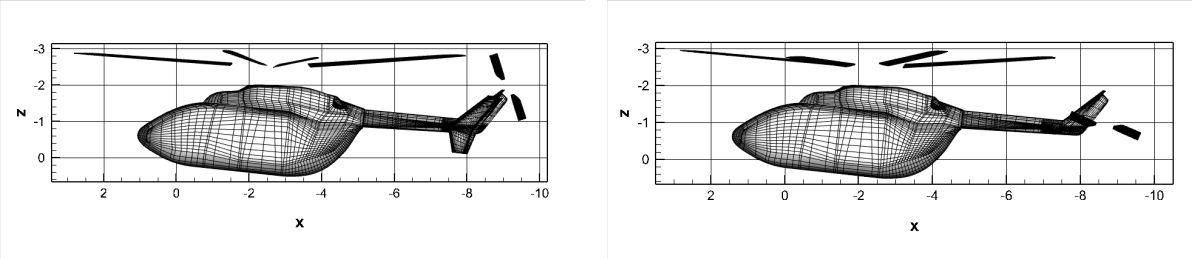

(a) Original model.

(b) Modified model.

Figure 3.8: Lateral view of the helicopter models used in UPM.

3.5. Verification of Level Flights

The verification is done for the helicopter model BK117-C2, presented in the previous section, based on data from the flight test. Since the last flight tests of the BK117-C2 were performed in the early 2000s, the data are more limited due to the lack of digital documentation, and only a few flight cases could be used. The parameters checked for verification will mainly be the main rotor torque, pitch attitude, roll attitude, collective angle on the main rotor, and the tail rotor collective angle. The coupled simulations for the verification are run in trim

configuration and for ten coupled iterations to guarantee acceptable convergence. In the UPM simulations, the simulation is run for seven main rotor revolutions with a time step of 3 degrees. The exact specifications of the UPM parameters are detailed in Table 3.2. Additionally, the compressibility correction is deactivated because it is a computation applied after finding the solution to the helicopter flow. Thus, the compressibility effect on the flow field is not considered, so the relation between the helicopter control and the flow physics is unrealistic. If one is only interested in the helicopter controls, then the compressibility and profile drag could be activated. Still, since this thesis is also about analysing the helicopter flow field and how it relates to the helicopter controls, it is deactivated. The flight conditions at which the helicopter is simulated are specified for the high-weight level flights in Table 3.3 and for low-weight level flights in Table 3.4.

Table 3.2: UPM simulation parameters.

Parameter	Value
Simulation duration	7 main rotor revolutions
Main rotor azimuth time step	3°
Tail rotor azimuth time step	16.974°
Main rotor vortex core radius for panels	5.76 cm
Tail rotor vortex core radius for panels	2.5 cm
Particles vortex core radius	5.76 cm
Particle split length	17 cm

Table 3.3: Flight conditions of the flight tests used for high weight simulations verification.

Flight Code	T.A.S [kts]	Rate of Descent [fpm]	Density Altitude [ft]	Weight [kg]
ft0016	41.800	-5.315	6007.600	3620.000
ft0036	34.200	60.630	5298.500	3572.000
ft0158	31.900	94.094	3251.700	3592.000
ft0158*	40.600	0.000	3287.800	3592.000
ft0158**	39.200	94.094	3287.800	3592.000
ft0235	33.500	21.754	5117.100	3612.000
ft0235*	33.400	6.246	5033.300	3612.000
ft0235**	42.900	-16.281	5074.400	3612.000
ft0235***	42.600	-15.789	4986.900	3612.000
ft0729	29.300	-63.955	5157.000	3454.000
ft0729*	42.500	-86.332	5113.500	3454.000

Table 3.4: Flight conditions of the flight tests used for low weight simulations verification.

Flight Code	T.A.S [kts]	Rate of Descent [fpm]	Density Altitude [ft]	Weight [kg]
ft0015	40.400	0.000	5903.400	2754.000
ft0017	40.300	-102.400	5329.500	2712.000
ft0019	41.800	-20.100	5699.000	2654.000
ft0154	33.300	-69.500	5817.100	2860.000
ft0154*	42.300	63.200	5887.600	2860.000
ft0154**	43.200	9.400	5893.300	2860.000

The results obtained from the high-weight level flights from flight test data are compared with the averaged results of the last 4 Gensim coupled iterations and illustrated in Figure 3.9. It is observed that the main rotor collective is similar for all flight tests considered with a minimum deviation of 0.432º and a maximum of 1.982º which can be attributed to the fact that the compressibility was deactivated, so the thrust for the same collective is less, which results into a higher collective over the coupled iterations. Additionally, the vortex core radius used in the particle solver can also have an effect since it will relate the induced flow field with the circulation from the blades. The tail rotor collective also presents similar results but with a higher variability between flight tests; the minimum deviation is 0.520º, and the maximum is 2.582º. These discrepancies can be attributed first to the same

factors as in the main rotor but added to the fact that the required tail rotor thrust might not be the same as in the flight test, whose data is unavailable since the main rotor torque from the simulations is different. Therefore, the difference in thrust is already a difference in the tail rotor collective. Moreover, the main rotor wake interaction also influences the tail rotor collective. The roll attitude is the variable presenting the most deviations between the coupled simulations and flight test with a minimum of 0.085º and a maximum of 1.384º. These differences are related to the low accuracy in the predicted roll moment from the main rotor and the difference in tail rotor thrust, which will need to be compensated with the roll attitude for a trimmed flight. The pitch attitude is more accurate and presents a minimum deviation of 0.464º and a maximum of 3.015º, which are mainly related to the pitch moment prediction from the main rotor and also affected by the drag prediction of the helicopter. Finally, the main rotor torque is observed to be very similar to the results from the flight test. These results are accepted considering that the computation of the main rotor torque from the flight tests carries a cumulative error due to the indirect measurement of this variable. The main rotor torque is measured from the total power computed from the two engines' torques and rotational speeds; then an estimation of the electrical power is subtracted from which afterwards the variable power losses from the transmission shaft and engine shaft are also subtracted to compute the torque with the main rotor rotational speed finally. Hence, the predicted main rotor torque from the flight test can present minor deviations due to the accuracy of the calculation. Nevertheless, the results from the coupled simulations show an overall lower main rotor torque prediction with a minimum deviation of 545.535 Nm and a maximum deviation of 3215.268 Nm, mainly attributable to the profile drag not computed in the simulations. Notice that the deviations from flight tests and the simulation results can also be affected scarcely by the not perfectly trimmed flight from the flight test since a pilot controls the helicopter. Overall, the results obtained from the coupled simulations are within the accuracy required for this thesis investigation.

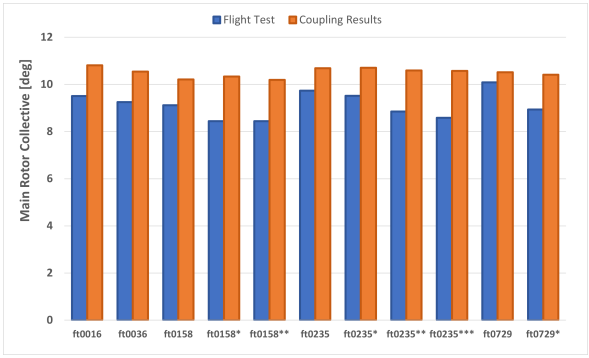

(a) Main rotor collective.

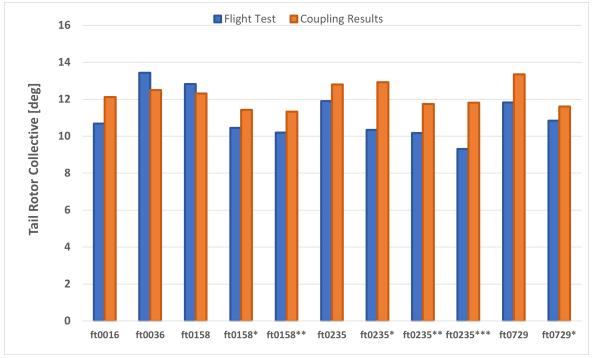

(b) Tail rotor collective.

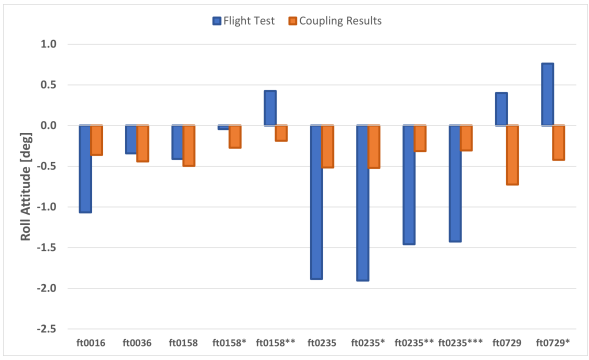

(c) Roll attitude.

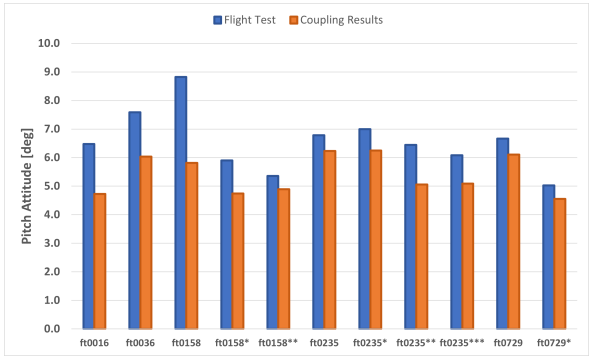

(d) Pitch attitude.

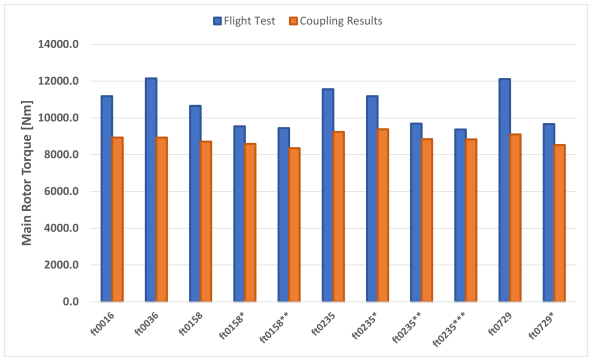

(e) Main rotor torque.

Figure 3.9: Coupling verification with flight test data for high-weight flights.

Low-weight flights are also verified to assess the accuracy of the numerical tool better. The results in Figure 3.10 show a minimum difference in the main rotor collective of 0.372º and a maximum of 1.495º, giving similar results between flight tests and numerical simulations. The tail rotor collective difference ranges from 0.232º to 4.465º, presenting higher variability between the flight tests. The roll attitude changes a minimum of 0.410º and a maximum of 1.711º, while the pitch attitude changes a minimum of 0.185º and a maximum of 2.464º. The main rotor torque has a minimum difference of 27.281 Nm and a maximum difference of 3680.082 Nm. Overall, the verification for low-weight flights shows that the accuracy is slightly better while still manifesting similar deviations for the same reasons.

(a) Main rotor collective.

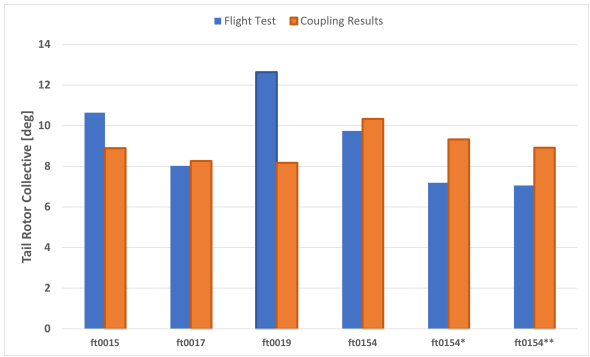

(b) Tail rotor collective.

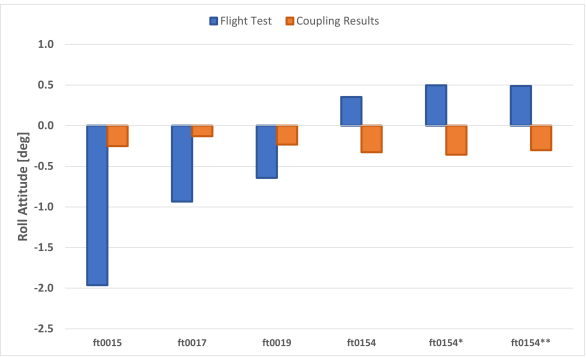

(c) Roll attitude.

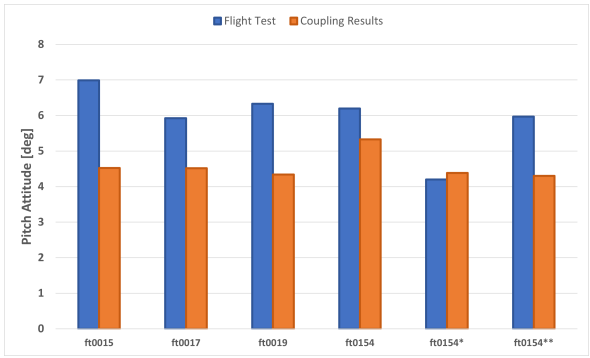

(d) Pitch attitude.

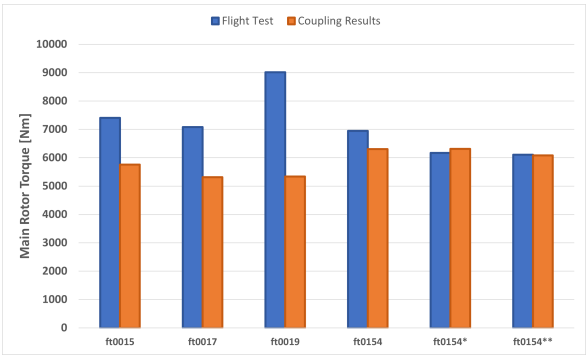

(e) Main rotor torque.

Figure 3.10: Coupling verification with flight test data for low-weight flights.

To summarise, the results for the verification demonstrate an acceptable level of accuracy suitable for the aims of this thesis investigation, where exceptionally high precision is not the primary requirement. Instead, the focus lies on accurately representing the flow physics in a feasible amount of time allowed with the panel method and particle solver formulation. It is worth noting that the available flight test data only covers level flights at velocities ranging from 30 to 40 knots, omitting verification of the helicopter's performance in sideward flights and direct validation of flow physics. However, the combination of the current verification, the standalone verification conducted at DLR for UPM, and insights from Airbus flight physics experts collectively instil sufficient confidence in the results to proceed with the investigation.

3.6. Research Approach

The flight mechanics code is coupled with an aerodynamics code to find answers to the research question. The reason for it is decided to use a coupling between a flight mechanics code, Gensim, and a panel method combined with a particle solver, UPM, which is considered to be a mid-fidelity tool and not a coupling with a higher fidelity code such as CFD is that panel method and particle method codes allow for lower simulation times. Although

they cannot predict skin friction loads at the lifting surfaces due to their formulation, their accuracy is considered high enough to investigate unintended yaw. Additionally, the BK117-C2 is used for the simulations since it is a helicopter representative of its class with an open tail rotor. This section explains the setup of the simulations, whose results are presented in the next chapter. The methodology followed is justified for each research question, and a small snippet of the expected output is mentioned.

RQ1: "Is there a flight condition that causes uncontrollable unintended yaw?"

To answer this question, we have decided to run trim flight simulations. This is because trim flights are the desired flight conditions when a pilot is flying a helicopter due to the equilibrium of forces and moments. Therefore, these simulations will allow us to know if the aircraft can maintain yaw trim, meaning that no flight configuration is causing the loss of the yaw trim without the ability of the pilot to stop it. Moreover, the trim simulation allows us to compare the results easily between different flight states as all of them are in equilibrium. From this simulation, it is also expected to know what tail rotor thrust is needed for trim and what tail rotor collective is required to create this thrust while checking if it is within the operational limits through the computation of the pedal position. Hence, if it is found that a case needs a pedal position close to the limit, it will indicate that the remaining range to manoeuvre is low and would pose a critical flight condition. The pedal position is computed directly from the tail rotor collective and its operational limits so that a 0% pedal position indicates the maximum left pedal and a 100% pedal position indicates a maximum right pedal. The simulations are to be run for all 360-degree freestream velocity azimuths and speeds from 10 knots to 30 knots, as these are possible wind gust speeds that the helicopter could experience in hover to some extent and are also the typical velocities for transition flights or low-speed flights, where is observed to appear most accidents classified as unintended yaw accidents. As discussed in the literature study, unintended yaw accidents occur most often on these kinds of flights, as confirmed by internal Airbus experts with experience in the industry. Following these results, the influence of other helicopter configurations is also evaluated.

For instance, to explore other tail rotor configurations, the tail rotor is moved down to the tail boom height, as is the case for many lightweight single-engine helicopters. The helicopter model used for these simulations is shown in Figure 3.7b and Figure 3.8b. For this configuration, the end plates of the model in UPM are removed to avoid possible relevant modifications of the flow field with the tail rotor freestream that could change the tail rotor performance. Note that for this modified configuration, it is assumed that the Gensim parameter, which accounts for the modified induced velocities at the vertical stabiliser due to the tail rotor suction, is the same. This configuration will also be simulated with trim flights and for the same range of velocities and wind azimuths as the original configuration of the BK117-C2. Therefore, it is expected to observe how having the tail rotor further away from the main rotor affects the results.

Another insightful simulation set-up that will be tested is to rotate the tail rotor in the opposite direction, top forward. This configuration is motivated since there are still helicopters flying with a top forward configuration, such as the old Bell UH-1 and the MD500. To achieve this, the tail rotor blade is rotated 180º around the spanwise axis so the leading edge is in front when rotating and mirrored to the tail rotor plane. Hence, the airfoil generates the loads in the correct orientation. This configuration will be simulated through trim flight simulations, and the same flight states will be tested in the original configuration. From these simulations, the interference from the main rotor wake is expected to be noted.

Trying to recreate typical helicopters with a low tail rotor location at the tail boom height, the disk loading of the main rotor was still representative of the BK117-C2, which is much higher than the usual helicopters with this type of configuration. Hence, trim simulations with the lower location of the tail boom will also be tested for a lower main rotor disk loading and all the same velocities and wind azimuths as was done for the original configuration. This is the closest configuration of such light-weight helicopters. However, the tail rotor sizing is still the same as the BK117-C2. Therefore, this will reduce the disk loading at the tail rotor since it can already be anticipated that the main rotor torque will be reduced. So, the expected outcome will be the influence of lower main rotor and tail rotor disk loadings on the trim capabilities of the modified helicopter.

RQ2: "Is a coupling between a flight mechanics code and an aerodynamics code needed to study unintended yaw?“

The answer to this research question is found by analysing the trimmed flight simulations obtained as a consequence of the first research question. In particular, a comparison is needed between a standalone Gensim simulation and a Gensim simulation that has received feedback from the aerodynamics code by exchanging differences in loads and induced velocities. This is achieved by comparing the first Gensim simulation in the coupled results (standalone Gensim simulation) and the last Gensim simulation, whose results are now affected by the results from UPM. The amount of main rotor torque, the needed anti-torque, the tail rotor collective for the original helicopter model and the pedal position are cross-checked to judge if the coupling workflow is required to study unintended yaw. Therefore, the expected outcome is a conclusion on whether the information from the aerodynamics code is necessary to perform an investigation on unintended yaw.

RQ3: "How do main rotor wake interactions and tail rotor vortex ring state affect tail rotor aerodynamics, and are they important for starting unintended yaw?"

The main rotor wake interactions and the possible appearance of a vortex ring state at the tail rotor need to be assessed for this research question. To do so, the tail rotor aerodynamics shall be addressed. This is done by partially reusing the simulations from the first research question. First, the yaw trim results can be used to analyse such phenomena by linking the relationship of the needed thrust with the collective causing this. Comparing the results for the tail rotor rotating in the opposite direction with the original configuration will also give a sense of the main rotor wake interactions. However, to study these interactions and rotor aerodynamics in detail, the UPM simulations from the coupled simulations shall be analysed by extracting the rotor loads and computing the flow field additionally. To compare the influence of specific changes in the helicopter configurations, such as tail rotor rotation or location, the same helicopter and blade motion must be compared so the results are strictly related to that change. Hence, it is expected that with the flow field solution and the rotor loads, the tail rotor vortex ring state and the main rotor wake interactions with the tail rotor can be quantified and addressed for the unintended yaw case.

RQ4: "How do the physical effects related to unintended yaw affect the handling characteristics?"

The methodology to answer the fourth research question will be to search for flight situations where the pilot would need to do higher workloads on the pedal or non-intuitive pedal positions during dynamic flights. The trim results are used as a reference to answer this question.

RQ5: "Is unintended yaw recoverable and what pilot control inputs are needed"

Time domain simulations are needed to analyse if it is possible to recover unintended yaw. Since a recovery method is a manoeuvre, the coupled time domain simulation set-up explained previously will give an understanding of such techniques. It was decided to perform a landing manoeuvre simulation since it was observed from accident analysis that this was one of the most frequent cases of unintended yaw accidents appearing when not in a hover or a slow flight.

Taking as reference the data from an actual accident in the German army, which was classified as an unintended yaw during an approach for landing, the initial flight state is considered similar, and the duration of the manoeuvre is similar to some of the pilot decisions. In Figure 3.11, an overall schematic is shown to understand the simulations' configurations. For instance, the simulation starts with a trimmed flight with 40 knots forward speed and a rate of descent of 200 feet per minute. The intention is to reduce the forward speed and the rate of descent. From this trim state, the simulation starts with 3 seconds, where the helicopter maintains the same flight state. Afterwards, the pitch is increased by around 10 degrees in 3 more seconds to reduce the forward speed. The helicopter is controlled by the autopilot from Gensim, which controls the heading with the tail rotor collective, the bank angle with the lateral cyclic, the pitch with the longitudinal cyclic and the vertical speed with the main rotor collective. When the simulation reaches 9 seconds from the start, the helicopter has approximately 27 knots forward speed and 128 feet per minute rate of descent. Here, the heading control is deactivated, simulating a pedal blockage, as was observed in real accident investigations where the pilot thought he had reached a maximum left pedal. This state is maintained until $t = 15.12\,s$.

Different scenarios are considered from this point, and other pilot decisions that worsen the loss of yaw control are simulated. A first scenario is considered where the same flight configuration is set until the helicopter reaches a yaw rate of around 100 deg/s. Then, a second scenario is also considered where the pilot increases the collective input by 20% during 6 seconds until $t = 21.12s$.

Finally, the recovery simulated in both scenarios will apply three magnitudes of left pedal input in 0.5 seconds. Also, two recovery techniques are tested for the scenario where the main rotor collective was increased. The first would be to apply the left pedal and decrease the main rotor collective back to the value at $t = 15.12s$ where the pilot manually changed it simultaneously. The second would be just to apply left pedal input while maintaining the main rotor collective. In the case of recovering the yaw rate to zero, the autopilot controls for the attitudes and a zero vertical speed are activated again. With these variations in the simulations, the effect of the magnitude of a left pedal input is assessed, and the help of decreasing the main rotor collective is also tackled.

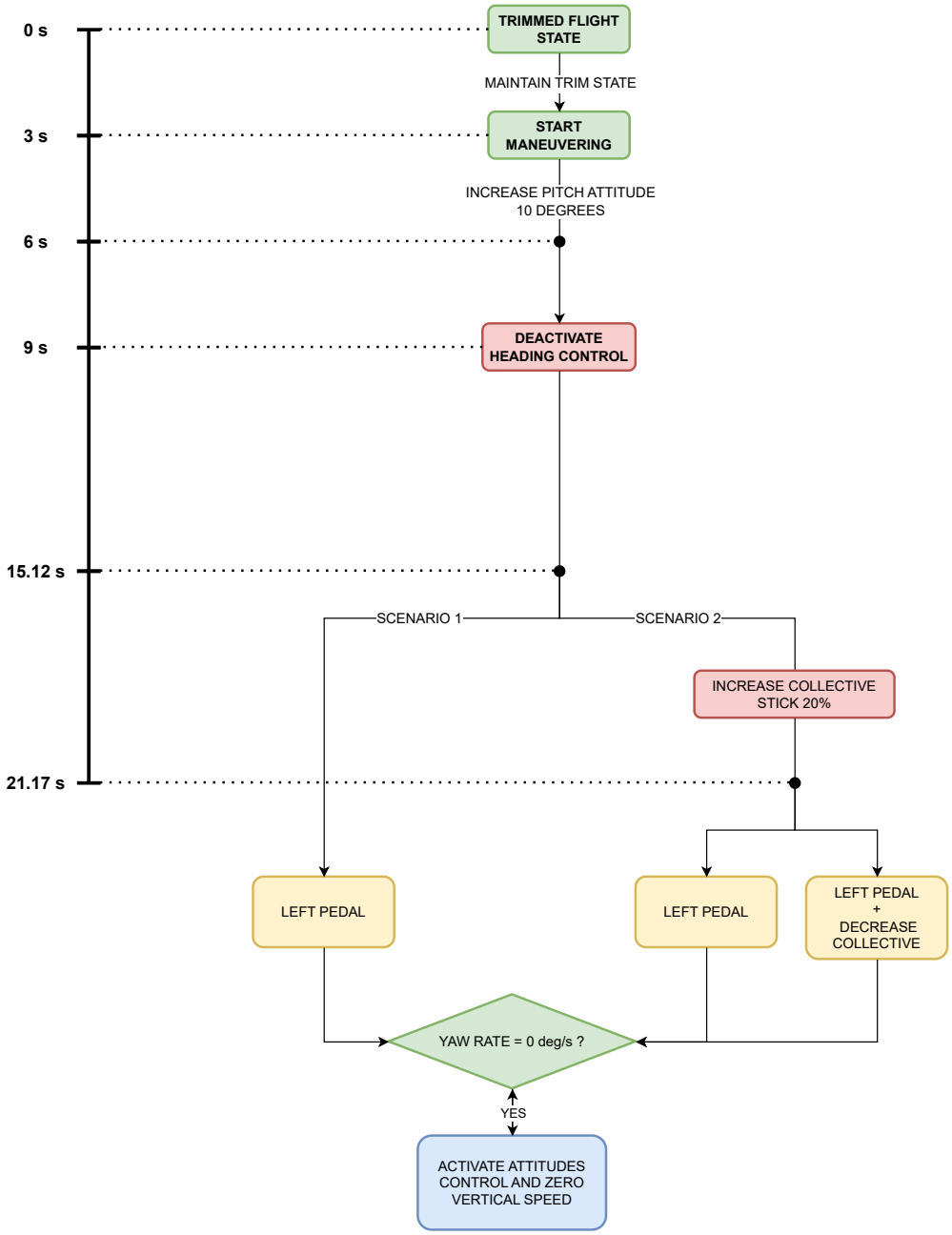

Figure 3.11: Flowchart of the approach for landing manoeuvre simulations.

3.6.1. Numerical Set Up

The approach followed to answer each research question is explained in the previous section. Now, the most important simulation parameters for UPM, Gensim, and the coupling used to obtain the results in each case are summarised.

The Gensim simulations need the geometry specified for the BK117-C2 and the polars for all aerodynamic surfaces. For trimmed flight simulations, the tolerances for the equilibrium are summarised in Table 3.5. These tolerances represent the limit from which the solver will stop to iterate and give the solution as converged. The time domain simulations also need specific inputs to be specified, such as the maximum rates or the limits for the

control inputs, shown in Table 3.6. Also, specific inputs need to be specified; the parameters are self-explanatory, but they limit the controls within the pilot's limitations in the real helicopter.

Table 3.5: Gensim simulation parameters for trimmed flights.

Load	Tolerance
Fx	25 N
Fy	25 N
Fz	50 N
Mx	25 Nm
My	50 Nm
Mz	50 Nm

Table 3.6: Gensim simulation parameters for time domain flights.

Control parameter	Value
Maximum rate of change of the collective control	23.42 deg/s
Maximum rate of change of the lateral cyclic control	35.0 deg/s
Maximum rate of change of the longitudinal cyclic control	35.0 deg/s
Maximum rate of change of the pedal control	90.0 deg/s
Maximum value of the collective control	21.2 deg
Minimum value of the collective control	3.8 deg
Maximum value of the lateral cyclic control	4.5 deg
Minimum value of the lateral cyclic control	-7.4 deg
Maximum value of the longitudinal cyclic control	6.6 deg
Minimum value of the longitudinal cyclic control	-13.3 deg
Maximum value of the pedal control	26.3 deg
Minimum value of the pedal control	-6.3 deg

After verifying the coupled simulations in the previous section for trimmed flights, the UPM simulation parameters that will be used are detailed in Table 3.2. To save computational time, in UPM simulations, the main rotor and the tail rotors are modelled as lifting surfaces, and all the rest of the components are modelled as bluff bodies. Thus, they do not create any wake; only the no penetration condition is imposed. This is justified due to the low-speed range of the simulations where the stabilisers don't play a critical role, which is also agreed upon by internal Airbus experts. The geometry used for all cases is the BK117-C2 model except for the variations in tail rotor configurations, which are custom configurations. Note that when the tail rotor is lowered to the tail boom height, the end plates of the model are removed.

The settings for the coupled simulations are more basic, and it is only information referring to the global flight case, i.e. the weight of the helicopter, the flying altitude and temperature, then, from the numerical perspective, the minimum number of coupling iterations that are run for every iteration are stated. The values are specified in Table 3.7. These values are decided based on the flight tests used to verify the coupling workflow and also agreed with the Airbus Helicopters experts to be a representative flight case close to the operational limits. The results for the coupling are generally taken as an average of the last four coupled Gensim simulations to have more relevant results. Additionally, the coupling convergence is assessed by computing the standard deviation of those previous four coupled iterations and checking for high standard deviation values, indicating high fluctuations during the last iterations and, hence, not converged solutions.

Table 3.7: Coupling workflow parameters.

Minimum number of coupled iterations	10
Helicopter weight	3620 kg
Helicopter weight for low disk loading	1900 kg
Pressure altitude	5248 ft
Density altitude	6000 ft
Outside Air Temperature	11.1 °C

4

Results

To find the operational conditions in which the helicopter could start an unintended yaw, the first approach is to run trimmed helicopter simulations to understand the helicopter demands to maintain yaw stability. Furthermore, these flights allow for a more clear description of the results as the incoming freestream velocity is well-known. However, in reality the helicopter almost never flies in a trimmed flight, i.e. there is not a zero net forces and moments balance, but very close to it. Therefore, manoeuvring simulations are also performed to account for non-trimmed flights and possible recovery methods. The simulation setup and the considerations proposed in the previous chapter are taken to perform the simulations presented in this chapter. For instance, the trimmed simulations to assess the required tail rotor capabilities to maintain yaw stability are first presented. These results include the required anti-torque, tail rotor thrust, collective angles, and pedal control input for different wind speeds and side-slip angles. This is followed by a comparison of the Gensim standalone results with the coupled Gesim with UPM simulation results. Afterwards, tail rotor loads and flow field explanations of the most interesting effects involving main rotor wake interactions and tail rotor vortex ring state are presented. Additionally, all the results are also assessed for other helicopter configurations and for other simulation setups to better understand the results. Following the results of the trimmed flights, the flight manoeuvres of potential unintended yaw accidents are presented together with the proposed recovery method and discussion of the results.

4.1. Trimmed Flights

Unintended yaw can occur when the thrust generated by the tail rotor is insufficient to provide enough anti-torque against the yaw moment exerted by the other helicopter components. Trimmed flight simulations are first run to find the flight regimes in which the helicopter might lose the yaw control. These simulations run for the original BK117-C2 helicopter configuration specified in chapter 3 for freestream velocities from 10 to 30 knots and 360-degree wind azimuths. First, the needed tail rotor thrust to maintain trim is investigated, followed by the analysis of the collective, which is causing this amount of thrust to assess the pedal limits. Finally, the results for other tail rotor configurations are presented.

4.1.1. Tail Rotor Thrust

The required tail rotor thrust for trimmed flights ranging from 10 to 30 knots and for all wind azimuths is displayed in Figure 4.1. These results represent the average over the last four Gensim coupled simulations, and one standard deviation is used as the error bar. Furthermore, the results are considered converged by checking both the evolution of the delta loads and observing a low value of the standard deviation. The required thrust results from the amount of anti-torque needed to compensate for the yaw moments exerted by the other helicopter components to find the equilibrium and fly trimmed, which is the most significant main rotor torque. From Figure 4.1, it is already observed that a trimmed solution is found for all wind azimuths and velocities where the positive wind azimuths present an increase of tail rotor thrust demand with the freestream velocity. On the other hand, for the negative

wind azimuths, the tail rotor thrust demands decrease with the freestream velocity, and the shape is flattened as a function of the wind azimuth. Now, to evaluate the dependency of the tail rotor thrust on the wind azimuth, let's assume that the helicopter is starting from 180-degree wind azimuth; if the helicopter begins to turn the nose to the left due to pedal input, this means that the wind is coming from the negative wind azimuths. Therefore, the demands of tail rotor thrust will start to reduce and then increase slowly until around -45° wind azimuth, where the needed tail rotor thrust rises more rapidly with the wind azimuth. For the 30 knots curve, the needs in tail rotor thrust increase locally at -90° azimuth. Moving toward positive wind azimuths, the needed tail rotor thrust increases steeply until around 90° wind azimuth, where it also starts to decrease very fast to the initial 180-degree wind azimuth. Therefore, it is observed that the wind azimuth has a significant impact on the tail rotor thrust demands. The dependency on the wind velocity amplifies the curve's amplitude while slightly reducing the average needed tail rotor thrust overall wind azimuths.

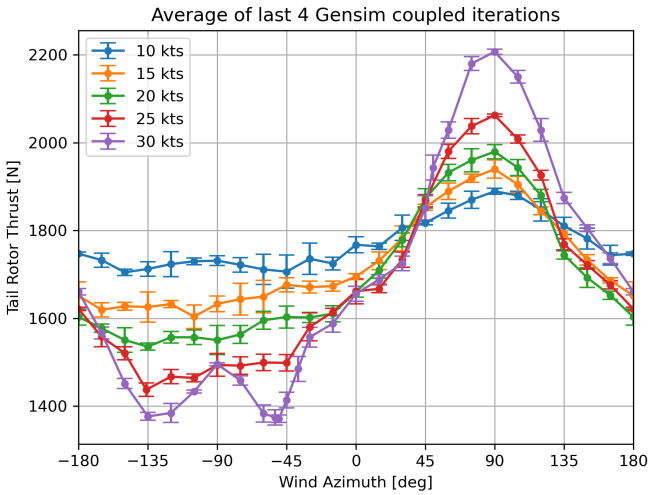

Figure 4.1: Tail rotor thrust required to maintain trim. The error bar is one standard deviation over the last four coupled Gensim simulations.

To understand the needs in tail rotor thrust, the anti-torque created can be checked since it is the primary function of the tail rotor. To do so, the average over four Gensim coupled simulations is taken and used as an error bar one standard deviation. Then, the yaw moments concerning the helicopter frame exerted by each helicopter component are split. For instance, the results for 10 and 15 knots are displayed in Figure 4.2. Notice that since the z-axis is pointing downwards, a positive z-moment represents a right yaw. It is observed that the main contributor is the generation of positive yaw moment, as it is a counterclockwise rotating helicopter. The relative differences in the values for the main rotor yaw moments concerning the wind azimuth are difficult to appreciate since the helicopter speeds are low. However, it was noticed that the main rotor's torque was higher for the negative wind azimuths. The second most important contributor to the yaw moments is the vertical stabiliser, which creates a positive yaw moment at a zero wind azimuth, increases for positive wind azimuths and decreases for negative wind azimuths. The fuselage is the third contributing to positive yaw moments, which creates almost no moment for a zero wind azimuth. Similarly to the vertical stabiliser, increase the moment for positive wind azimuths and decrease for negative wind azimuths. The least contributing component is the horizontal stabiliser, which does not create any noticeable yaw moment, as expected. Since the horizontal stabiliser is oriented, the wing creates lift in the z-direction. Thus, it is barely creating any moment concerning this axis. Finally, the amount of anti-torque will be a yaw moment equal to the negative sum of all the helicopter yaw components to achieve a trim state.

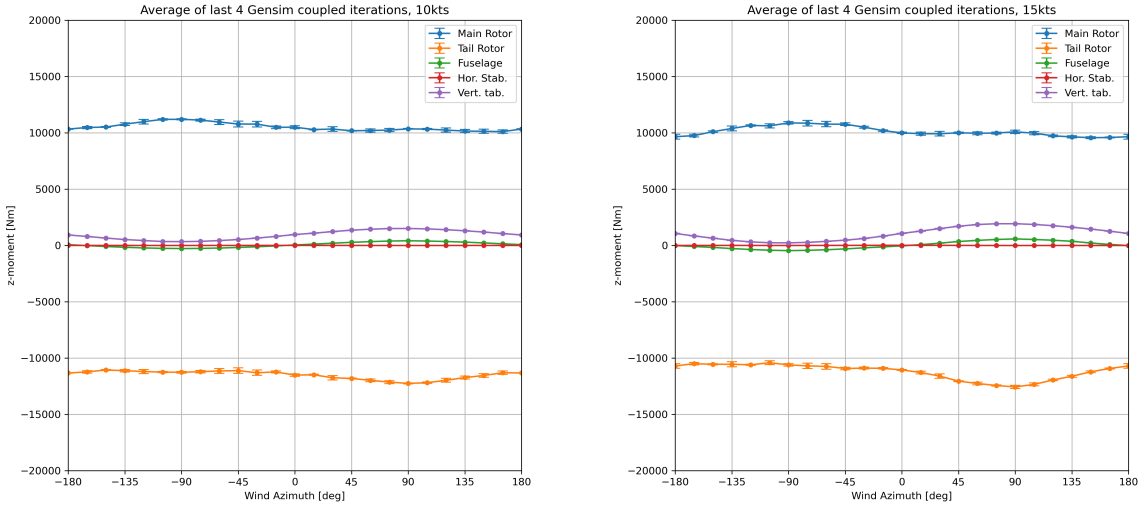

(a) Yaw moments for 10 knots.

(b) Yaw moments for 15 knots.

Figure 4.2: Yaw moments averaged over the last four Gensim coupled iterations and one standard deviation taken as error bar.

When the freestream velocity increases, the relative effects become more apparent, as illustrated in Figure 4.3. It can be observed that the main rotor torque shows two wind azimuth regions with increased torque demands. A more pronounced increase is around -90 degrees wind azimuth, and a less prominent increase is at 90 degrees wind azimuth. To understand why the main rotor torque demands behave like this, the helicopter attitudes and the main rotor torque and thrust are revised to explain the increase in main rotor torque. The roll attitude for the last Gensim coupled iterations is illustrated in Figure 4.4a, and the main rotor torque from the rotor fixed reference system averaged over the previous UPM iterations is shown in Figure 4.4b. As expected, the main rotor torque from the rotor fixed reference system follows a similar trend to the one observed for the yaw moment exerted by the main rotor from the helicopter reference frame illustrated previously in Figure 4.2 and Figure 4.3. The explanation for this trend can be better understood if the roll attitude in Figure 4.4a is checked. It is seen that the roll angle of the main rotor decreases when the helicopter is moving to the left to create a thrust component towards that side that compensates for the helicopter drag and the tail rotor thrust, which is directed to the right-hand side. Thus, the main rotor will need to generate more thrust in this direction, meaning that the collective and torque are increased. Towards the other side, the roll angle is higher to point the thrust vector towards the right and compensate for the helicopter drag; however, in this case, the tail rotor thrust also contributes to this thrust component, which results in a not-so-high main rotor torque.

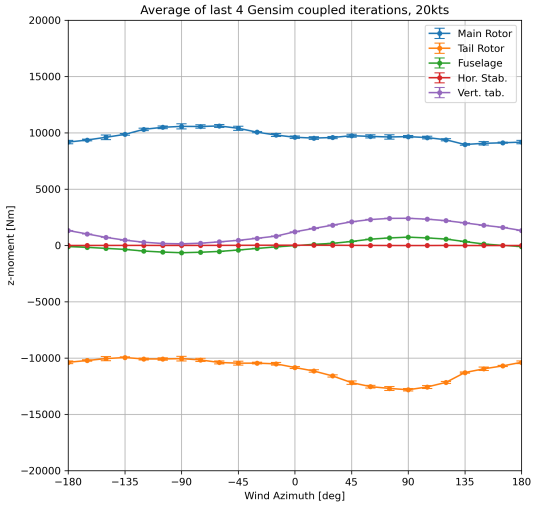

(a) Yaw moments for 20 knots.

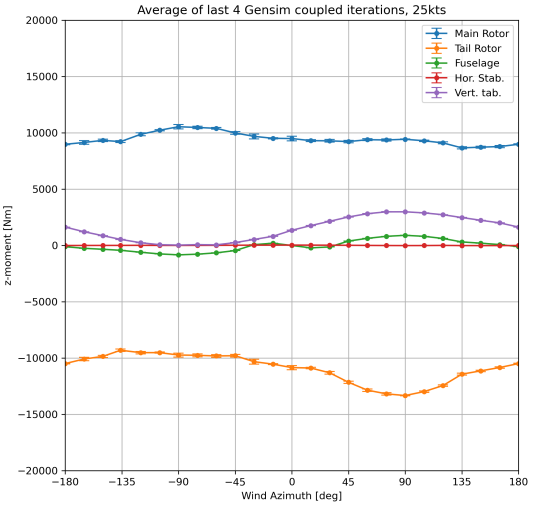

(b) Yaw moments for 25 knots.

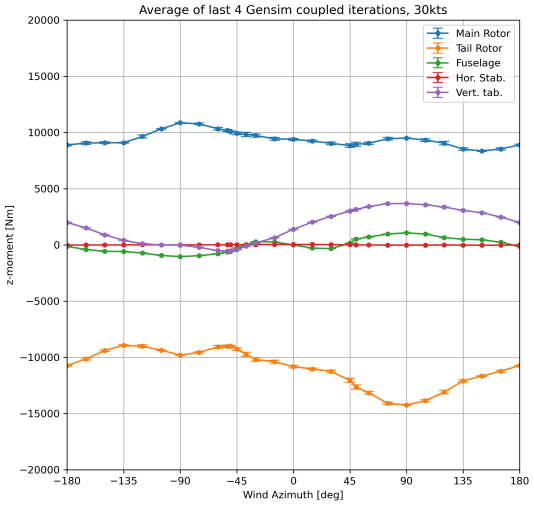

(c) Yaw moments for 30 knots.

Figure 4.3: Yaw moments averaged over the last four Gensim coupled iterations and one standard deviation taken as error bar.

The main rotor torque demands are understood now, and the vertical stabiliser loads will be analysed. For a forward flight, the vertical stabiliser creates a positive z-moment, requiring the tail rotor to produce more thrust. This occurs because of how the vertical stabiliser loads are computed in Gensim. The forces created by the aerodynamic surfaces are calculated by considering the velocity magnitude that the component sees, the sideslip angle and the angle of attack. Then, these values are used to retrieve the loads from a 3D polar of the element that is provided as input in Genism. The critical factor is, therefore, to compute these three components of the velocity seen by the vertical stabiliser. In Gensim, the freestream velocity is added to an induced velocity caused by the tail rotor operating near the fin to compute such velocity. This induced velocity is calculated as a factor of the tail rotor thrust. Although this is a simple model, the accuracy is considered enough for the thesis's purposes. Additionally, a more complex methodology has been shown in the previous chapter, where this model was tried to be improved. Still, it was unused due to time constraints and no significant improvement. When the helicopter is translating at a higher velocity, the yaw moment created by the vertical stabiliser increases, but only for somewhat positive wind azimuths. In contrast, for negative wind azimuths, it decreases to almost zero moments. There is a small exception for 30-knot winds and slightly negative wind azimuths where the vertical stabiliser creates some

anti-torque. This low yaw moment created by the fin is due to the freestream velocity opposing the tail rotor flow direction, which Gensim adds up and creates a dynamic pressure close to zero. Hence, the vertical stabiliser did not contribute significantly to creating an anti-torque for these azimuths.

The fuselage loads are also calculated from 3D polars in Gensim; therefore, the velocity magnitude, sideslip and angle of attack angles must be computed from a model. This model considers the freestream velocity added to the main rotor induced velocities seen by the fuselage in terms of a correction factor. Overall, the yaw moment created by the fuselage is zero for a forward flight independently of the wind velocity. This moment increases for positive wind azimuths and decreases for negative azimuths since the polar gives the local moment contributions of each pressure and friction force around the fuselage concerning the centre of gravity. However, its contribution to the overall required anti-torque by the tail rotor is low. Finally, the horizontal stabiliser does not create any yaw moment since the airfoil creates aerodynamic forces in a plane parallel to the z-axis.

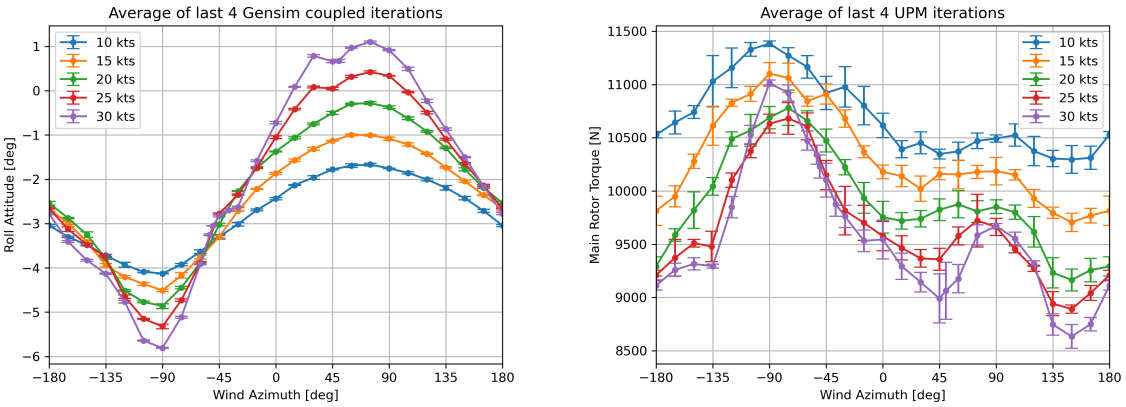

(a) Roll attitude for several wind velocities from Gensim results.

(b) Main rotor torque from UPM results.

Figure 4.4: Roll and main rotor torque. Results are averaged for the last four coupled iterations, and one standard deviation is taken as an error bar.

The needed tail rotor thrust showed previously in Figure 4.1 is now understood. The flat trend of tail rotor thrust over the negative wind azimuths around -90 wind azimuths is a consequence of the compensation of increased main rotor torque with the decrease in vertical stabiliser and fuselage yaw moments. However, this compensation is not more effective for 30 knots, where the increase in main rotor torque is higher than the increase in anti-torque from the vertical stabiliser, creating a small region with relatively higher needed tail rotor thrust. Instead, when the helicopter starts to increase the wind azimuth by yawing, the vertical stabiliser is not affected so much by the tail rotor thrust; therefore, the increase in yaw moment from the vertical stabiliser is added to the slight increase in torque from the main rotor and the rise in yaw moment from the fuselage which results in a significant increase in needed tail rotor thrust by reaching its maximum at a 90-degree wind azimuth. After this point, the tail rotor thrust decreases because of the decrease in the fin and fuselage yaw moments and the decrease in main rotor torque until it reaches a sufficient negative wind azimuth again so the moments from the fin are not decreasing so rapidly and the tail rotor thrust is constant over some wind azimuths.

4.1.2. Tail Rotor Collective

So far, it is observed that a trim state for the helicopter has been found for all the wind velocities and wind azimuths. To generate this amount of tail rotor thrust, a certain collective angle of the tail rotor blades is needed where the rotor aerodynamics gives the relation between the collective and its respective thrust. Since the tail rotor collective is controlled by the pedal position from the cockpit, the needed collective might be outside of the pedal limits, so it wouldn't be possible to find a trim. Therefore, the tail rotor collective, which creates the required thrust, is investigated.

The tail rotor collective needed for trim is illustrated in Figure 4.5 for the range of velocities and wind azimuths together with the corresponding needed tail rotor thrust again for argumentation purposes. First, focusing on the

positive wind azimuths in Figure 4.5b, the relation between the tail rotor thrust and the collective is proportional since a higher collective creates a higher rotor thrust for all wind velocities. This is because, under normal flow field conditions, a rotor in hover or with an axial velocity component going towards the wake direction creates more thrust the higher the pitch collective since the local angle of attack of the blades is increased even though the increase in thrust means that the axial-induced velocities also increase, whose effect is compensated. The impact of expanding the freestream velocity in these positive wind azimuths is to improve the tail rotor collective to generate the same thrust as the local angle of attack is reduced due to the higher freestream axial velocity and axial induced velocity caused by higher disk loading. Although this argumentation is for an idyllic case where the freestream velocity is perpendicular to the rotor, the results in Figure 4.5 for a wind azimuth of 90 degrees where the helicopter has a slight roll angle, as observed in Figure 4.4a, can be taken as an example of such effect. The rest of the positive wind azimuths also present a similar trend. Still, they become more affected by the sideslip angle, and the low positive wind azimuths start to be interfered with by the main rotor wake interacting with the tail rotor.

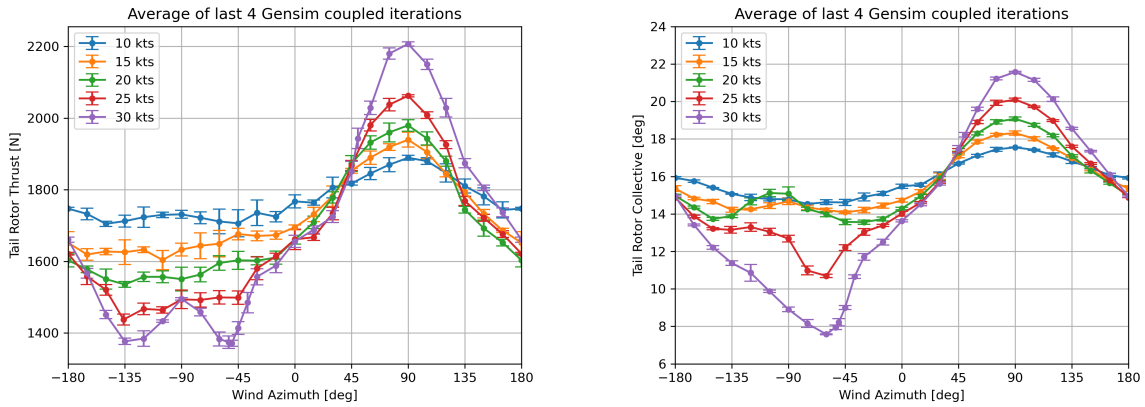

(a) Tail rotor thrust.

(b) Tail rotor collective.

Figure 4.5: Tail rotor thrust and corresponding collective. Averaged over the last four coupled Gensim simulations, the error bar is one standard deviation.

For negative wind azimuths, the freestream velocity starts to gain an axial velocity component which opposes the wake direction. For general rotor operating conditions, the decrease in freestream axial velocity increases the effective local angle of attack of the blade section, which increases thrust. This is the case for the wind azimuths close to 0 or -180 degrees since the freestream velocity component perpendicular to the rotor is low enough. For instance, for a wind azimuth of -15 and -30 degrees and a velocity of 25 and 30 knots in Figure 4.5, the tail rotor thrust is almost the same as it is the helicopter roll angle from Figure 4.4a. At the same time, the collective is much lower for a higher velocity. A similar case appears for wind azimuths of -165 degrees.

The tail rotor collective for the flights with wind azimuths around -90 degrees needs to be more intuitive to understand. Considering the velocities from 10 to 20 knots at a wind azimuth of -90 degrees, it is observed that for almost the same tail rotor collective and roll attitude, the higher the velocity, the lower the thrust created by the tail rotor. This is counterintuitive since it was expected that an increase of the velocity against the rotor wake, if the collective is fixed, would lead to a higher integrated thrust due to a lower inflow that leads to a higher effective angle of attack on the blades. Since a dampening effect seems to appear, it is already suspected that a vortex ring state is appearing at the tail rotor plane. From the literature, it is known that the vortex ring state on the main rotor reduced the rotor thrust due to the organised recirculation of the tip vortices from the blades, which are reinjected, creating an increased inflow that reduces the effective angle of attack, especially around the tip of the blades. This can also appear for the tail rotor but can be more dependent on the helicopter's attitude. For example, such reduction in thrust is also observed for the thrust trim curve at 25 knots, where the needed thrust from -45 to -135 degrees is very similar and slowly decreasing; however, the collective experiences a sudden decrease followed by a rapid increase afterwards due to this loss in thrust. Note that the effect is not so significant for higher velocities since some smaller recirculation lies above the rotor, which has a lower influence on the rotor inflow. A detailed analysis of these effects will be carried out in the following sections; however, the current results show that a vortex ring state can appear.

4.1.3. Different Helicopter Configurations

Several modifications were performed to the BK117-C2 model as specified in chapter 3 to make the results more widely applied over other helicopter configurations. The same results presented for the original configuration are now analysed for different tail rotor configurations, which include the tail rotor rotating top-forward, meaning that the blade is moving forward when is at the top of the rotation, the tail rotor located at a lower height, at the tail boom height, and a low main rotor disk loading with the lower height tail rotor location.

4.1.3.1. Tail Rotor Top Forward

The required thrust and the corresponding tail rotor collective for the tail rotor rotating top forward are illustrated in Figure 4.6. The required thrust seen in Figure 4.6a is almost the same as for the original tail rotor configuration seen in Figure 4.5a, the slight differences appear due to the small change in performance of the tail rotor which also influences the trim state. The collective which is causing this thrust illustrated in Figure 4.6b also presents a similar behaviour to the original configuration observed in Figure 4.5b, where the positive wind azimuths behave in a proportional trend with the required thrust while the negative wind azimuths present regions with an inverse proportion between the thrust and the collective. There are two ways to observe this phenomenon; the first would be to observe that similar collectives are needed for a wind azimuth of -90 degrees, where the freestream velocity is against the tail rotor wake direction. At the same time, the thrust generated is reduced for higher velocities. This wouldn't be the case for a standard operating rotor, as the inflow reduction would increase the effective angle of attack of each blade station and the thrust. Another way of checking this effect is to follow the collective trim curve for the velocities of 20 and 25 knots, for example, and observe that the collective increases for more negative wind azimuths. At the same time, the thrust of the tail rotor decreases slightly. Therefore, this can be associated with a recirculation forming around the tail rotor plane called a vortex ring state.

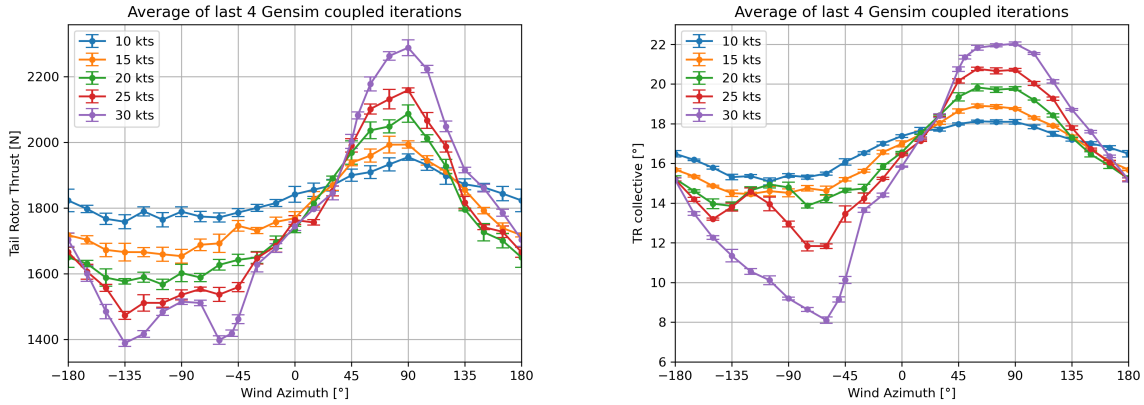

(a) Tail rotor thrust.

(b) Tail rotor collective.

Figure 4.6: Tail rotor thrust and corresponding collective for the tail rotor rotating top forward. Averaged over the last four coupled Gensim simulations, the error bar is one standard deviation.

The effect of rotating the tail rotor in the opposite direction of the original tail rotor configuration must be studied by comparing the tail rotor collective needed to maintain the trim state for each configuration. Although the required tail rotor thrust for trim observed in Figure 4.6a is slightly different than in Figure 4.5a, the comparison is still fair since the differences in thrust are negligible. In Figure 4.7, the tail rotor collectives are compared for 10 and 15 knots. The first observation is that the two curves are very similar for wind azimuths, which are closer to the 180 wind azimuth, i.e. the helicopter is flying backwards. Instead, the flights with a wind azimuth closer to 0 degrees are more affected. In particular, the required collective for the trim increases for the top forward configuration while creating the same amount of thrust as the top aft configuration.

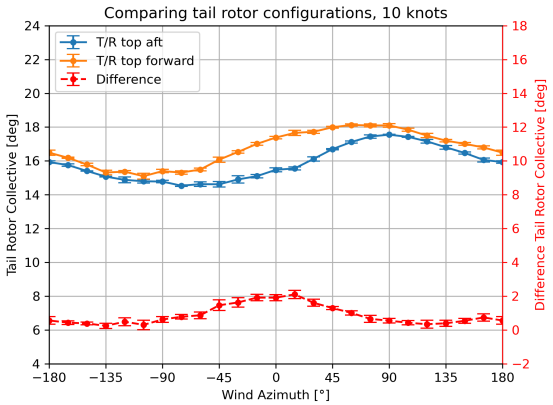

(a) Tail rotor collectives for 10 knots flights.

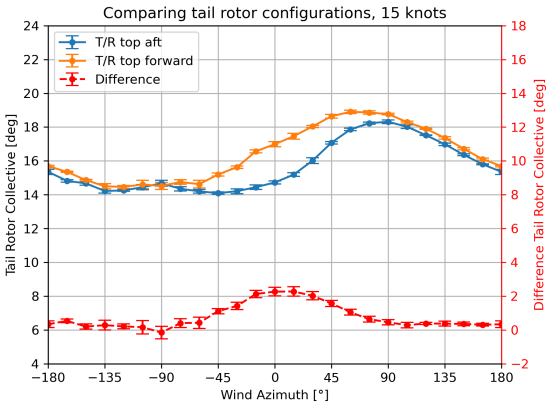

(b) Tail rotor collectives for 15 knots flights.

Figure 4.7: Tail rotor collective for the top aft configuration compared to the top forward configuration. The difference is shown in the secondary axis. The average over the last four coupled Gensim simulations and error bar is one standard deviation.

For even higher velocities, the required collective is compared in Figure 4.8. It is observed that the affected region remains smaller for these velocities. However, it is observed that the affected wind azimuths are not equally affected. Instead, it is always noticed that the 45-degree wind azimuth is the most affected. For instance, there is a sudden increase in interference when moving to a 45-degree wind azimuth from a higher wind azimuth. If the wind azimuth is further decreased, the interference slowly decreases. Additionally, it is observed that when flying at a speed of 25 knots, the wind azimuths between -90 and -135 degrees are also affected. The results for velocities from 10 to 30 knots already show that there is a dependency on the rotation direction for wind azimuths close to the forward flight; since the only change was the rotation direction of the tail rotor, this effect can be related to an interaction of the main rotor wake with the tail rotor. This interference is studied in more detail in the following sections.

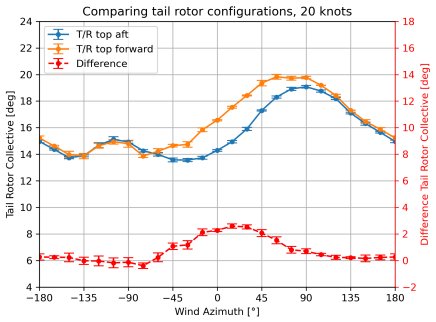

(a) Tail rotor collectives for 20 knots flights.

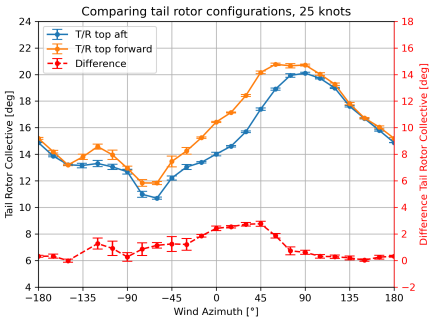

(b) Tail rotor collectives for 25 knots flights.

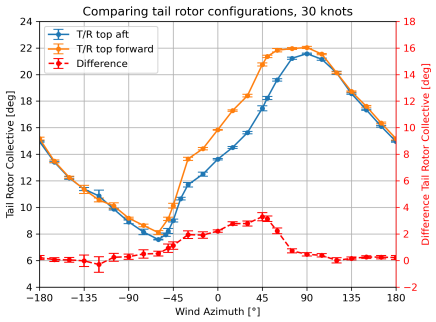

(c) Tail rotor collectives for 30 knots flights.

Figure 4.8: Tail rotor collective for the top aft configuration compared to the top forward configuration. The difference is shown in the secondary axis. The average over the last four coupled Gensim simulations and error bar is one standard deviation.

4.1.3.2. Tail Rotor at Tail Boom Height

Shifting the tail rotor downwards at the tail boom height gives the results for the required tail rotor thrust and the tail rotor collective to maintain trim as shown in Figure 4.9. As in the tail rotor rotating top forward, in this case, the required thrust by the tail rotor, seen in Figure 4.9a, is almost identical to the required thrust from the original tail rotor configuration in Figure 4.5a. This is expected since there is practically no effect on the other simulated aerodynamics code components by lowering the tail rotor location. The roll attitude is most affected since a lower tail rotor location is changing the roll moment, which will need to be compensated by the roll attitude of the helicopter. This can be confirmed if the helicopter's roll attitude from the original tail rotor configuration in Figure 4.4a is compared with the roll attitude for the lower tail rotor position in Figure 4.9c. The collective for the positive wind azimuths and this tail rotor configuration behave similarly as observed in the two previous cases. However, for the negative wind azimuths, the required collective differs in some aspects from the original tail rotor configuration. For instance, it is observed that a change in the slope of the collective trim curve appears for all freestream velocities and occurs around a wind azimuth of -90 degrees. At the same time, the maximum is reached for wind azimuths that are slightly more negative than -90. In the original tail rotor configuration, this was observed to appear clearly at speeds close to 20 knots and was vanishing for higher speeds. Therefore, by lowering the tail rotor location, the recirculation around the tail rotor plane due to the re-ingestion of the wake still appears at higher velocities.

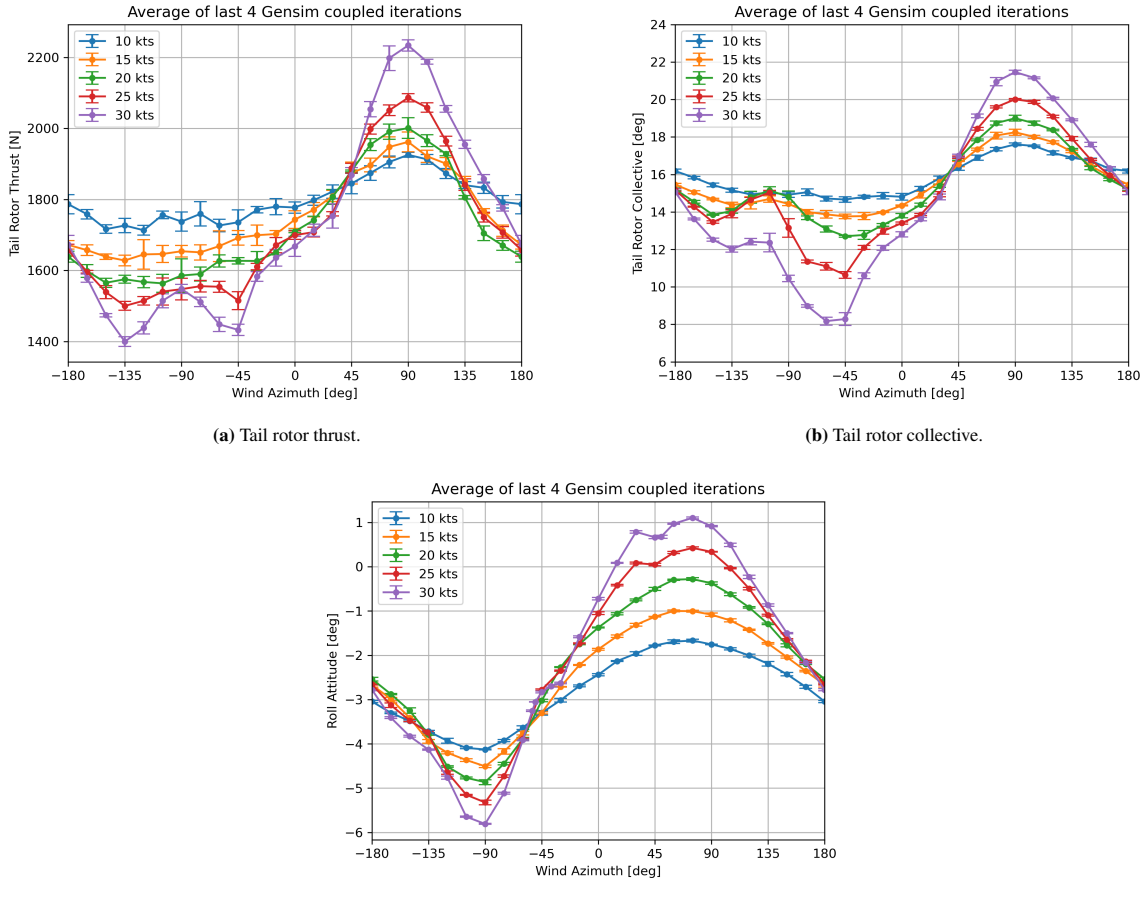

(a) Tail rotor thrust.

(b) Tail rotor collective.

(c) Roll attitude.

Figure 4.9: Tail rotor thrust, the corresponding collective and the helicopter's roll attitude for the tail rotor at tail boom height. The average over the last four coupled Gensim simulations and error bar is one standard deviation.

Comparing the trim curve for the needed collective of the original case with the tail rotor at the tail boom height case for each velocity gives the results shown in Figure 4.10 and Figure 4.11. Focusing first on the lower velocities illustrated in Figure 4.10, the required tail rotor collective for the lower tail rotor position is observed to

be almost identical to the original case. The minor deviations are due to the small changes in roll attitude, causing the tail rotor to operate in a slightly different orientation. However, the deviations are small enough to assume that no difference with the original helicopter configuration exists at 10 and 15 knots.

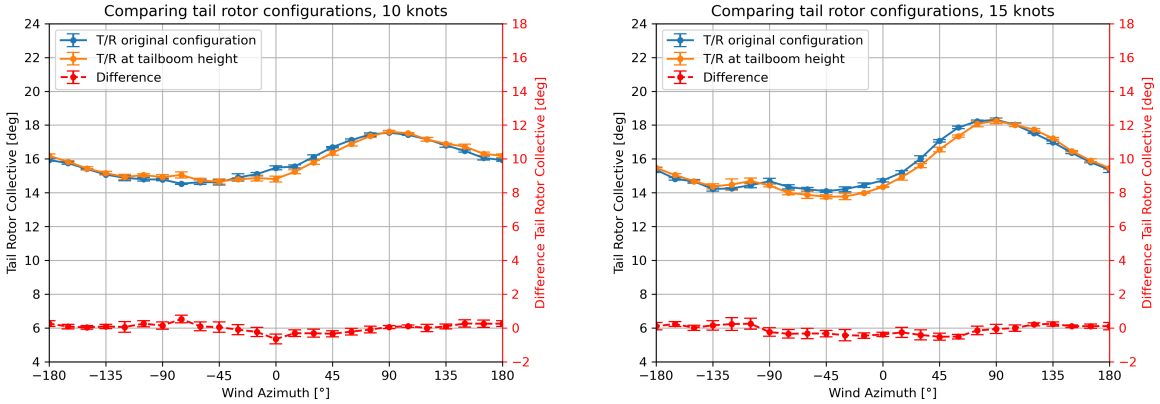

(a) Tail rotor collectives for 10 knots flights.

(b) Tail rotor collectives for 15 knots flights.

Figure 4.10: Tail rotor collective for the top aft configuration compared to the top forward configuration. The difference is shown in the secondary axis. Averaged over the last four coupled Gensim simulations, the error bar is one standard deviation.

The comparison of the tail rotor collective between the original helicopter configuration and the lower tail rotor location for higher velocities of 20, 25 and 30 knots is shown in Figure 4.11 for all wind azimuths. The first observation is that at 20 knots, the most significant difference occurs at a wind azimuth of around -45 degrees, where the lower tail rotor location configuration requires less collective to maintain the trim. This can be explained by the lower tail rotor thrust needed for the trim state due to the different roll attitudes. For 25 and 30 knots, these minor deviations are observed around the wind azimuths from -45 to 45 degrees. However, more significant differences in the collective compared with the original configuration are observed around the -90-degree wind azimuth for 25 and 30 knots. As discussed before, if the thrust is also brought into the discussion, these deviations indicate that a re-circulation around the tail rotor plane is happening when the tail rotor location is at a lower height, which reduces the tail rotor thrust and needs to be compensated with a higher collective. The hypothesis is that placing the tail rotor at a lower location less interferes with the main rotor, so the vortex ring gains strength for accumulating vorticity around the rotor. Hence, this state persists until larger freestream velocities are strong enough to interfere with the rotor inflow. This effect is studied in more detail in the following sections.

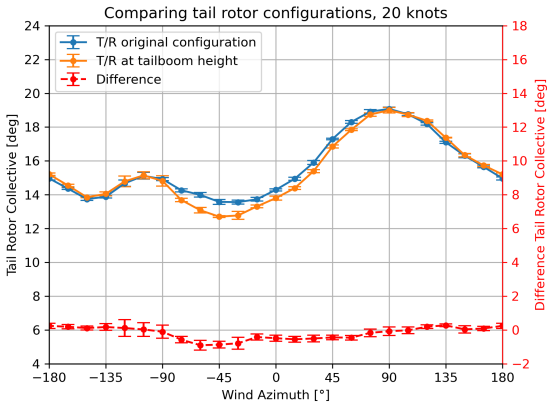

(a) Tail rotor collectives for 20 knots flights.

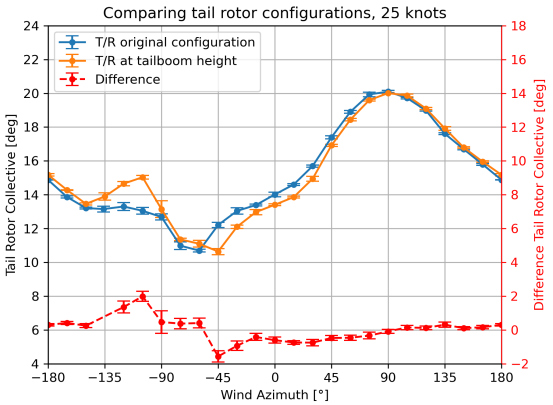

(b) Tail rotor collectives for 25 knots flights.

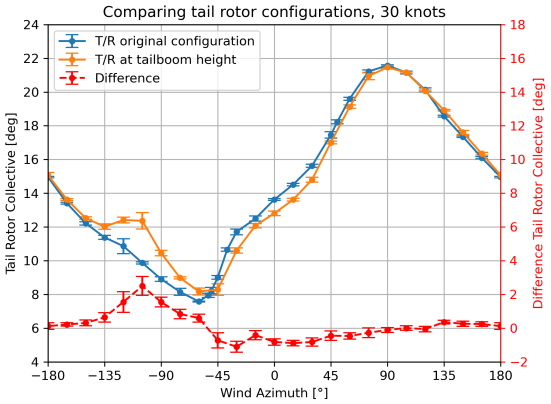

(c) Tail rotor collectives for 30 knots flights.

Figure 4.11: Tail rotor collective for the top aft configuration compared to the top forward configuration. The difference is shown in the secondary axis. The average over the last four coupled Gensim simulations and error bar is one standard deviation.

4.1.3.3. Low Main Rotor Disk Loading

The following investigated helicopter configuration was the lowered main rotor disk loading. This case aims to evaluate the influence of a lightweight helicopter with a tail rotor located at the tail boom height, as is usually the case for such helicopter types. Nevertheless, note that only the main rotor disk loading is equivalent to such helicopters; the tail rotor disk loading is lower than it is in these helicopters since the tail rotor size was not modified.

The required tail rotor thrust and tail rotor collectives for the freestream velocities from 10 to 30 knots and all wind azimuths are illustrated in Figure 4.12. Since the main rotor disk loading is lower for this case, the main rotor torque is also lowered, causing the tail rotor thrust required for trim to be lower, as observed in Figure 4.12a. The required thrust is almost half of the needed for the higher disk loading, and the tail rotor moved at the tail boom height presented in Figure 4.9a. Focusing now on the tail rotor collective shown in Figure 4.12b, it is observed that the positive wind azimuths present a very similar trend with the previous cases discussed so far. At the same time, the most significant change is a much overall lower collective. On the other hand, for the negative wind azimuths, incredibly close to -90 degrees, the collective is observed to increase while the thrust is maintained at a similar value. This is again due to the vortex ring state appearing at the tail rotor plane. However, due to the lower main rotor disk loading, the required tail rotor thrust is lower, and since the tail rotor radius has not changed, the tail rotor disk loading is also lowered. This is causing the induced velocities from the tail rotor to be lower. Hence, the vortex ring state appears at lower freestream velocities, as can be observed in Figure 4.12b, where the curve at 15 knots is already presenting a reversed slope region around -90 wind azimuth. The freestream velocity from which the vortex ring state disappears is also lower, which can be observed to be at 20 knots for the present results.

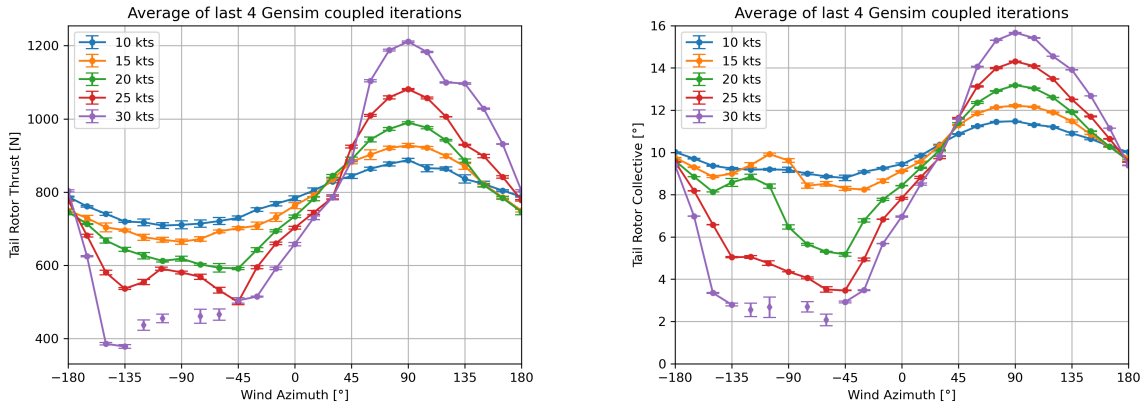

(a) Tail rotor thrust.

(b) Tail rotor collective.

Figure 4.12: Tail rotor thrust and the corresponding collective for a lower main rotor disk loading. Averaged over the last four coupled Gensim simulations, the error bar is one standard deviation.

Since the tail rotor thrust is lower, the disk loading is also lower, which can cause numerical convergence problems based on the flight mechanics code. This was the case for the 30 knots curve, where the wind azimuths from -60º to -120º had numerical convergence problems during the coupling. Finding a trimmed solution for these wind azimuths is also difficult because the rotor operates close to the windmill state. It was noticed that the tail rotor collective evolution over the coupled iterations for these azimuths was oscillating considerably with a constant amplitude until it reached an iteration where the Gensim simulation crashed. On the other hand, the main rotor collective evolution did not present this behaviour during the coupled iterations; therefore, the tail rotor collective has a strong sensitivity to the tail rotor thrust. The oscillation during the coupled iterations was due to the too-high change in the tail rotor collective coupling iterations, which also significantly changed the predicted tail rotor thrust from the UPM simulations. One option would be to apply a relaxation factor. However, the thesis time constraints wouldn't allow this option to be coded. Therefore, a time domain simulation with the autopilot controlling all the attitude rates was performed to find a solution for almost all the wind azimuths presenting difficulties except for -90º. The time domain simulation departs the last found trimmed solution from the Gensim coupled iterations, which was already the standalone Gensim simulation for some cases, and 60 intervals are simulated, resulting in a total real-time of 9.072 seconds. The results of this time domain simulation are not what they would be in reality since, in the first seconds, the autopilot controls adjust the transferred loads from UPM that were missing from the first trimmed simulation. So, this procedure effectively smooths the transfer of loads and allows the helicopter controls to converge slowly to the final solution. It would be the closest to a tight coupling where each interval can be considered a coupled iteration. However, these simulations come at the cost of higher computational time. To illustrate this, in Figure 4.13, the evolution of the tail rotor collective for the investigated wind azimuths with this method is shown. The flight at a wind azimuth of -90º could not be converged since the Gensim time domain simulation crashed. It can be concluded that even the tiny collective changes from the time domain autopilot are too significant to handle.

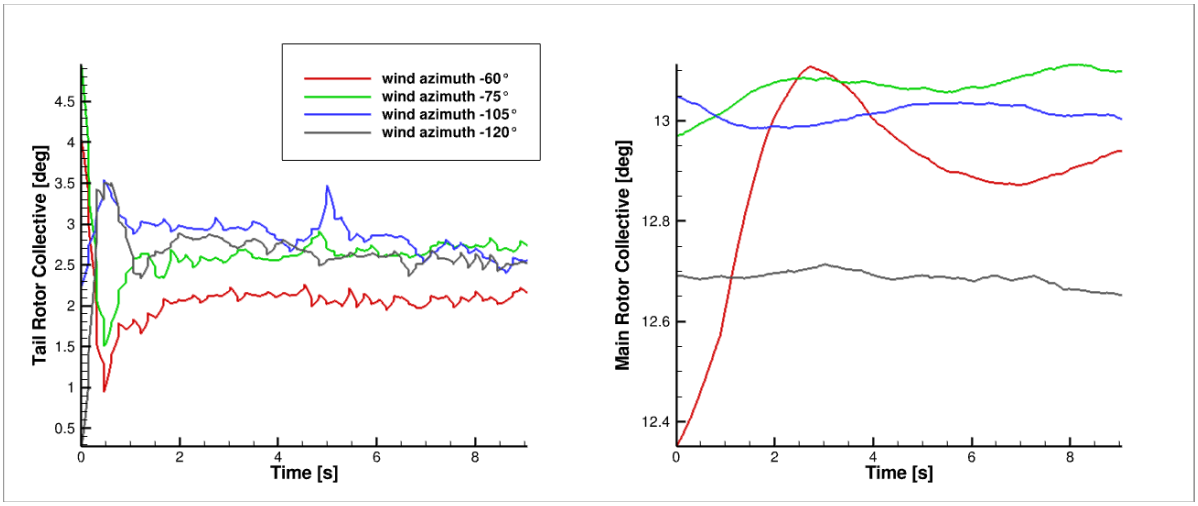

Figure 4.13: Evolution of tail rotor collective over time for the pseudo time domain simulations to obtain coupling convergence.

4.1.4. Pedal Demands

The different helicopter tail rotor configurations have been discussed in the previous sections regarding tail rotor thrust and tail rotor collective needed for the trim state in different freestream velocities and wind azimuths. This section aims to assess whether the collective demands are within the pedal limits. The pedal limits are the minimum and maximum collectives that the pilot can input from the cockpit; therefore, if a case is found where the required collective is outside this range, this would mean that even though a trimmed solution was numerically found, the pilot wouldn't be able to apply such pedal control and would suffer insufficient anti-torque. To compute the pedal position, considering a counterclockwise rotating main rotor, a linear correlation is used between the tail rotor collective corresponding to a maximum left pedal position (zero per cent), which would mean maximum tail rotor collective, and a maximum right pedal position (one-hundred per cent) that would be a minimum tail rotor collective. Notice that a 50% pedal position means that the pilot has the pedals in a neutral position, and the same amount of right and left pedals is applied. Now, the pedal in percentage can be formulated as follows:

$$Pedal\,[\%] = 100 \cdot \frac{\theta_{max} - \theta}{\theta_{max} - \theta_{min}} \tag{4.1}$$

where θ_{max} is the tail rotor collective corresponding to a maximum left pedal position, θ_{min} is the tail rotor collective corresponding to a maximum right pedal position, and θ is the actual tail rotor collective angle. The pedal limits are specific for each helicopter model, and using the data presented in chapter 3, the pedal for the BK117-C2 can be computed as,

$$Pedal\,[\%] = 100 \cdot \frac{26.3 - \theta}{(26.3 - (-6.3))} = 100 \cdot \frac{26.3 - \theta}{32.6} \tag{4.2}$$

So far, using the numerical tools, it was observed that a trim state was obtained for all the evaluated points except for the low main rotor disk loading, where a trimmed solution could not be found due to high collective inputs during the coupling iterations. In Figure 4.14, the pedal requirements for all four investigated helicopter configuration cases are presented for all the studied velocities and all wind azimuths. The pedal position for all cases is within the operational limits of the helicopter. For that reason, no such case starts to yaw without the pilot's intervention.

Comparing the four helicopter configurations and considering the discussion in the previous sections, it is noted that the tail rotor configuration where the tail rotor rotates top forward requires a higher left pedal position for the wind azimuths that experience a main rotor wake interaction. This means that the pilot will have less room for possible manoeuvrings, as the recovery of unintended yaw, where the more left pedal is needed. Therefore, this configuration is not preferred over the original tail rotor configuration. The configuration where the tail rotor is located at the tail boom height affects the pedal demands, especially in the negative wind azimuths, as was discussed in the previous section; in particular, it facilitates the appearance of a vortex ring state at the tail

rotor since it is less disturbed by the main rotor. The consequence is that pilots must apply more left pedals to the affected wind azimuths if yaw trim is desired. Pilots must apply more left pedals if yaw trim is desired for the affected wind azimuths. Consequently, this configuration is also not preferred over the original tail rotor configuration.

The last helicopter configuration case investigated was the lowered disk loading for the main and tail rotors. This case cannot be directly compared with the original helicopter configuration since it represents a strongly modified helicopter in terms of weight. However, it shows the pedal demands for lower main rotor and tail rotor disk loading helicopters with the tail rotor located at the tail boom height. The most noticeable effects include a lower freestream velocity where the vortex ring state at the tail rotor starts to appear due to the lower tail rotor disk loading and the non-converged trim cases for high freestream velocities and wind azimuths close to -90 degrees due to fluctuations in the tail rotor collective.

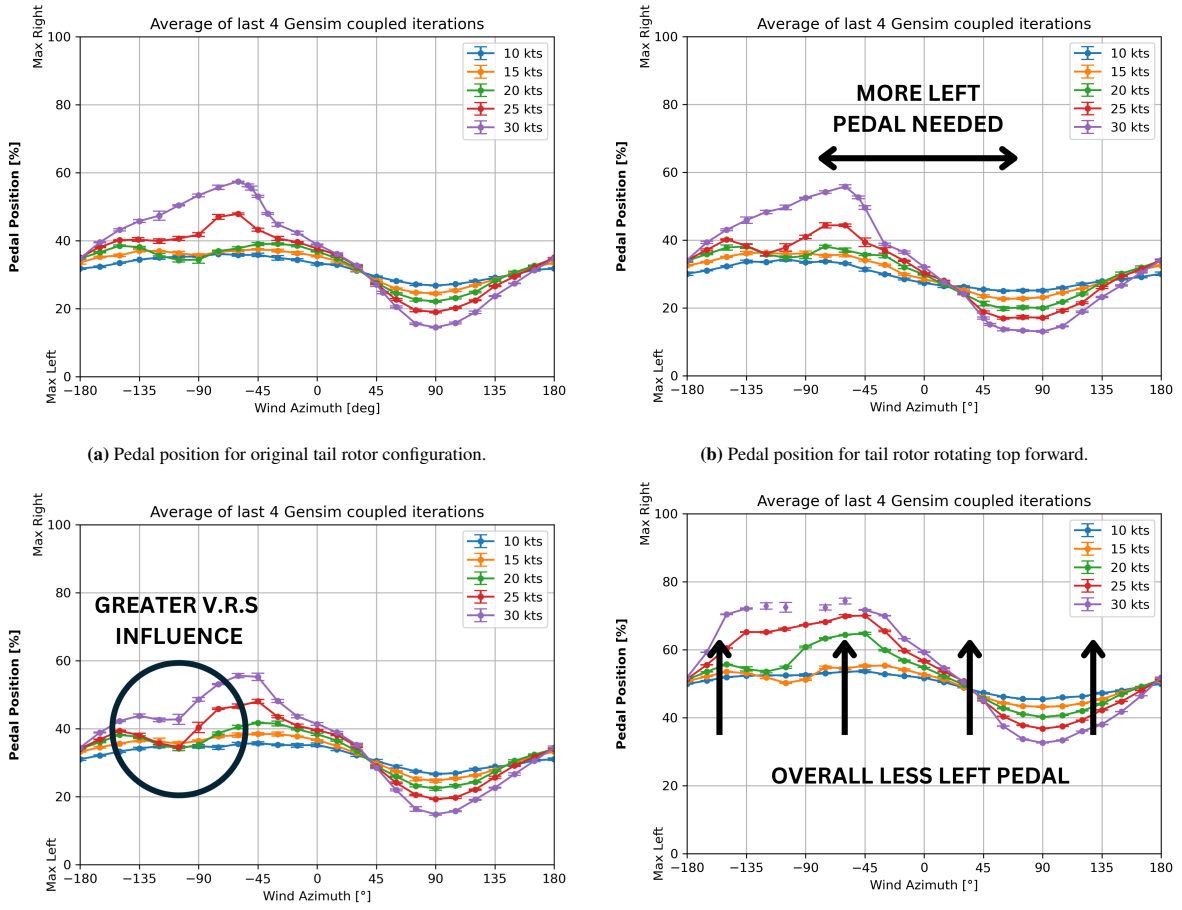

(a) Pedal position for original tail rotor configuration.

(b) Pedal position for tail rotor rotating top forward.

(c) Pedal position for tail rotor located at tail boom height.

(d) Pedal position for lower main rotor disk loading and tail rotor at tail boom height.

Figure 4.14: Pedal position for all the tail rotor configurations and main rotor disk loading evaluated. Averaged over the last four coupled Gensim simulations, the error bar is one standard deviation.

4.1.5. Summary

Before assessing how unintended yaw can start, a summary of the observed aerodynamic effects changing the required tail rotor collective is presented. Two main effects were observed to alter the tail rotor collective for trim curves for the different wind velocities and wind azimuths. The first is the appearance of a vortex ring state around the wind azimuths where the freestream velocity is directed against the tail rotor wake; this requires more tail rotor collective, so more left pedal, for a range of low velocities, then, when the freestream velocity is higher, the vortex ring state is moved above the rotor so the effect is reduced. The rotor regains thrust, which is when the effect is gone. The second phenomenon is the interaction from the main rotor wake with the tail rotor, which will

cause the tail rotor to create more thrust, as could be observed by comparing the tail rotor rotating top aft with the tail rotor rotating top forward, and requiring less left pedal for the trim. Additionally, the affected areas are only those where the tail rotor interacts with the main rotor wake, as could also be proved from Figure 4.7 and Figure 4.8. An illustrative image to clarify which areas are affected by what effect is shown in Figure 4.15.

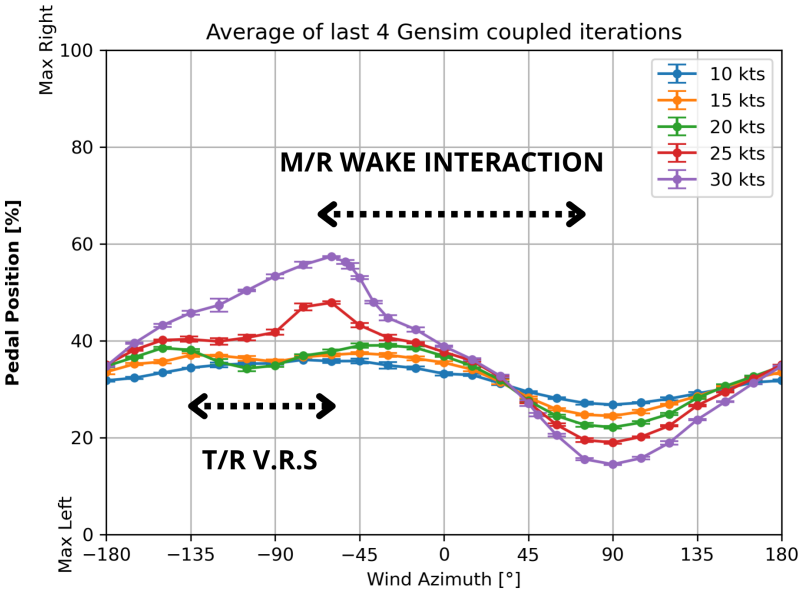

Figure 4.15: Affected wind azimuths by tail rotor vortex ring state and main rotor wake interaction.

Based on the results presented in the previous sections, no flight condition causes the start of unintended yaw since a trimmed case can be found. Furthermore, the start of the unintended yaw is unrelated to the helicopter's design malfunction. Instead, it is caused by aerodynamic effects or pilot inputs of the collective or pedal. This is because the aerodynamic effects, namely the tail rotor vortex ring state and the main rotor wake interaction with the tail rotor, are modifying the required pedal for each wind azimuth curve to have a trim flight for the different freestream velocities. Furthermore, notice that such curves exist for each helicopter model and depend on the air temperature and density. Additionally, a change in the main rotor collective will have a direct impact due to the related increase in torque. Consequently, it will require more left pedal (more tail rotor collective). Since these effects are not apparent to the pilot and require pedal adjustments to maintain a trimmed flight, they could cause the pilot to be flying in those affected wind azimuths and apply the wrong pedal inputs. Moreover, if the pilot makes collective changes, the trim curve for the pedal position to achieve trim will be shifted, and the pedal needs to be adapted accordingly.

Let's consider the scenario illustrated in Figure 4.16, where the pilot is flying with a freestream velocity of 25 knots and 0-degree azimuth. If the pilot wants to yaw to the right, the pilot will need to apply a correct pedal step input, decreasing the tail rotor thrust, and the helicopter will start to yaw to the right, decreasing the wind azimuth. Consequently, the helicopter will continue to yaw to the right until it reaches a wind azimuth where the required pedal for yaw trim equals the pilot's current pedal position. If the pilot tries to apply the same right pedal step when the wind azimuth is around -60 degrees, the wind azimuth will start to decrease, and the pedal position needed for yaw trim will be with the more left pedal. Therefore, suppose the pilot needs to apply the left pedal quickly enough. In that case, the helicopter will increase the yaw rate without stopping because the pedal position the pilot currently has does not intercept the pedal curve at any wind azimuth. For this flight speed, due to the tail vortex ring state, the point from where the pilot needs to apply the left pedal again while decreasing the wind azimuth is reached earlier. As an additional example, for a speed of 20 knots, two points exist where the pilot needs to apply the left pedal after reaching a maximum right pedal position while decreasing the wind azimuth (yawing to the right) due to the vortex ring state at the tail rotor which can be confusing since these two points are not far from each other in terms of azimuth range.

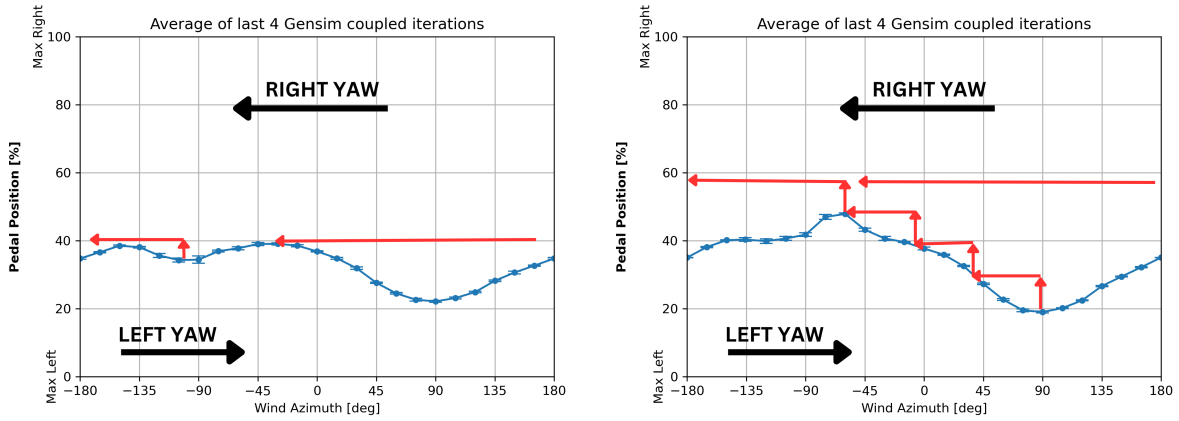

(a) 20 knots.

(b) 25 knots.

Figure 4.16: Example of the start of unintended yaw at constant speeds of 20 and 25 knots.

4.2. Coupling Necessity

This section evaluates the necessity of coupling the flight mechanics code Gensim and the aerodynamics code UPM to investigate unintended yaw-related accidents. To do so, the results of the standalone Gensim simulations and the coupled Gensim simulations for the original helicopter configuration will be compared and discussed. In particular, the tail rotor thrust and the tail rotor collective for both cases will be compared.

4.2.1. Tail Rotor Thrust

The tail rotor thrust required for the trim if only Gensim was used and the one obtained from an average of the last 4 coupled Gensim iterations is illustrated in Figure 4.17. The coupled Gensim results in Figure 4.17a are already discussed in the previous sections and understood. Instead, the tail rotor thrust results from standalone Gensim simulations in Figure 4.17b must be analysed in detail first. There is a first big difference between the two results as it is observed that the tail rotor thrust obtained from standalone Gensim simulations shows an overall higher thrust required for a trim for all wind speeds and azimuths. In addition, the wind azimuths that require the most tail rotor thrust are those close to 90 degrees, which is the same behaviour obtained in the coupled Gensim results. Also, the negative wind azimuths around -90 degrees behave similarly where the slope of the thrust to the wind azimuth is reduced. Even though the trends are similar, the results when using the coupling change considerably, so these differences are explained in detail in the following paragraphs.

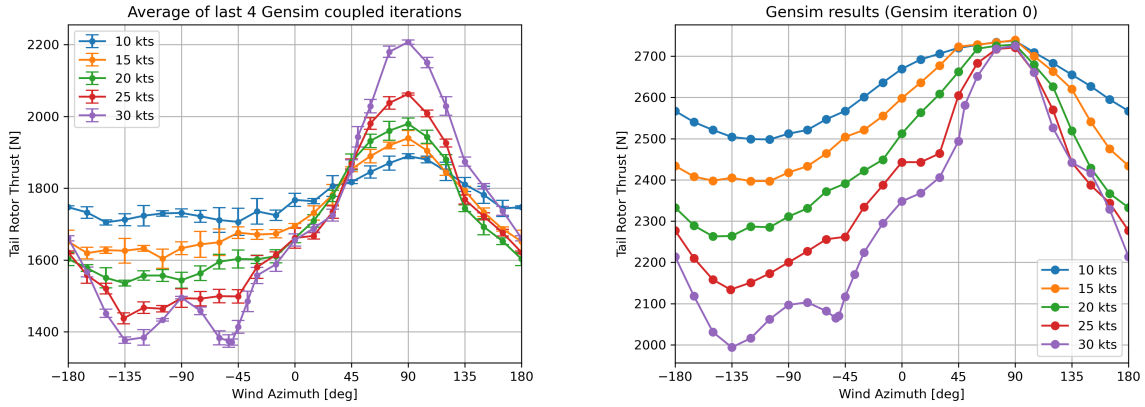

(a) Coupled Gensim results.

(b) Standalone Gensim results.

Figure 4.17: Tail rotor thrust for standalone Gensim simulations and coupled Gensim simulations.

The first relative difference investigated is the difference in the thrust required for a wind azimuth of 90 degrees, where the standalone Gensim simulations show that a constant thrust is needed for the different evaluated freestream velocities. Instead, in the coupled results, the thrust required increases with the velocity magnitude. To assess the cause of these results in both cases, the yaw moment for each helicopter component at a wind azimuth of 90 degrees is shown for the evaluated velocity magnitudes for the Gensim standalone and the coupled simulations in Figure 4.18. It can be seen that for the coupled results, the main rotor torque decreases with the increase in velocity. At the same time, the vertical stabiliser yaw moments also increase while the fuselage yaw moment slowly grows. This results in a total amount of torque to be compensated, which increases with the freestream velocity; therefore, the required tail rotor thrust also increases. For the standalone Gensim simulations, it is first observed that the main rotor torque is much higher than the one obtained from the coupling for the same velocity. Then, the main rotor torque decreases at a much faster pace when the helicopter velocity is increased. The vertical stabiliser and fuselage yaw moments increase at the same rate as in the coupled results. Coincidentally, the rate at which the main rotor decreases and the vertical stabiliser and fuselage increase is the same. Therefore, the total amount of anti-torque required by the tail rotor is constant over the freestream velocities. This is why the tail rotor thrust for these velocities at a wind azimuth of 90 degrees is kept constant. The reason for the overprediction in the torque from Gensim alone is that the rotor model in Gensim is a simple analytical model that does not account for the local blade interactions, and it assumes a linear inflow distribution like if the rotor had an infinite number

of blades instead; thus, it lacks prediction on the induced power due to a finite number of blades.

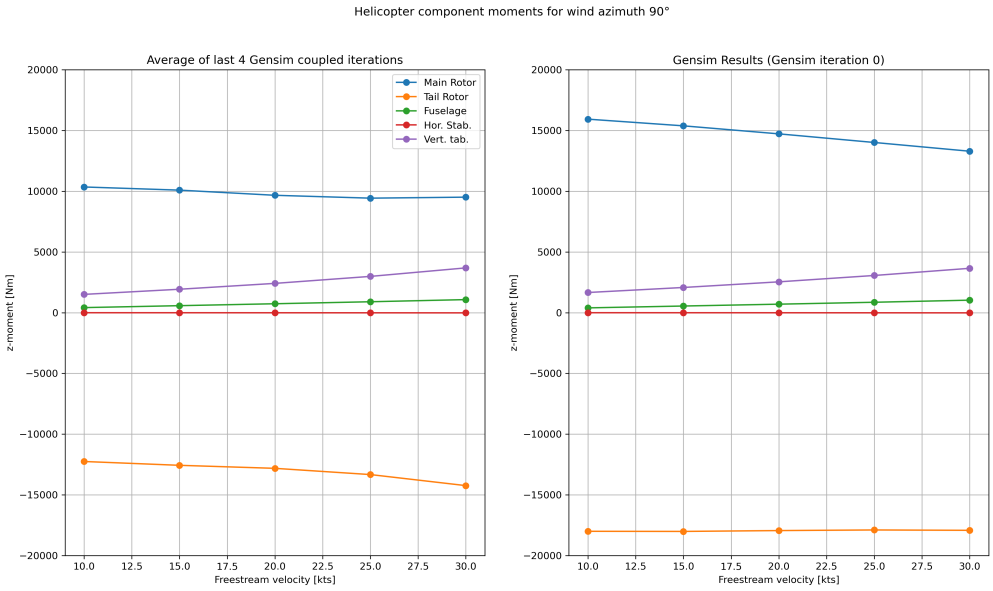

Figure 4.18: Yaw moments for each helicopter component depending on the freestream velocities.

The rest of the wind azimuths also present differences in the results; for example, at a freestream velocity of 30 knots, the yaw moments of each helicopter component depending on the wind azimuth are pictured in Figure 4.19. The amount of yaw moments for each component is equal except for the main rotor and the tail rotor, which are decreased. This is directly related to the fact that in the UPM simulations, only the main and tail rotors are modelled, so the vertical stabiliser, fuselage and horizontal stabiliser are unaffected. However, the transfer of loads and induced velocities from the aerodynamics simulation affects helicopter attitudes. Hence, this is why, for some wind azimuths, the yaw moments of the vertical stabiliser and the fuselage are changing. Therefore, considering the results from the flight test used to verify the coupling in chapter 3, the coupling is improving the accuracy of the torque.

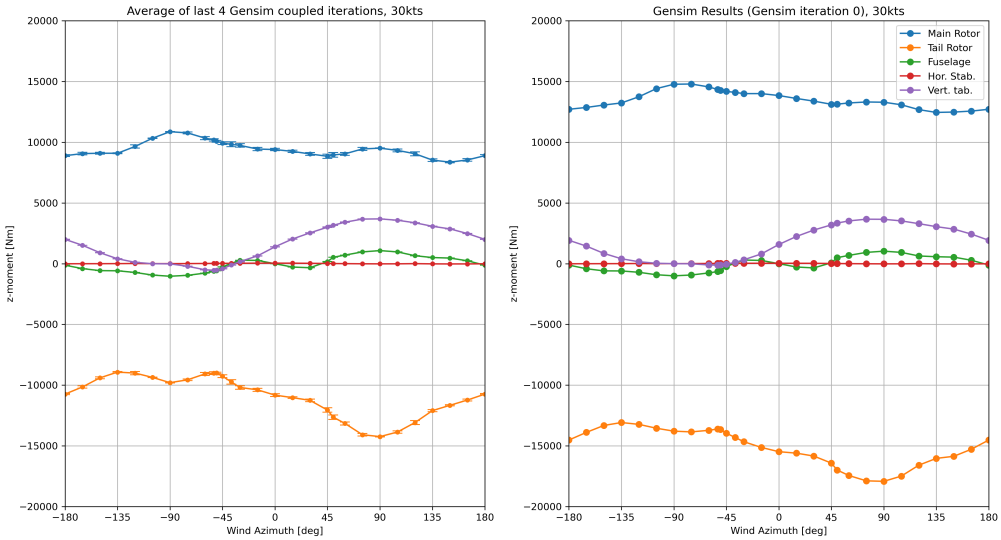

Figure 4.19: Yaw moments for the helicopter components depending on the wind azimuth for a freestream velocity of 30 knots.

To better understand how much the transfer of loads during the coupled iterations affects the results for the different wind azimuths, the delta loads for the main rotor and the tail rotor are extracted for each wind azimuth. In Figure 4.20, the difference in the moments concerning the z-axis between the flight mechanics code and the aerodynamics code during each coupled iteration is averaged over the last four exchanges for the main rotor and the tail rotor. This z-moment represents the moments in the helicopter reference frame; in general, the changes in z-moment for the main rotor are due to changes in the main rotor torque, while the z-moment variations for the tail rotor are due to the tail rotor thrust changes. This difference in loads for the main rotor and the tail rotor over the wind azimuths indicates discrepancies in the loads when the same motion is simulated from both codes. Therefore, it is observed that the main rotor increment loads are almost constant with the wind azimuth as other components do not influence the main rotor, and it always operates in similar freestream conditions as the wind azimuth is not affected. The difference in the z-moment is negative for the main rotor, meaning that the UPM simulations give a lower torque than the Gensim simulations and have an averaged absolute value of around 3000 Nm for the velocities evaluated. The difference observed for the tail rotor yaw moment strongly depends on the wind azimuth. This is expected since the tail rotor operates in various conditions due to the change in wind azimuth, which directly changes the sideslip of the rotor and, at the same time, is influenced by the main rotor wake. From a physical point of view, it is expected that the simulated cases at a wind azimuth of 180 degrees are not affected by the main rotor wake; hence, this wind azimuth is taken as a reference for the difference in loads of an isolated tail rotor. The difference in yaw moment is due to deviations in the tail rotor thrust, which is around 4500 Nm and changes slightly with the freestream velocity. When the wind azimuth changes, this difference is affected by the main rotor wake interactions and the vortex ring state appearing at the tail rotor. The difference in z-moments exerted by the tail rotor is generally favourable. Be aware that in the flight mechanics reference system, the z direction is pointing downwards. Hence, the tail rotor is causing a negative torque, the anti-torque. This means that a positive difference represents that the yaw moments predicted by UPM are lower than those predicted by Gensim. This occurs due to the lower thrust predicted by UPM for the tail rotor compared to Gensim while operating with the same tail rotor collective. However, it is interesting to observe that for a wind azimuth of -90 degrees, the difference becomes negative for high speeds and more favourable for lower speeds. As discussed in previous sections, the wind azimuths where the freestream velocity is against the direction of the wake, a vortex ring state occurs at the tail rotor, which causes the tail rotor to lose thrust. A loss in the thrust will lower the yaw moments, so the difference between UPM and Gensim will become more positive since Gensim does not predict any loss in thrust. For higher speeds, UPM predicts the vortex ring to be above the rotor so a gain in tail rotor thrust appears. This gain is such that the UPM predicted tail rotor thrust surpasses the Gensim thrust; thus, the difference is now negative.

Another interesting phenomenon, although it is hard to observe, is noted that the central wind azimuths have a decreased difference in tail rotor yaw moment; hence, as discussed before, this relates to an increased tail rotor thrust. For that reason, when the tail rotor is operating around the central wind azimuths, under the interaction of the main rotor wake, it is observed that the tail rotor is gaining thrust. These results show that an interaction that increases the tail rotor thrust is present without testing other tail rotor configurations. Note that the argumentation presented in this part is valid because Gensim doesn't account for any interaction models or vortex ring state models for the tail rotor.

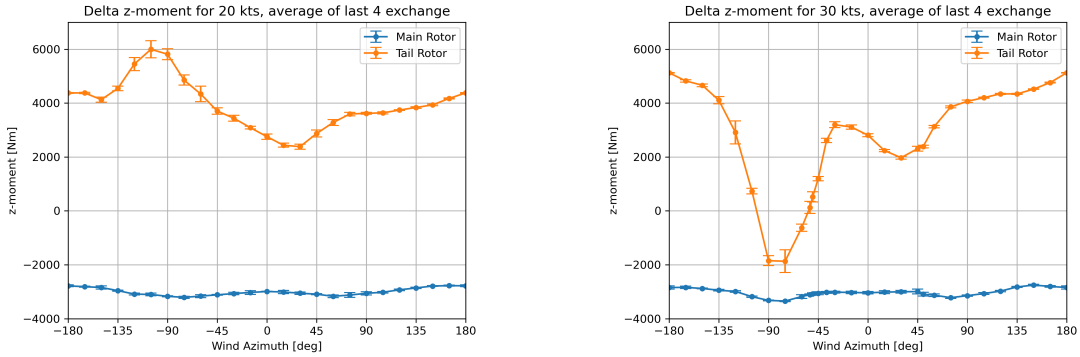

(a) Difference in loads for 20 knots.

(b) Difference in loads for 30 knots.

Figure 4.20: Difference in loads between UPM and Gensim simulations during the coupled iterations. Results are an average of the last 4 coupled iterations and one standard deviation is shown as an error bar.

4.2.2. Tail Rotor Collective

The relation between the thrust created by a rotor and the collective pitch causing this thrust is related to the aerodynamics modelling of the rotor. For instance, Gensim uses an analytical model that assumes a linear inflow distribution over the rotor azimuth and a radial distribution that depends on the induction factors. Instead, in UPM, the local loads for each blade section rely on the flow field modelled from the vortex particle method. The previous section shows that the predicted main rotor torque when the coupling is used is lower than what Gensim predicts alone. It was observed that the tail rotor thrust was also generally lower for the coupled results. Nevertheless, the tail rotor collective, which creates a given rotor thrust, is strongly influenced by the flow field around the rotor. Therefore, it can already be suspected that the Gensim results will need more accuracy since the flowfield is not considered. Because of the lack of flow field prediction from Gensim, to compare the tail rotor collective values between the coupled Gensim results and the standalone Gensim results, the tail rotor collective values from the standalone Gensim simulations are shifted to the values from the coupling at a wind azimuth of 180 degrees. Since the main rotor wake does not interact with the tail rotor when flying at a wind azimuth of 180 degrees, the predicted collective from the standalone Gensim simulations is expected to be the closest approximation to the coupled Gensim simulations. Therefore, this shift will isolate the relative effects between the two results.

In Figure 4.21, the tail rotor collective angles are shown for the standalone Gensim simulations and the final coupled Gensim simulations. The relative difference between the two results once the Gensim standalone simulation results are shifted to the values of the coupled Gensim results at a wind azimuth of 180 degrees is also shown in the same plots with a second axis. First, the 10 knots curve for the standalone Gensim simulation has been shifted down more degrees than for the 15 knots case. However, this shift is related to the rotor model in Gensim but also the required tail rotor thrust which is dependent on the modelling of the rest of the components; therefore, it can be related to the difference in the rate of decrease of the main rotor torque with the increase in velocity, shown in Figure 4.19, between Gensim standalone and the coupled Gensim results where Gensim standalone main rotor torque was decreasing at a faster rate. Since the tail rotor collective from the Gensim rotor model is a simple model, the tail rotor collective will decrease with the decrease in required tail rotor thrust for all wind azimuths. Now, for these low speeds of 10 and 15 knots, the relative differences in tail rotor collective don't exceed two degrees and are higher for 15 knots than for 10 knots. Specifically, the central wind azimuths are the flight cases which are most affected. This is expected since these wind azimuths interact with the main rotor wake. The rest of the wind azimuths are not observed to have significant relative differences since the dependence of the aerodynamics of the tail rotor concerning the wind azimuths for these velocities without any interactions can be estimated with the rotor model from Gensim.

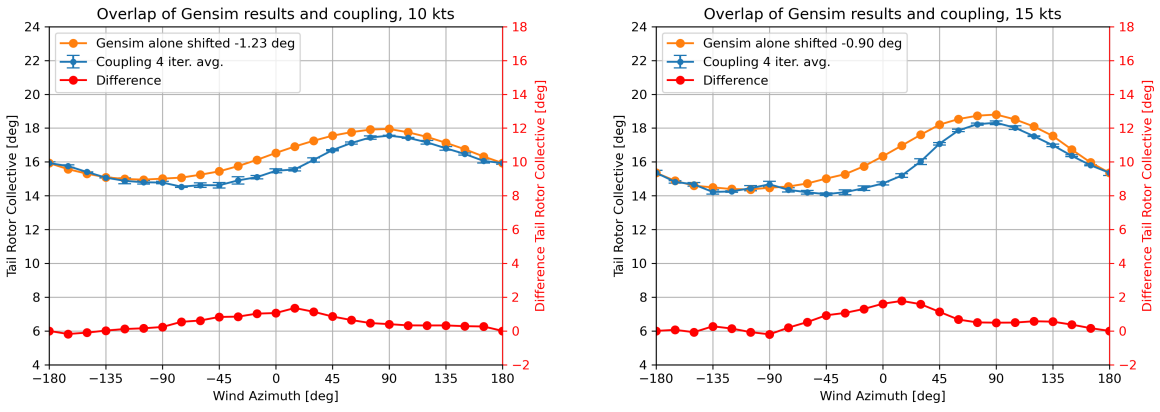

(a) Overlap for 10 knots.

(b) Overlap for 15 knots.

Figure 4.21: Difference in required tail rotor collective between standalone Gensim and the coupled Gensim results for speeds of 10 and 15 knots. Shifted standalone Gensim results to match 180° wind azimuth tail rotor collective.

The tail rotor collective for a freestream velocity of 20, 25 and 30 knots is shown in Figure 4.22. The results show that the tail rotor collective for the standalone Gensim simulations tends to decrease with the velocity increase, as explained for the cases of 10 and 15 knots. However, for 20 knots, the tail rotor collective starts to present more relative differences between the two results since it is observed that not only the central wind

azimuths are now affected due to the main rotor wake interacting with the tail rotor, but the wind azimuths close to -90 degrees wind azimuth are also presenting some differences. When the coupling is used, the tail rotor collective is higher due to the reduction in thrust from a vortex ring state, which causes a higher needed collective. For 25 knots flights, the differences become higher over a broader range of wind azimuths from -100 degrees to 90 degrees since the negative wind azimuths become more affected by the wake reinjection, which is not captured in Gensim standalone. Going up to the 30 knots flight cases, the differences between standalone and coupled Gensim simulations are increasing even more. It is noted that the most significant difference occurs at wind azimuths close to -90 degrees, where the increased velocity has moved the wake reinjection above the rotor which is causing a thrust that can be unpredictable by Gensim standalone. Finally, the difference in the tail rotor collectives is directly related to the difference in loads presented in the previous section in Figure 4.20 because in the coupled Gensim iterations, the increment in loads are applied at the fuselage so that the rest of the components will adjust the controls considering these extra loads.

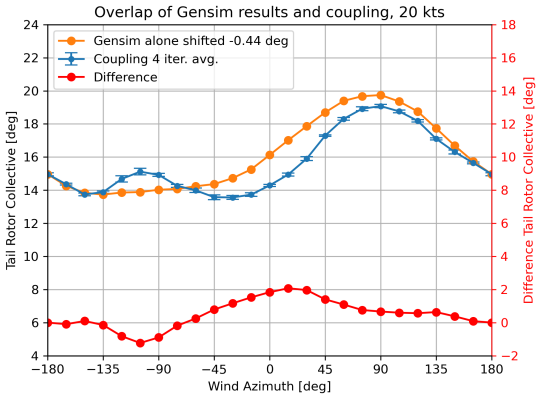

(a) Overlap for 20 knots.

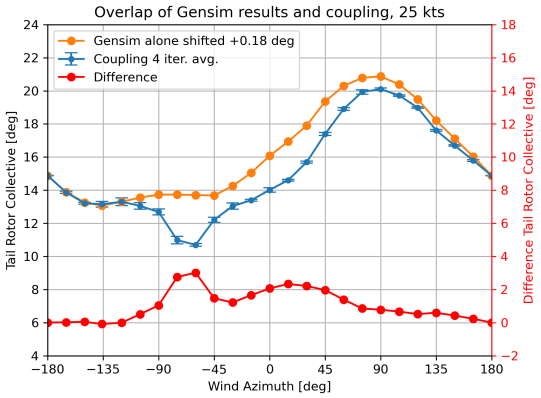

(b) Overlap for 25 knots.

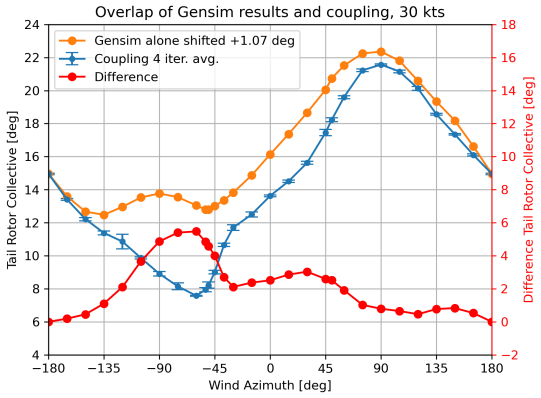

(c) Overlap for 30 knots.

Figure 4.22: Difference in required tail rotor collective between standalone Gensim and the coupled Gensim results for speeds of 20, 25 and 30 knots. Shifted standalone Gensim results to match 180° wind azimuth tail rotor collective.

4.2.3. Summary

The differences when not using the coupling with the aerodynamics code have been examined and observed to be significant. The coupling between a flight mechanics code and an aerodynamics code is essential to investigate unintended yaw since the tail rotor performance must be assessed carefully. This means that it is mandatory not to miss critical flow physics such as vortex ring state or main rotor wake interactions with the tail rotor, which can only be captured with the help of an aerodynamics code. The flight mechanics code fails to predict rotor aerodynamics, which are out of the typical rotor operation. Furthermore, it was observed that the higher the velocity, the higher the discrepancies in tail rotor collective for those wind azimuths involving tail rotor vortex ring state and main rotor wake interaction.

4.3. Flow Physics

From the results in the previous sections, the rotor aerodynamics could be analysed indirectly by comparing tail rotor thrust and collective for different wind velocities and azimuths together with different helicopter configurations. Throughout these sections, the tail rotor vortex ring state appearing at the tail rotor plane surroundings and the main rotor wake interactions with the tail rotor have been continuously mentioned due to the observed influences in the tail rotor thrust and collective. Moreover, when comparing standalone Gensim simulations, these effects could also be noted. However, these phenomena have been only proven from indirect measurements provided by the flight mechanics code, Gensim. Therefore, the present section aims to present the results of a detailed investigation of the tail rotor vortex ring state and main rotor wake interactions through the analysis obtained from the aerodynamics code, UPM. This thorough analysis will directly prove the existence of such effects, and then the results will be discussed to evaluate how they can influence unintended yaw.

4.3.1. Tail Rotor Vortex Ring State

Main rotor vortex ring state studies have been provided in the literature. These studies investigated the rotor aerodynamics when the rotor is descending where the freestream velocity is against the rotor wake direction. In normal operating conditions, the rotor releases a tip vortex for each blade, which travels downstream in a helical tubular structure. However, when an opposing freestream velocity appears, the tip vortices start to be convected upstream towards the rotor. If the freestream velocity is sufficient enough, the tip vortices will travel at around the rotor height, and they will be sucked into the rotor again due to the low pressure above the rotor. This creates an accumulation of tip vortices around the rotor, forming a toroidal vortex ring; the rotor is under a vortex ring state. The consequences of such a vortex ring are related to the fact that the vortex ring state is a consequence of the tip vortices accumulating, which also does their vorticity. As a result, the inflow over the rotor blades is significantly increased. Therefore, an increase in the rotor inflow is causing a reduction in the effective angle of attack for each local blade section. The integrated thrust results in a lower thrust value compared to normal operating conditions. This decrease in thrust can have severe consequences; in the case of a main rotor, the helicopter will increase the rate of descent, which can cause potential damage. However, when the freestream velocity grows, the tip vortices accumulate above the rotor, where the influence in the rotor inflow is reduced, and the rotor regains the thrust. The rotor does not operate in the windmill region yet but operates under a fluctuation of thrust, which is slightly influenced by the accumulating vortices above the rotor. Therefore, in the case of a main rotor, the helicopter would fall faster due to the decrease in thrust, but it would regain thrust once the decent rate increases.

In the case of a tail rotor, the rotor aerodynamics are the same; however, the orientation of the rotor changes concerning the helicopter reference frame. Therefore, since the vortex ring state occurs when the freestream velocity is against the wake direction, the tip vortices are convected towards the rotor, and the tail rotor will mostly be affected by the wind azimuth and the freestream velocity. This is already observed from the results of the tail rotor thrust and tail rotor collective for trimmed flights. To assess how the vortex ring state affects the helicopter's yaw trim, the aerodynamic simulations from UPM obtained during the coupled iterations from the trimmed flight simulations obtained in section 4.1 are studied for the different helicopter configurations as needed. It is already expected that for the tail rotor, the vortex ring state will require differences in the tail rotor collective when the helicopter is flying in wind azimuths close to -90 degrees since for a counterclockwise rotating main rotor, the tail rotor wake is directed towards the left-hand side. Notably, it was noted that when flying with wind azimuths, where the perpendicular component to the tail rotor plane started to be significant, the tail rotor collective increased. In contrast, the tail rotor thrust remained at a considerably constant value. Additionally, when comparing the standalone Gensim simulations and the coupled in section 4.2, there were remarkable differences in both the loads transferred during the coupling shown in Figure 4.20 and the tail rotor collective observed in Figure 4.21 and Figure 4.22 for the negative wind azimuths. Thus, without having checked the rotor loads, flow field or blades' angles of attack, the tail rotor blades had to increase the blade pitch to maintain the trim.

To start with the investigation, the flow field around the helicopter is visualised for a flight with a wind azimuth of -90 degrees with streamlines around the tail rotor to check if the flow recirculates. In Figure 4.23, the streamlines for a flight at 20 knots and -90 degrees wind azimuth are shown twice in the last UPM simulation in the coupled iterations. The streamlines revolve around the rotor plane, and the volume around the tail rotor is shown in Figure 4.23 with green colour, creating a ring around the blade tips trajectory. However, this ring only appears for one part of the rotor azimuths. In particular, the part closer to the main rotor does not present

recirculating streamlines around the tail rotor. Instead, the streamlines around the closer part between the main rotor and the tail rotor are circulating the main rotor due to the tip vorticity of the main rotor blades. Therefore, what is happening is that the tip vortices from the main rotor are disturbing the formation of the vortex ring state at the tail rotor at the azimuths closer to the main rotor. It is observed that the formation of the vortex ring state around the tail rotor is very unsteady, and the vorticity around the tip of the tail rotor blades changes in magnitude and location over time. It is also observed that the streamlines closer to the main rotor blades always have a vertical velocity component due to the main rotor tip vortices. Furthermore, the disturbed region due to the main rotor tip vorticity momentarily accumulates some vorticity until a new blade introduces a perpendicular vorticity that is combined with the tail rotor tip vorticity, which results in a dominated flow field by the stronger main rotor tip vortex.

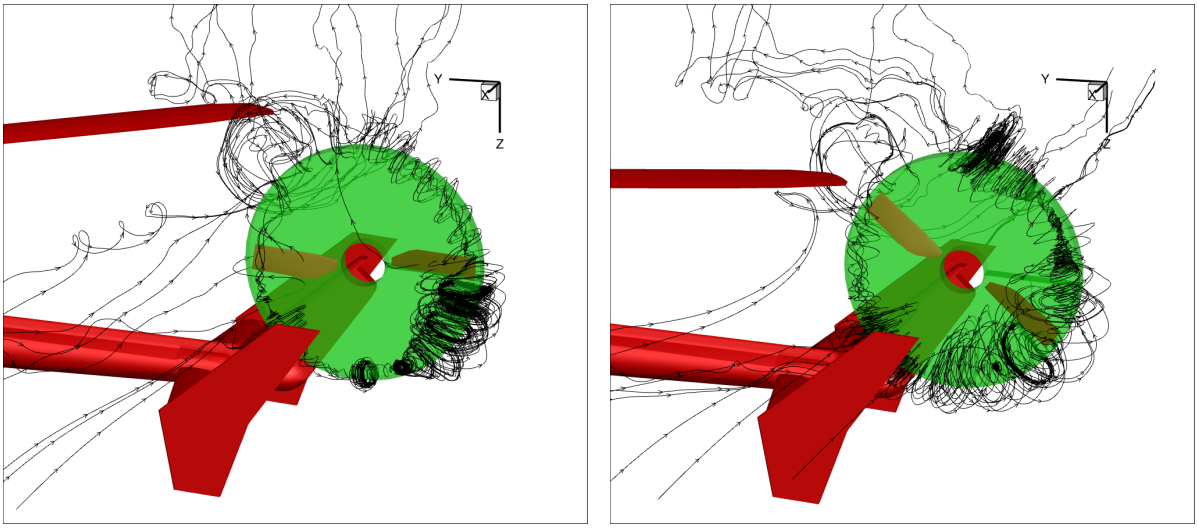

(a) Streamlines at $t = t^*$.

(b) Streamlines at $t = t^* + 2.9 \cdot 10^{-3}$.

Figure 4.23: Instant snapshots of the streamlines around the tail rotor for a difference in time of 2.95ms, equivalent to a main rotor azimuth step of 70 degrees. Wind azimuth is -90 degrees, and freestream velocity is 20 knots. The tail rotor volume is shown in green.

Now, to better assess the formation of this disturbed vortex ring around the tail rotor, the flow field is averaged over time to eliminate the local periodicity of the solution due to the blade frequency. As a consequence, the shape of the disturbed vortex ring can be better visualised. The streamlines are again illustrated in Figure 4.24, where it is shown that the vortex ring appears throughout the tail rotor volume, but it is concentrated on the regions away from the main rotor disturbance as was also observed in the instant snapshots from Figure 4.23. The azimuths from the tail rotor plane, which are closer to the main rotor, present a vorticity component in the freestream direction, caused by the main rotor tip vortices, that is stronger compared to the vorticity from the tail rotor tip vortices. Thus, the flow is disturbed by the vortices shedding from the main rotor blades, so the tail rotor does not present a fully developed vortex ring state. The flow around the tail rotor azimuths located between the main rotor and the tail boom has a main velocity component, which is a combination of the vorticity from the main rotor blades and the tail rotor blades, which results in the streamlines to travel towards the main rotor while still having, with less strength, a swirl component around the tip of the tail rotor blades. It is also noticed that the size of the recirculating regions is lower for the averaged flow compared to the instant flow due to the dampening caused by the integration of the peaks from the instant flow field solutions.

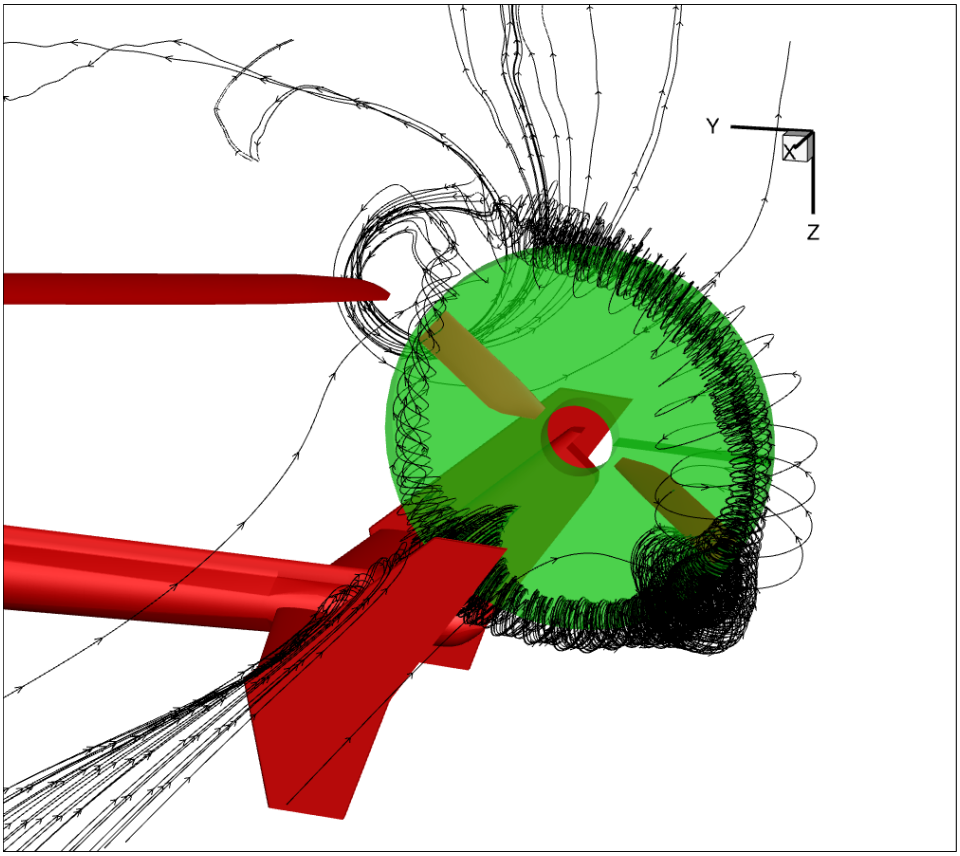

Figure 4.24: Averaged flow field around the tail rotor volume over two main rotor revolutions. Wind azimuth is -90 degrees, and freestream velocity is 20 knots. The tail rotor volume is shown in green.

Since the results from the trimmed flight simulations showed differences in the relation of the tail rotor thrust-collective when the freestream velocity was changed, the influence of the freestream velocity on the formation of the disturbed vortex ring state is assessed for the trimmed helicopter simulations. A slice through the middle of the helicopter tail rotor is performed in Figure 4.25 to observe the streamlines in a 2D plane for the different velocities. Note that these flight cases correspond to the last coupled UPM simulation. Therefore, the tail rotor blades have different collectives. Also, notice from Figure 4.5b that the 10, 15 and 20 knots trim cases are flying with the same tail rotor collective while the 25 and 30 knots cases are flying with the same tail rotor thrust, as can be checked in Figure 4.5a. The accumulated vortices are observed to be of a lower strength for the side closer to the main rotor for all the evaluated freestream velocities, and the location of the vortices is moved from below the rotor for the lower velocities to above the rotor for increased velocities. The 10 knots flow field shows that the wake of the tail rotor is still propagating below the rotor until the freestream velocity convects the flow towards above the rotor. The streamlines are circulating a wide, vast vortex of low strength, and the flow upstream is still affected by the tail rotor wake; for this velocity, the inflow at the tail rotor is not affected by the vortex ring state, so there is no significant influence on the tail rotor thrust. For 15 and 20 knots, the wake from the tail rotor is convected further up the tail rotor plane, and the streamlines circulation's core is very close to the rotor blades plane. In addition, the circulation regions are now more compact and influence the tail rotor blades' inflow. This can be observed by checking that the tail rotor thrust is being reduced while the tail rotor collective is approximately the same. Checking the results for a freestream velocity of 25 knots, the rotor is still under the influence of the disturbed vortex ring state, which presents a different location for the circulating streamlines. For instance, the vortex close to the main rotor is located downstream of the tail rotor, and the vortex away from the main rotor is located upstream of the tail rotor. Instead, for a freestream velocity of 30 knots, all the vortex is located downstream of the tail rotor. The effect of the vortices is more prominent for 25 knots than for 30 knots since at 25 knots; the tail rotor is set at a higher collective pitch than the 30 knots case while the thrust is approximately the same.

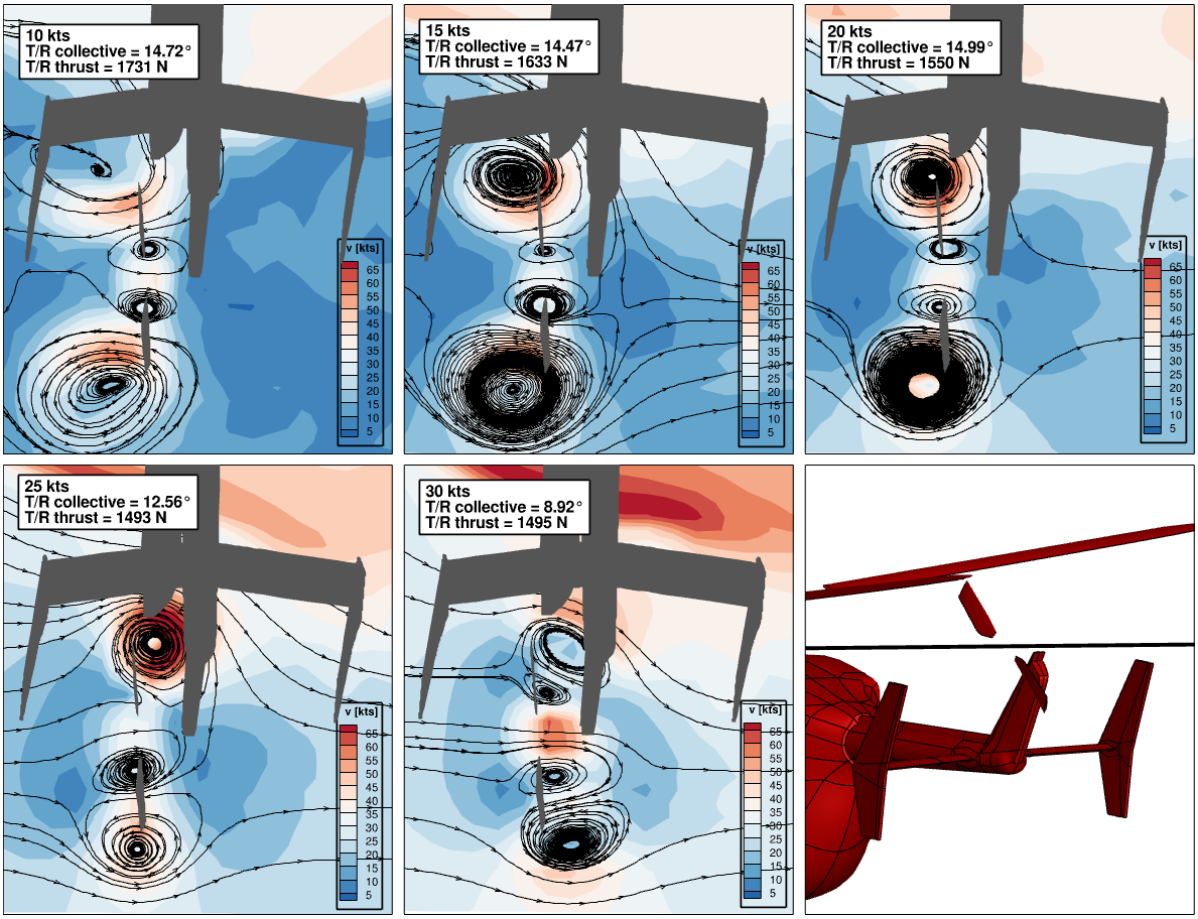

Figure 4.25: Slice of averaged flow field over two main rotor revolutions through tail rotor centre showing streamlines for different freestream velocities and a wind azimuth of -90 degrees. The last picture in red shows the location of the slice through the helicopter.

To investigate the effect of the vortex ring state as a function of the freestream velocity, a trimmed helicopter motion is considered for 20 knots, with which UPM simulations are run for three velocities with the same motion: 10, 20 and 30 knots. This is done because if the results shown previously were to be compared, the different helicopter attitudes would make the comparison more vague and more complex. Therefore, this will effectively isolate the effect of the freestream velocity on the rotor aerodynamics and the formation of vortices around the tail rotor. However, the helicopter will not be trimmed for the 10 and the 30 knots cases. The streamlines in the 2D plane through the tail rotor are not shown again since they are very similar to the results obtained in Figure 4.25, for further interest, they are shown in Figure A.1. The thrust for each case is shown in Figure 4.26a where the thrust for the 20 knots case is lower than that for the 10 knots case. The local distribution of loads over the tail rotor plane is illustrated for further interest in Figure A.2. This wouldn't be expected if it wasn't for the appearance of a disturbed tail rotor vortex ring state that increases the inflow over the rotor and reduces the effective angle of attack at the blade stations. When the velocity is further increased, the tail rotor thrust increases again. It reaches higher values than for the 10 knots case since the vortices from the disturbed vortex ring state are further away from the rotor, so the influence in the inflow is reduced, and the effective angle of attack is increased again. The difference in the effective angle of attack concerning the 20 knots case is shown in Figure 4.26b. The difference in angle of attack is positive for both 10 and 30-knot cases for most of the rotor plane, resulting in an increased tail rotor thrust. The negative difference in the angle of attack at 10 knots is located at radial stations, which are close to the root, so the increased thrust from the rest of the rotor azimuths compensates for the lower thrust from those azimuths. Notice that for 30 knots, the increase in angle of attack is more substantial around the root and, to a lesser extent, at the tips for some rotor azimuths. The root vortex is weaker than the tip vortex. Therefore, the influence of this vortex on the root sections disappears faster than the tip's. Nevertheless, the tip increase in the angle of attack is not insignificant and is what, in the end, is contributing the most to the thrust. This can be confirmed by comparing the relative increase in the effective velocities at the tail rotor plane shown in Figure A.3

to be low.

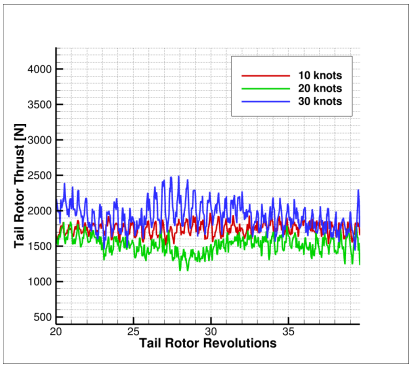

(a) Tail rotor thrust where 5.658 tail rotor revolutions are one main rotor revolution.

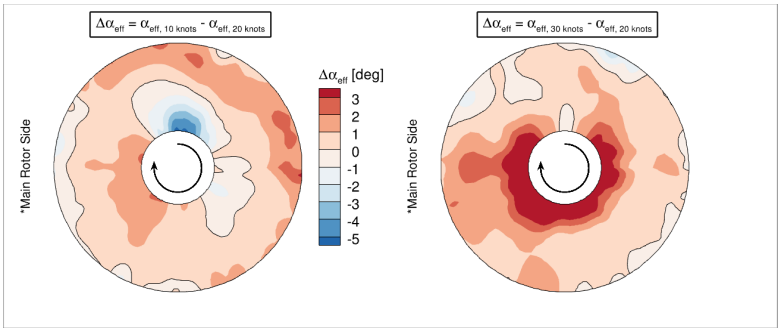

(b) Absolute difference in angle of attack to the 20 knots case. The right figure is for 10 knots, and the left is for 30 knots. The solid line is the border between positive and negative values.

Figure 4.26: Thrust and effective angle of attack for isolated freestream velocity influence. All simulations have the same helicopter motion from the trim at 20 knots except for the freestream velocity. Hence, only the 20 knots case is trimmed.

The effect of the disturbed vortex ring state on the tail rotor aerodynamics has been assessed only for a wind azimuth of -90 degrees. However, when the helicopter flies with wind azimuths close to -90, the tail rotor is also affected by the disturbed vortex ring state. Going back to the results for the trimmed flights and wind azimuths close to -90 degrees, the tail rotor thrust from Figure 4.5a remains almost constant for the wind azimuths close to -90 degrees while the collective from Figure 4.5b is increasing when the wind azimuth decreases. Therefore, the disturbed vortex ring state is also affecting these azimuths. This trend is most noticed for freestream velocities of 25 and 30 knots. For 25 knots, this can be noticed already from the required tail rotor collective for trimmed flights in Figure 4.5b, where the collective increases while the thrust from Figure 4.5a remains reasonably constant. For 30 knots, the tail rotor collective has increased since a wind azimuth of -60 degrees; however, the tail rotor thrust is also growing. This changes after the wind azimuth is more negative than -90 degrees, where the thrust decreases while the collective increases. On the other hand, the tail rotor collective variation concerning the wind azimuth at 20 knots is not so significant, and the trend is smooth. Therefore, the flow field dependence on the wind azimuth, which is more noticeable for higher speeds, is causing the vortex ring state to appear for wind azimuths lower than -90. Meanwhile, for more positive wind azimuths, it is not so significant. The average flow streamlines for wind azimuths of -75 and -105 degrees for 25 knots and -120 and -60 degrees for 30 knots are computed to prove this dependence on the wind azimuth. These wind azimuths are chosen because the tail rotor creates a similar thrust to be compared more easily. The results are illustrated in Figure 4.27. Flying at 30 knots and a wind azimuth of -60 degrees does not create any circulating streamlines around the tail rotor plane. Therefore, the tail rotor inflow is unaffected, and less collective is needed to have similar effective angles of attack and generate a similar thrust.

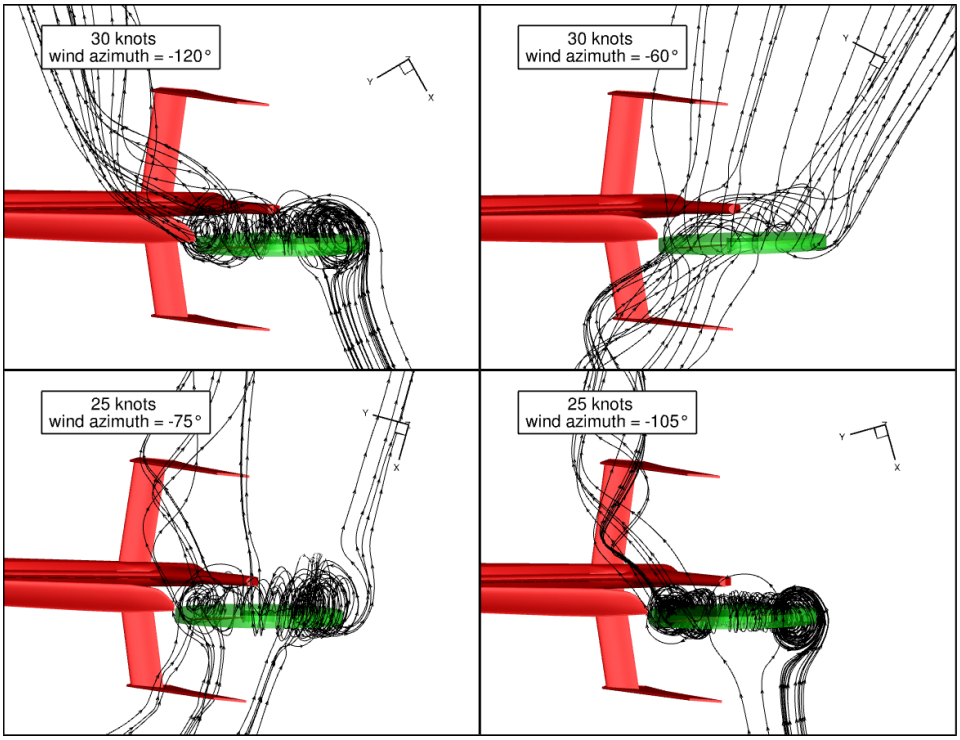

Figure 4.27: Streamlines from the averaged flow field at wind azimuths -75° and -105° for 25 knots; -60° and -120° for 30 knots.

4.3.1.1. Tail Rotor at Tail Boom Height

From the results in section 4.1, it was noticed that the tail rotor aerodynamics were affected by the disturbed vortex ring state for a broader range of freestream velocities compared to the original tail rotor configuration. So, it is intended to look over the influence of lowering the tail rotor height to the tail boom's height when it comes to the appearance of the vortex ring state. In Figure 4.28, 3D images are shown for the flow field at a freestream velocity of 20 knots for two instants in time separated by roughly 70 main rotor degrees and the averaged flow field over two main rotor revolutions. It is observed that the vortical structures, regions where the streamlines circulate the most, around the tail rotor tips are not so disturbed compared to the results observed for the original tail rotor location in Figure 4.24. This occurs because the tail rotor blades are further away from the main rotor. Therefore, the strength of the accumulated vorticity around the tail rotor blades' tip is higher, as can also be observed comparing Figure 4.28 with Figure 4.23 and Figure 4.24.

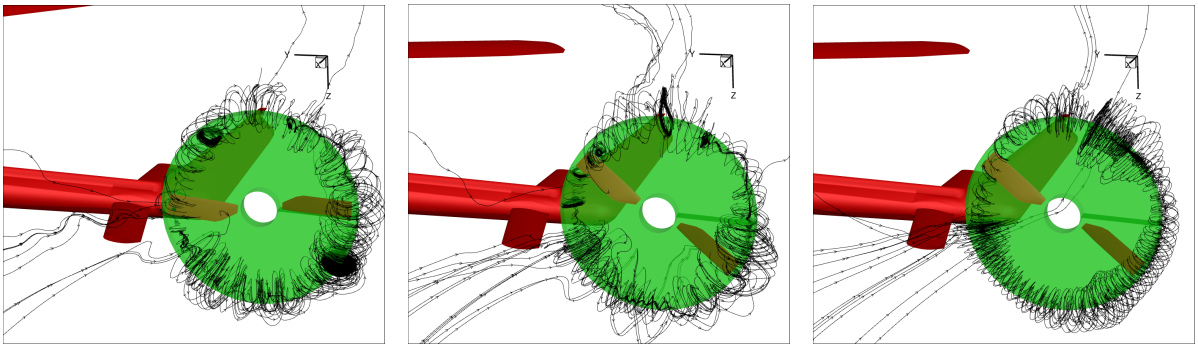

(a) Instant streamlines at $t = t^*$.

(b) Instant streamlines at $t = t^* + 2.9 \cdot 10^{-3}$.

(c) Averaged flow field streamlines.

Figure 4.28: Instant and averaged streamlines through the tail rotor volume, depicted in green, located at the tail boom height.

Following the same procedure as the original tail rotor configuration, the streamlines for a wind azimuth of -90 degrees are plotted for all the range of freestream velocities. This results in the figure illustrated in Figure 4.29.

The vortex ring state around the tail rotor blades' tip is observed to behave similarly to the original tail rotor configuration. In particular, at lower speeds, the cores of the vorticity are located upstream, are large and have low strength. The location of the vortices moves from the left of the tail rotor to the right of the tail rotor if the freestream velocity is increased. Additionally, the vortices' size is reduced when the freestream velocity is increased, so the most affected wind velocities are around 20 knots. Although for a wind azimuth of -90º the 2D flow field is similar to the original tail rotor configuration, it is known from the 3D flow field pictures that lowering the tail rotor location causes less disturbance at the rotor azimuths closer to the main rotor blade's tip. The main difference caused by lowering the tail rotor location is to reduce the tail rotor thrust when the wind azimuths become more negative than -90º which is observed from comparing the thrust and tail rotor collectives already presented in section 4.1.

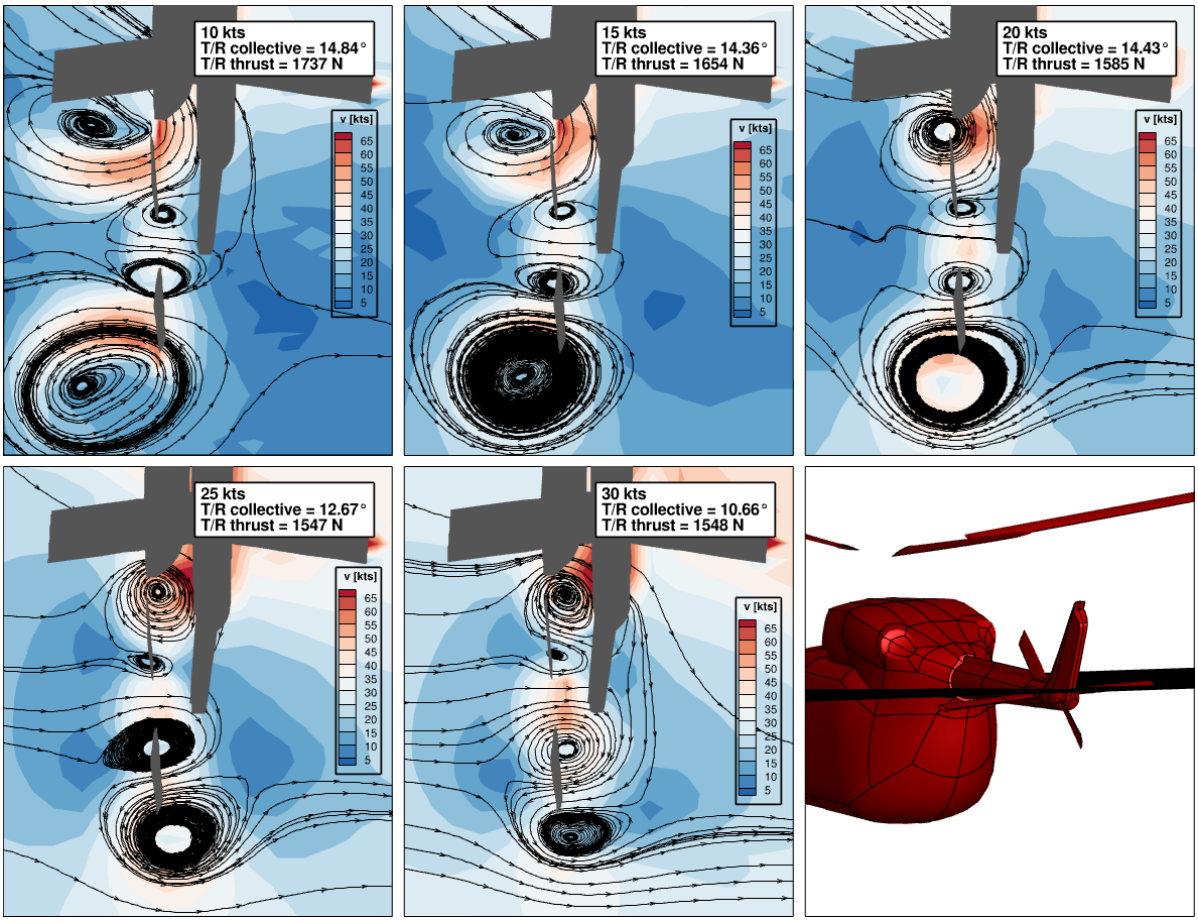

Figure 4.29: Slice of the flow field for tail rotor located at tail boom height averaged over two main rotor revolutions through tail rotor centre showing streamlines for different freestream velocities and a wind azimuth of -90 degrees. The last picture in red shows the location of the slice through the helicopter.

To prove the effect of lowering the tail rotor location at the tail boom's height, two simulations are run, with the only change being the location of the tail rotor. Since the most significant differences caused by lowering the tail rotor location are for wind azimuths around -90º to -135º, the influence of reducing the tail rotor location is investigated for a flight at 25 knots and wind azimuth -105º. The helicopter motion obtained from the trimmed flights at 25 knots and wind azimuth of -105º is simulated again by only lowering the tail rotor location to the tail boom's height. This will effectively isolate the influence of changing the tail rotor location since the helicopter controls are the same. The thrust obtained from the two simulations is compared in Figure 4.30a, where it is observed that lowering the tail rotor at the tail boom's height reduces the tail rotor thrust. The origin of this reduction in thrust is attributed to a decrease in the effective angle of attack as observed from the difference in the effective angle of attack over the tail rotor plane between the original configuration and the configuration with the lower tail rotor location shown in Figure 4.30b, where the difference is positive for almost all the rotor plane indicating that the angle of attack for the original configuration is higher for most of the rotor plane regions that

contribute the most to the integrated thrust (≈ 70% radial stations). The effective velocities at the blades' sections are slightly higher for the tail rotor at the tail boom configuration for most of the tail rotor plane. However, the relative change is minimal, so it does not contribute significantly to the change in thrust. Additionally, notice that the relative change in the effective velocity is positive for regions located close to the main rotor blades, indicating that the influence from the main rotor blades is reduced, as the relative difference in the induced velocities from the main rotor indicates in Figure 4.30c.

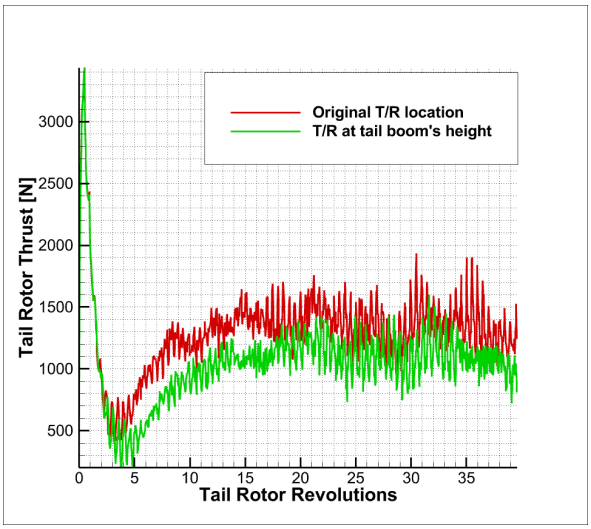

(a) Thrust comparison.

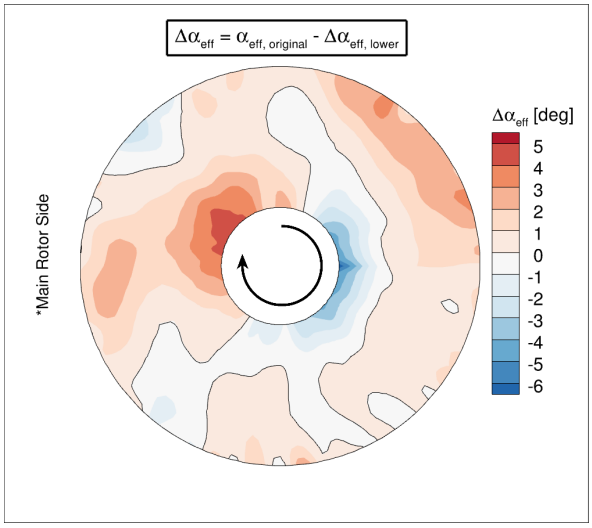

(b) Difference in the effective angle of attack. The solid line indicates the border between positive and negative values.

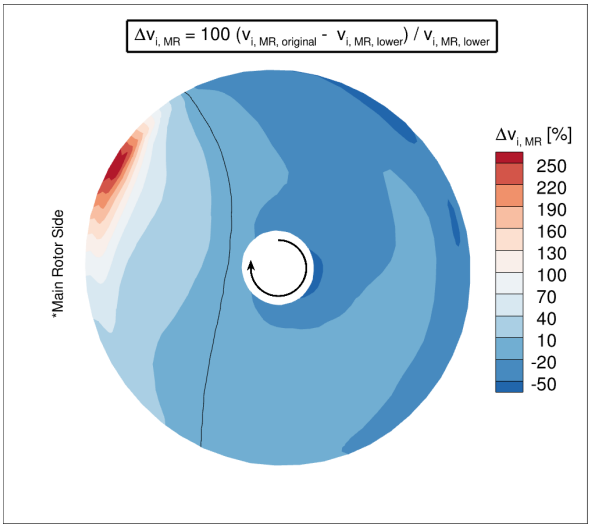

(c) Induced velocities from the main rotor.

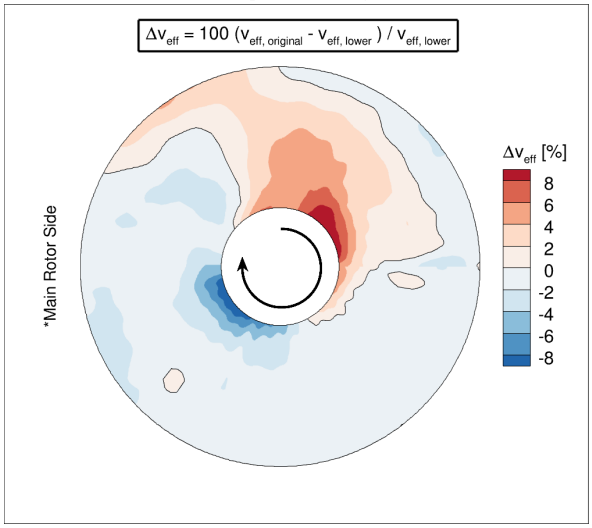

(d) Difference in the effective velocity seen at the blade sections. The solid line indicates the border between positive and negative values.

Figure 4.30: Thrust, effective angle of attack, induced velocity from the main rotor and effective velocity difference for original tail rotor configuration against tail rotor at tail boom's height.

Finally, the physical explanation of the decrease in tail rotor thrust is that the lower disturbance from the main rotor tip vortices helps the formation of a stronger vortex around the tail rotor blade tips. Therefore, the more organised the accumulated vorticity is, the more inflow will be produced on the tail rotor plane. In Figure 4.31, the streamlines of the averaged flow field for the two configurations with the same flight conditions evaluated in the last case are shown. The streamlines show higher accumulation around the tail rotor when the rotor's location is lower than the higher configuration, and this is especially noted at the rotor azimuth regions closer to the main rotor.

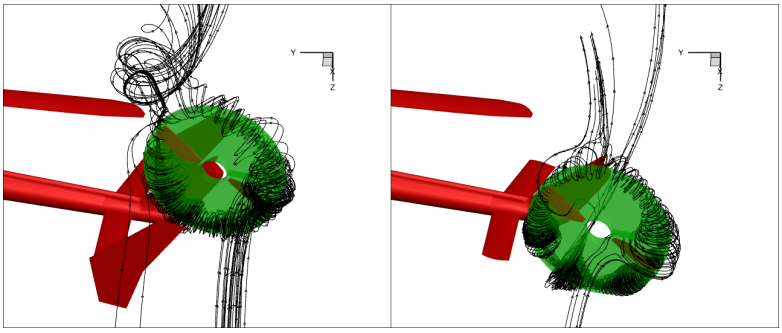

Figure 4.31: Streamlines of the averaged flow field for a freestream velocity of 25 knots (12.86 m/s) and wind azimuth of -105°. Left shows original tail rotor configuration and right shows tail rotor at the tail booms height.

4.3.1.2. Main Rotor not included

To prove that the main rotor is causing a disturbance on the tail rotor vortex ring state, a simulation was run with the same helicopter motion for a trimmed 20 knots and -90º wind azimuth case but without the computation of the main rotor component in UPM. Therefore, the loads and tail rotor aerodynamics can be directly compared, and the difference can be related to the main rotor influence. The comparison in the thrust Figure 4.32a shows that the tail rotor thrust is reduced when the main rotor is removed. Furthermore, it takes some time to reduce the thrust, which can be attributed to the formation of VRS at the tail rotor. The streamlines can be compared in Figure A.4 and Figure A.5. The cause of the reduction in thrust can be directly attributed to a decrease in the effective angle of attack at the blades, as observed in Figure 4.32d. Moreover, it is observed that the relative increment in effective velocities in Figure 4.32c is not very significant. However, it indicates that the regions closer to the main rotor side see an increased effective velocity, indicating that the main rotor was influencing those regions. Therefore, to summarise, the effect of the main rotor is to weaken the formation of the vortex ring state at the tail rotor.

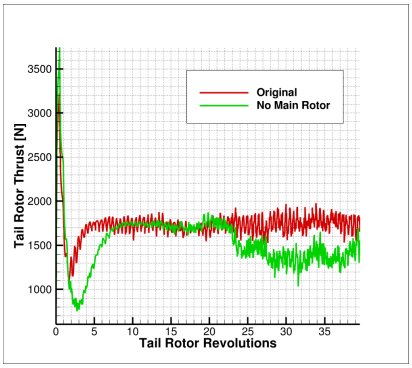

(a) Thrust over tail rotor revolutions.

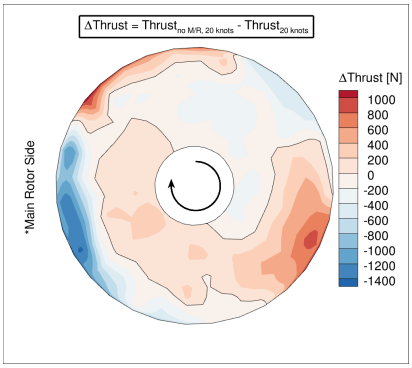

(b) Increment in tail rotor local thrust.

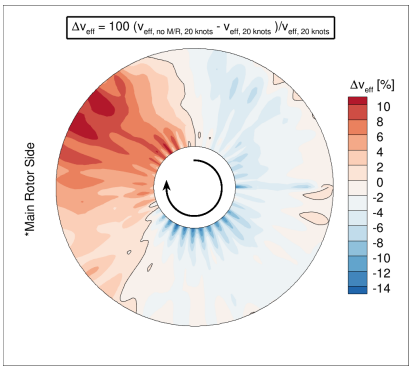

(c) Increment in tail rotor blades' effective velocity.

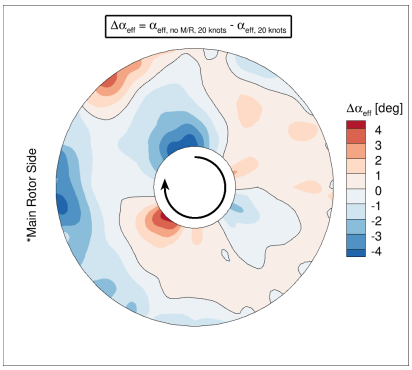

(d) Increment in tail rotor blades' effective angle of attack.

Figure 4.32: Comparing thrust, effective velocity and effective angle of attack over the tail rotor plane for the isolated tail rotor. Helicopter motion from trimmed 20 knots and -90º wind azimuth flight.

4.3.2. Main Rotor Wake Interactions

The tail rotor is especially vulnerable to the interference of the main rotor wake since it is located just behind the main rotor. I section 4.1, the interactions due to the main rotor wake were suspected when the results from the original tail rotor configuration were compared to the results from the tail rotor rotating in the opposite direction, top forward, were the latter was observed to require more collective to produce the same thrust. The comparison of the coupled Gensim results with the standalone Gensim simulations also showed a difference in the transferred loads during the coupling at the tail rotor when it was operating under the influence of the main rotor wake. However, how this interaction affects the tail rotor aerodynamics must be investigated, and the results are presented in this section. For the analysis, the first UPM simulation is compared between the top aft and top forward configurations since the first simulation has the same motion obtained from the first Gensim simulation and can indeed be compared.

The first analysis is to study the flow field around the tail rotor in a forward flight with a freestream velocity of 30 knots. A profile section of the helicopter and the velocity field are shown in Figure 4.33. Since the main rotor is creating thrust, it accelerates the flow in its control volume by adding a perpendicular velocity to the rotor plane and, in a lower amount, a swirl component, making the wake rotate due to the torque. Combining these induced velocities from the main rotor and the freestream creates the main rotor wake. It is observed that the wake is a region of higher local velocities and is tilted depending on the freestream velocity. Additionally, in a forward flight, the main rotor wake produces two super-vortices, resulting from the superposition of the tip vortices released from each blade thanks to the freestream convection. Note that when the freestream velocity is higher, these super-vortices will be more concentrated and have higher local velocity changes. From Figure 4.33, it is observed that the higher velocities from the main rotor wake interact with the tail rotor approximately for half of the tail rotor area.

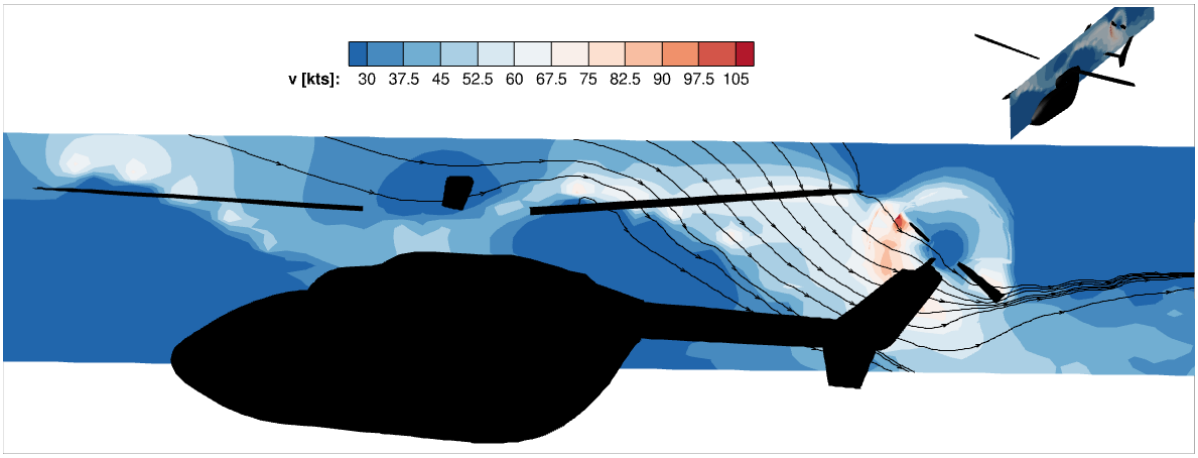

Figure 4.33: Flow field around the helicopter with tail rotor rotating top aft for a forward flight (0 degrees wind azimuth) and 30 knots. Showing a slice in the x-z plane through the tail rotor plane.

Such interaction increases thrust for the top aft configuration as shown in Figure 4.34a. In particular, the interaction modifies the effective velocity field around the tail rotor blades. For the tail rotor rotating top aft, the tail rotor blades are experiencing a higher relative tangential velocity due to the induced velocities from the main rotor wake in the x-z plane. To prove this, the difference in local tail rotor loads over the tail rotor plane are illustrated in Figure 4.34b for the tail rotor configuration rotating top aft and top forward. The first observation is that when the rotor is rotating top aft, the local loads are higher around the azimuths where the main rotor wake interacts most significantly with the tail rotor, which is the bottom left region and is indicated with a higher positive difference. On the other hand, the upper right area is experiencing a negative difference in local loads, meaning that the tail rotor rotating top aft is creating less thrust locally in that region. Nevertheless, notice that the minimum decrease in local thrust has a lower magnitude than the increase in local thrust; thus, the integrated thrust results in a higher tail rotor thrust. The interference of the main rotor wake with the tail rotor is increasing significantly the dynamic pressure, as can be observed from the difference in effective velocities over the tail rotor plane in Figure 4.34c. The effective velocity is directly proportional to the dynamic pressure from $q = \rho v_{eff}^2/2$ since the aerodynamics code is based on a constant density formulation. The effective angle of

attack is illustrated in Figure 4.34c, where the rotor azimuths are approximately divided into two areas, one where the top aft configuration shows higher effective angles of attack and the other where the top forward is higher. The increase in the angle of attack itself doesn't mean that the final loads will be higher, as observed for some rotor azimuths, since the dynamic pressure plays a vital role in this case as the increase in the dynamic pressure represents a high relative change, see Figure B.1b in the appendix for further information. The combination of the increment in the angle of attack and the increase in the dynamic pressure increases the local loads observed in Figure 4.20. In general, in the regions where the tangential velocity at the blades' coordinate system increases, the effective angle of attack also increases; this is the reason why the border between the positive and negative difference is similar to the border observed for the effective velocity as the differences in the effective velocities are primarily due to changes in the tangential velocity since the tail rotor is oriented perpendicular to the main rotor and parallel to the fin.

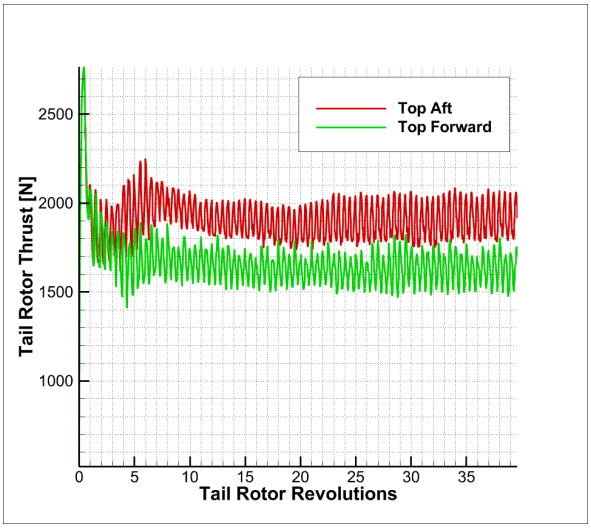

(a) Thrust over tail rotor revolutions.

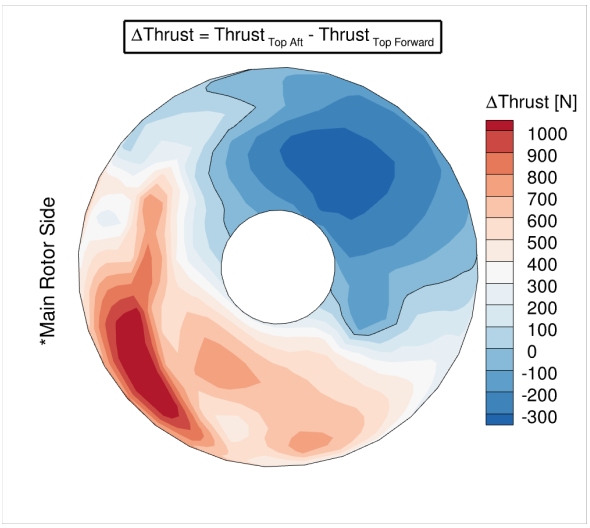

(b) Increment in tail rotor thrust.

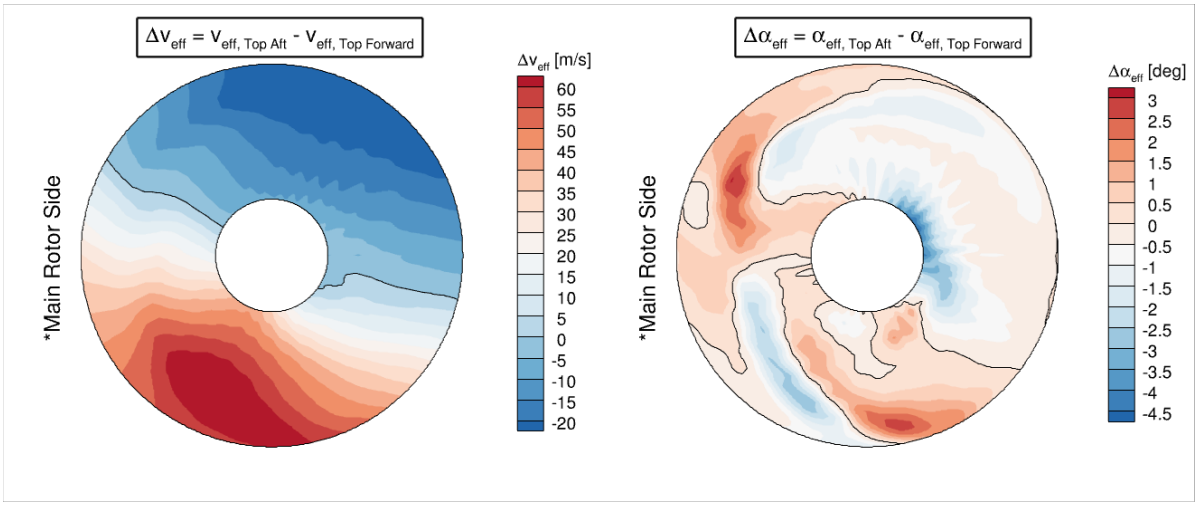

(c) Increment in tail rotor blades' effective velocity and effective angle of attack.

Figure 4.34: Comparing thrust, effective velocity and effective angle of attack over the tail rotor plane for the tail rotor rotating top aft and top forward. Freestream velocity is 30 knots, and wind azimuth is 0º. Solid lines indicate the border between positive and negative.

To assess how the main rotor wake interferes with the tail rotor for other wind azimuths, two cases are explored: quartering flight to the left and the right at 30 knots, which means wind azimuths of -50º and 50º degrees. The range of wind azimuths between -50º and 50º is expected to have the same interaction as observed in forward flight, with slight variations in the tail rotor aerodynamics due to the sideslip. However, when the helicopter's wind azimuth starts to be close to -50º and 50º, the interaction with the tail rotor by the super-vortices shedded from the main rotor plane due to the superposition of the individual blades' tip vortices is also of interest. This is

because of the possibility of having the super-vortex directed through the centre of the tail rotor and influencing all the tail rotor planes. Starting with a wind azimuth of -50 degrees, the two tail rotor configurations, top aft and top forward were evaluated since the effect can be noticed. The flow field of such flight condition is shown in Figure 4.35, where it can be observed that the streamlines gain a swirl component in the freestream direction, which finally interacts almost perpendicular to the tail rotor plane.

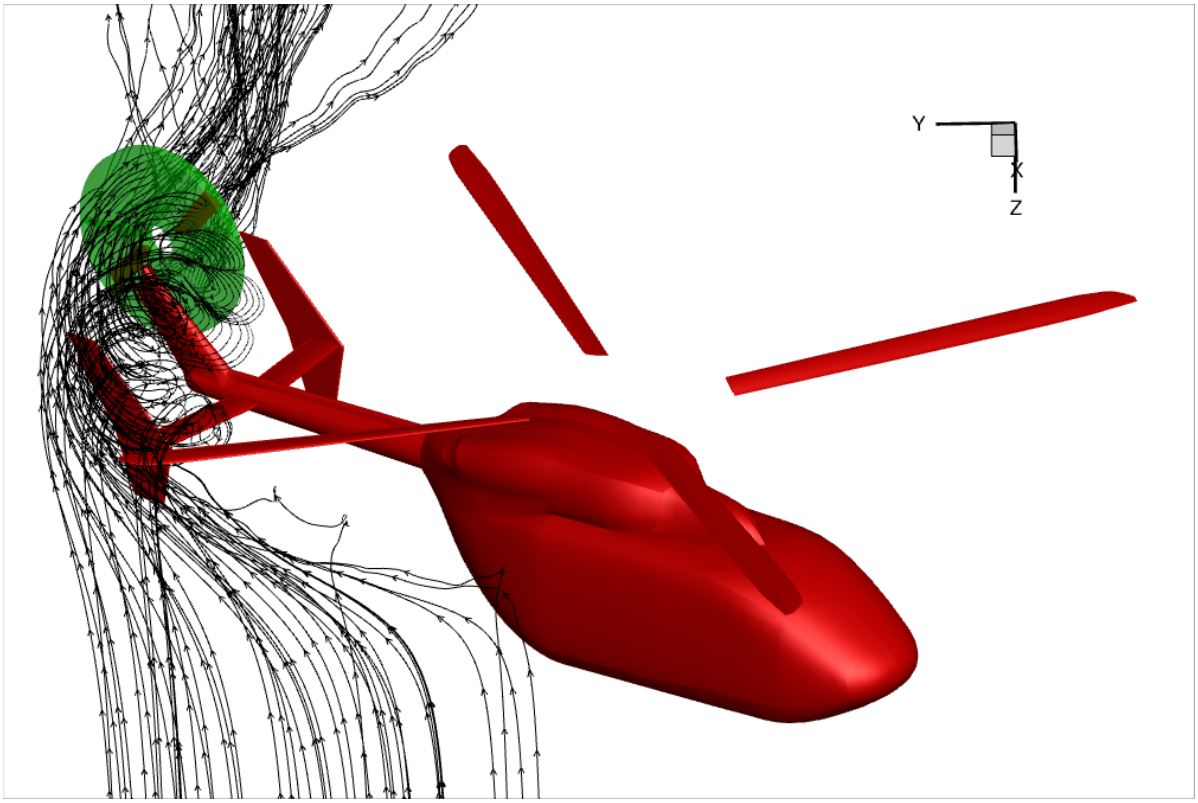

Figure 4.35: Streamlines of the flow field for the helicopter flying at 30 knots and a wind azimuth of -50°.

Comparing the two tail rotor configurations for the forward flight case results in the figures shown in Figure 4.36. The tail rotor thrust, shown in Figure 4.36a, is decreased for the top forward configuration, as was in the forward flight case, and as expected from the results in section 4.1. The local difference in the loads is higher for the bottom left azimuths and lower for the top right azimuths. Although the accumulated vorticity from the main rotor blades is interfering with the tail rotor, there is still a main rotor wake with high downwash that interferes with the corner of the tail rotor, which is closer to the main rotor plane in a similar way as for the forward flight. The influence of the super-vortices interfering with the tail rotor can be noted from a reduced negative difference in Figure 4.36b compared to the forward flight investigation observed in Figure 4.34b. If the change in the effective velocity at the tail rotor is analysed from Figure 4.36c, the rotor azimuths with a higher increment in the effective velocity are concentrated to the lower left corner of the rotor, due to the main rotor downwash still highly interfering with the tail rotor. However, the positive increment gained by using a top aft configuration is spread throughout a more considerable amount of tail rotor azimuths than the forward flight case thanks to the interaction from the super-vortices shedded from the main rotor. The effective angle of attack is increased for the majority of the tail rotor plane when the top aft configuration is used, thanks to the increase in the tangential velocity at the blade sections caused by the combination of the super-vortices and the main rotor downwash. Notice a small region with a negative increment in the angle of attack at the lower corner of the tail rotor. This is attributed to the downwash increasing the rotor inflow and reducing the effective angle of attack as it interacts with the tail rotor with a significant perpendicular component. The reduction of the negative increment zones at the tail rotor plane observed for the local thurst, effective velocity and effective angle of attack are caused because the freestream flow interacting with the super-vortices gain a significant velocity component on the y-z plane (plane perpendicular to the flying direction) which results into a spiral flow moving downstream and rotating in the negative x-direction, clockwise for the left side super-vortex as observed from the front. Therefore, since the tail

rotor top aft configuration rotates the blades in the counterclockwise direction as observed from the front, the interaction of the super vortex with the tail rotor is causing an almost complete increase in the effective velocity over the rotor plane. Hence, when the top forward configuration was tested, the exact opposite effect appeared. Nevertheless, the top forward configuration was generating more thrust than the top aft over a small region of rotor azimuths, which is attributed to the fact that the flow field is not only influenced by the super-vortices but also by the main rotor downwash, which is giving a strong velocity component in the x-z plane. This component influences the tail rotor aerodynamics, as was studied for the forward flight, where the main rotor wake positively impacted the lower half of the rotor plane for a top aft configuration.

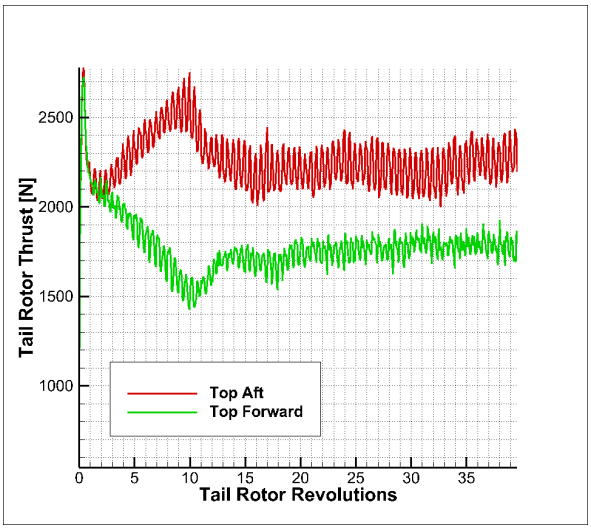

(a) Thrust over tail rotor revolutions.

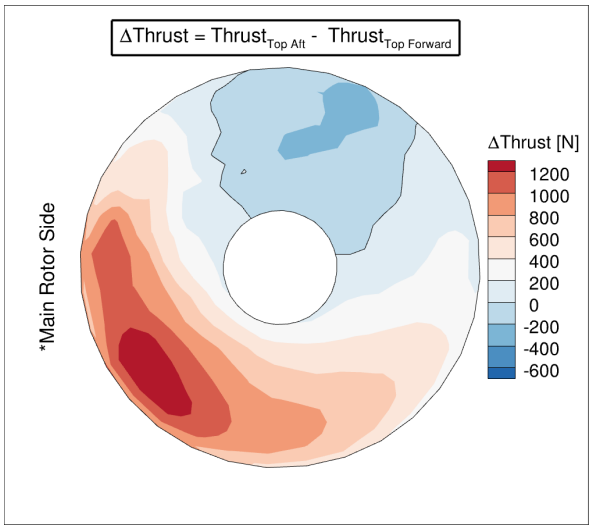

(b) Increment in local tail rotor thrust.

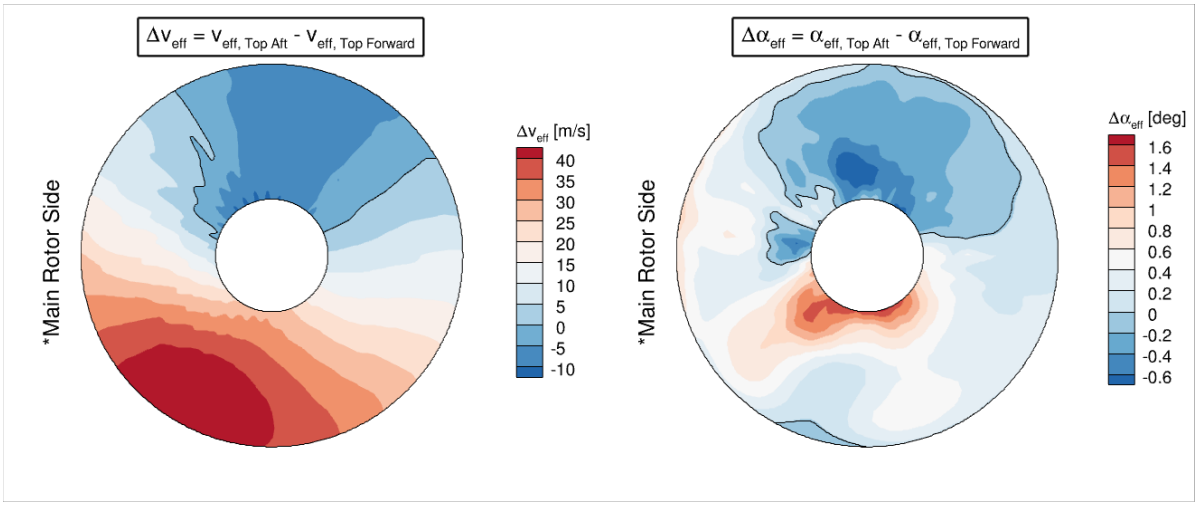

(c) Increment in tail rotor blades' effective velocity and effective angle of attack.

Figure 4.36: Comparing thrust, effective velocity and effective angle of attack over the tail rotor plane for the tail rotor rotating top aft and top forward. Freestream velocity of 30 knots, and wind azimuth is 50º. Solid lines indicate the border between positive and negative.

The opposite wind azimuth, 50º, is now being investigated. The average flow field streamlines for this case are illustrated in Figure 4.37. From this image, it can already be noticed that the streamlines are taking different paths compared to the previous case for a wind azimuth of -50º. Now, for a wind azimuth of 50º, the flow field interacting with the tail rotor is a priori the same as it was for -50º. However, a freestream velocity component is against the tail rotor wake. For this reason, the flow field behaves differently from the previously investigated case, and a small amount of recirculation appears at the tail rotor tips. However, the super vortex and the main rotor downwash greatly disturb the accumulation of vorticity at the tail rotor tips.

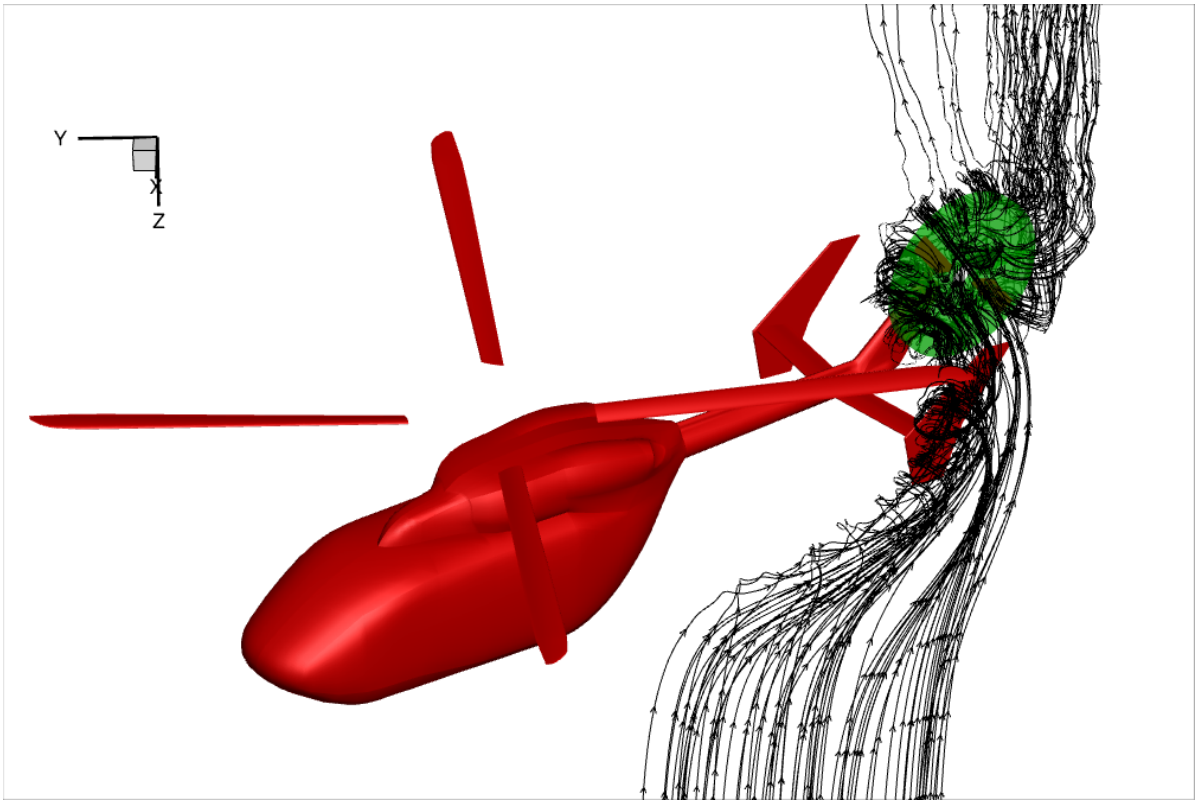

Figure 4.37: Streamlines of the flow field for the helicopter flying at 30 knots and a wind azimuth of 50°.

The tail rotor thrust for the top aft and top forward configurations from Figure 4.38a shows that there is almost no dependence on the tail rotor direction of rotation when the wind azimuth is -50º, where the tail rotor top forward indicates a slight reduction in thrust. From the difference in the local loads over the tail rotor plane in Figure 4.38b, the tail rotor rotating top aft shows a higher local thrust for the majority of the tail rotor plane areas and some decrease in a lower amount of regions. However, the value of such an increment is small, resulting in a slightly increased integrated thrust as observed from the thrust over the tail rotor revolutions. The results from the local thrust differences also show that the tips of the left rotor plane show a higher increment. Thus, these regions are more influenced by the main rotor wake and the rotation direction. Such a local thrust distribution results from changes in the effective velocities and angle of attack at the blade sections. For instance, the effective velocity increases for the lower left part of the tail rotor plane. In contrast, the upper tail rotor area experiences a reduction of the effective velocity. In parallel, the effective angle of attack shows small distributed positive and negative increments over the tail rotor area. Even though the increment in the effective velocity is higher for the lower tail rotor region and lower for the upper region, the combination with the changes in the angle of attack results in the distributed increment in local thrust. The slight increase in tail rotor thrust observed at the rotor azimuths closer to the main rotor when the tail rotor rotates top aft is because, in this case, the effective angle of attack has increased. Hence, it can be stated that for this wind azimuth, the differences in the local thrust over the tail rotor plane can be attributed to the differences in the angle of attack. On top of that, in the regions where the effective velocity changes the most, this increase or decrease in the effective velocity contributes the most and dominates the resulting local thrust. In conclusion, the differences between the tail rotor rotating top aft and top forward are insignificant for right quartering flights (positive wind azimuths), meaning that the main rotor wake is starting to lose its influence on the tail rotor. This is due to the freestream velocity component perpendicular to the tail rotor plane, which is beginning to cause the accumulation of vorticity at the tail rotor tips, indicating the development of the vortex ring state, so the combination of this vorticity with the vorticity induced by the main rotor blade tips passing results into a disturbance of the flow field at the tail rotor azimuths closer to the main rotor. Hence, the main rotor wake is less effective.

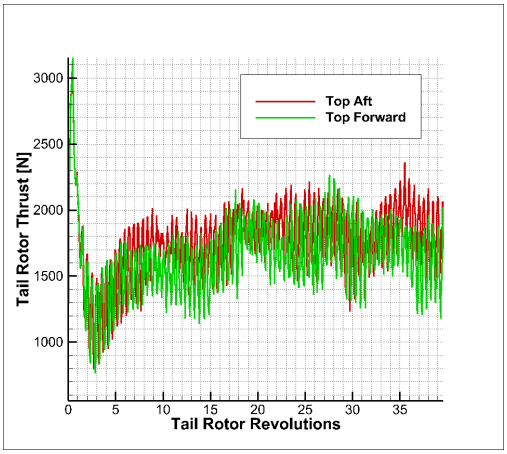

(a) Thrust over tail rotor revolutions.

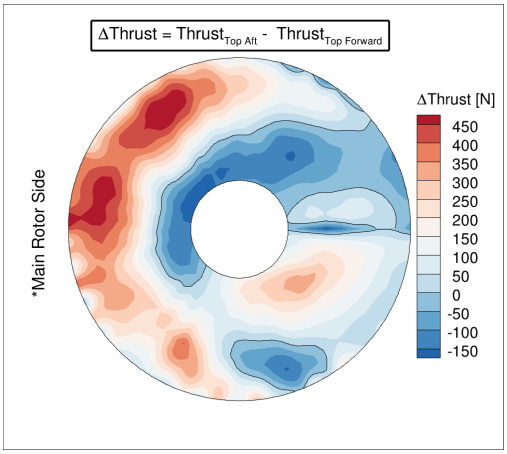

(b) Increment in local tail rotor thrust.

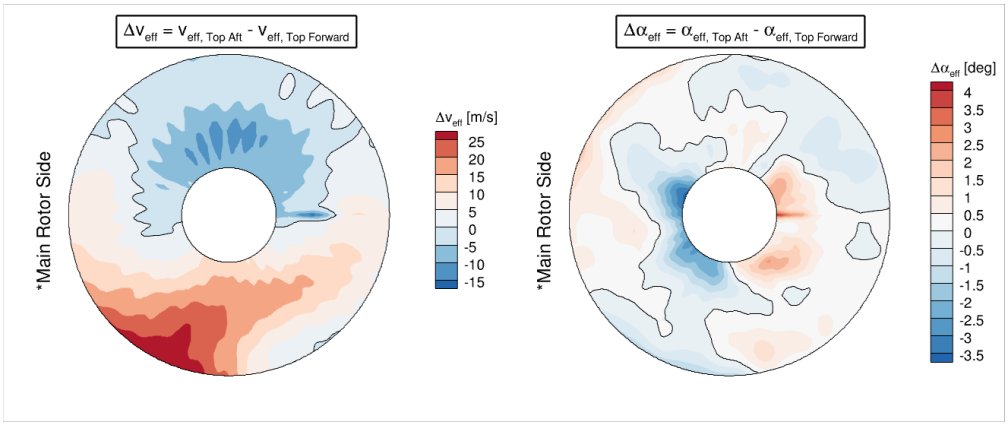

(c) Increment in tail rotor blades' effective velocity and effective angle of attack.

Figure 4.38: Comparing thrust, effective velocity and effective angle of attack over the tail rotor plane for the tail rotor rotating top aft and top forward. Freestream velocity of 30 knots and wind azimuth is -50°. Solid lines indicate the border between positive and negative.

4.3.2.1. Tail Rotor at Tail Boom Height

Lowering the tail rotor location to the tail boom height results in greater interaction between the main rotor wake and the tail rotor. This is observed from a flow field description shown in Figure 4.39 for a forward flight at 30 knots. The picture shows that the tail rotor is fully immersed in the main rotor wake.

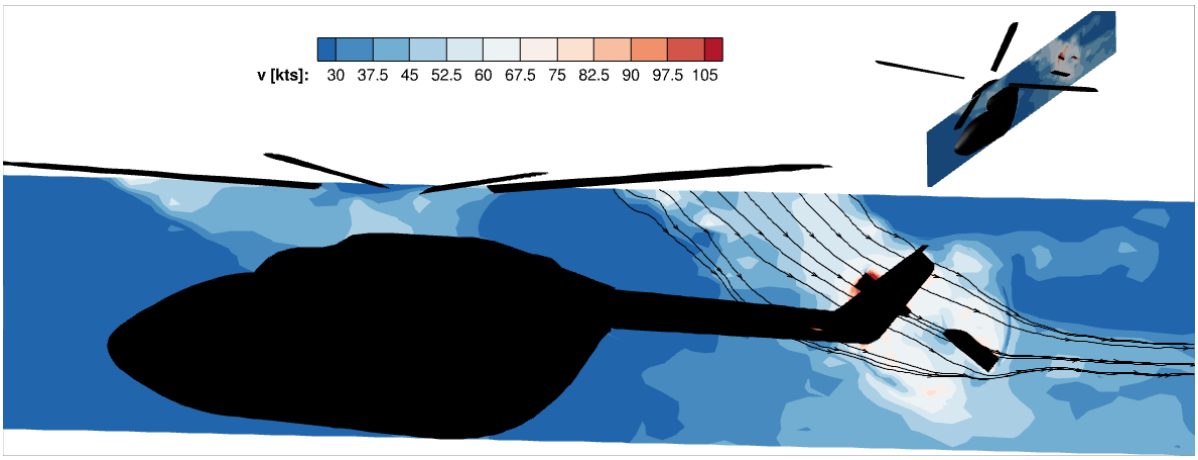

Figure 4.39: Flow field around the helicopter with tail rotor rotating top aft and located at the tail boom height for a forward flight (0 degrees wind azimuth) and 30 knots. Showing a slice in the x-z plane through the tail rotor plane.

To investigate the effects of the interaction of the main rotor wake with the tail rotor, the 30-knot forward flight is also simulated with a top forward configuration using the same helicopter motion. The thrust over the tail rotor revolutions is pictured in Figure 4.40a. The difference between the tail rotor rotating top aft and top forward is almost negligible compared to the results obtained for the higher tail rotor location from the original configuration. If the difference in the local loads from Figure 4.40b are considered, approximately the lower half of the tail rotor shows an increased amount of local thrust while the upper part shows a decrease. Nevertheless, the upper part is not entirely negative but contains a positive region. Therefore, the integrated thrust is slightly higher for the top aft configuration. The combination of a higher effective velocity at the lower half of the tail rotor and a distributed higher effective angle of attack results in the increased local thrust. Notice that for the upper part of the tail rotor, the positive regions are caused by the significant increase in the angle of attack that compensates for the decrease in the effective velocity. These results are expected since the tail rotor is fully immersed in the main rotor wake. Therefore, the rotation direction won't significantly affect the generated thrust. However, the slight difference in thrust is attributed to the orientation of the slightly tilted main rotor wake, and the tips of the tail rotor plane further away from the tail boom are less influenced compared to the inner sections.

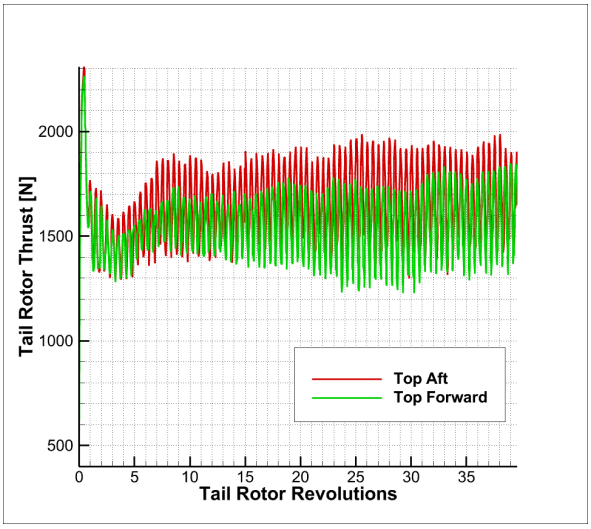

(a) Thrust over tail rotor revolutions.

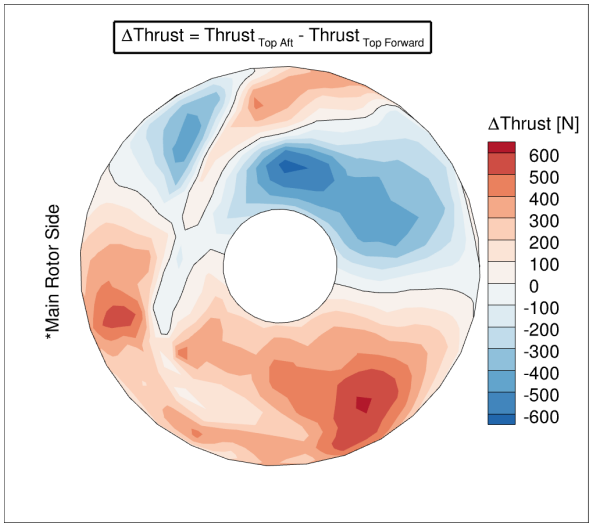

(b) Increment in local tail rotor thrust.

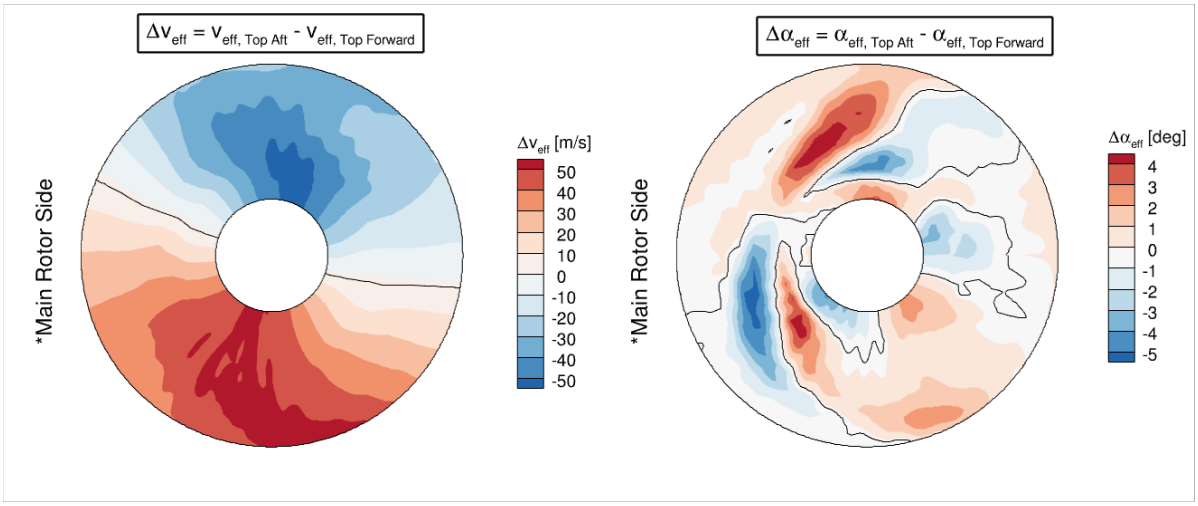

(c) Increment in tail rotor blades' effective velocity and effective angle of attack.

Figure 4.40: Comparing thrust, effective velocity and effective angle of attack over the tail rotor plane for the tail rotor rotating top aft and top forward. The Rotor is located at the tail boom's height, a freestream velocity of 30 knots, and a wind azimuth of 0º. Solid lines indicate the border between positive and negative.

4.3.3. Summary

The influence of the tail rotor aerodynamics on the tail rotor vortex ring state and the main rotor wake interference have been investigated in detail. It was observed that the tail rotor vortex ring state could instead be called disturbed vortex ring state at the tail rotor since the main rotor blades' tip vorticity is disturbing the flow field of the tail rotor azimuths closer to the main rotor plane, preventing a fully developed vortex ring state at the tail rotor. Nevertheless, the effect of the disturbed vortex ring state at the tail rotor is to reduce the integrated thrust due to a reduction in the effective angle of attack towards the tail rotor blade tips caused by the increased inflow over the rotor plane. The influence of the freestream velocity was to move the higher vorticity regions from the rotor's downstream to the upstream location of the rotor. As a result of the investigation at a wind azimuth of -90°, the disturbed vortex ring state at the tail rotor was observed to be reducing the thrust the most at freestream velocities close to 20 knots since the core of the accumulated vorticity was located right on the tail rotor plane. Additionally, the influence of the wind azimuth is a higher tail rotor thrust for wind azimuths closer to zero since the perpendicular component to the tail rotor is reduced and the main rotor wake is reducing the accumulation of vorticity at the tail rotor. The disturbed vortex ring state was observed to influence wind azimuths of -105 still ° or -120°, where the main rotor-induced velocity less influences the tail rotor plane. Lowering the tail rotor location reduced the thrust since the accumulated vorticity was observed to be higher due to the lower disturbance from the main rotor blade tip vortices. This was confirmed with the additional simulations run without the main rotor component simulated, which showed that the main rotor tip vorticity was weakening the formation of the vortex ring state at the tail rotor.

The influence of the main rotor wake on the tail rotor was assessed by analysis of the flow field, thrust obtained from the aerodynamics code, the local thrust, the effective velocities and the effective angle of attack over the rotor plane directly from the UPM simulations. The influence of the main rotor wake was noticed to be significant for forward flights, creating more thrust for a top aft configuration as a consequence of the partial interaction of the main rotor wake, which increased the effective velocity for a top aft configuration of those rotor azimuths which where interfered by the main rotor wake. For positive wind azimuths around 50°, the influence of the main rotor wake is mainly due to a combined downwash with the additional vorticity of the flow thanks to the superposition of the main rotor blades' tip vorticity which is then interfering with the tail rotor plane. Although the main rotor downwash is significant, it only intersects with the tail rotor at a limited rotor azimuth closer to the tail boom. In contrast, the other azimuths are affected mainly by the super-vortex interfering with the tail rotor and increasing the blades' effective velocity and angle of attack. For negative wind azimuths of -50°, the difference between the top aft and top forward configurations is barely noticed since the perpendicular freestream velocity component causes the disturbed vortex ring state to appear. Then, the main rotor wake influence is also not distinguished due to the dominant flow from the disturbed vortex ring state. Finally, lowering the tail rotor location to the tail boom height results in the tail rotor being directly immersed inside the main rotor wake; therefore, the differences between the top aft and top forward rotations are not remarkable, with minor discrepancies due to a slightly more influence at the inner tail rotor azimuths. Thus, the benefits of using a top aft configuration are only present for the tail rotor located at a high position.

4.4. Recovery Methods

This section aims to provide results to compare and discuss the recovery technique that must be used if the pilot is in an unintended yaw. From the previous sections, it has been proven that the helicopter will not enter an unintended yaw if the pilot is giving the correct pedal inputs to maintain the yaw trim. The manoeuvres and recoveries described in chapter 3 are considered for the simulation of an unintended yaw accident during an approach for landing; as described, the values for the manoeuvre variables that are controlled in the simulation are taken similarly from an actual accident of unintended yaw in the Airbus Helicopters fleet. In particular, the pilot's key actions are used as an orientation for setting up a realistic simulation. However, the control values are approximate, and the results can not be directly compared with the accident data since the helicopter was a H135. Three scenarios are considered: for. In contrast, three different pedal inputs are used in each case to recover the yaw trim.

The three scenarios share the same initial simulation phase. This phase consists of a slow-down manoeuvre from a forward velocity of 40 knots and a rate of descent of 200 feet per minute to a forward velocity of 26.67 knots and a rate of descent of 128 feet per minute in 6 seconds. To achieve this, the autopilot from Gensim controls all three helicopter attitude rates to zero to have a level flight. In contrast, it controls the vertical speed through main rotor collective changes. This level of flight is maintained for 3 seconds. Then, an increase in pitch attitude of 10 degrees is performed in the following 3 seconds to reduce the forward velocity effectively. The slow-down phase occurs in 6 seconds, ending at $t = 9\,s$. Afterwards, a pedal blockage is simulated, as was observed in the real accident, where the tail rotor collective is fixed to the value at $t = 9\,s$. Notice that when the helicopter slows down, the main rotor torque increases, requiring more left pedal input by the pilot. This inevitably increases the yaw rate since the helicopter is still slowing down, and the pilot is not applying any pedal input. Additionally, since the autopilot controls the helicopter's vertical speed, the main rotor collective is also increased to reduce the vertical speed, causing an increase in the main rotor torque that also contributes to the yaw rate. The three scenarios share the same solution until $t = 15.12\,s$. Then, in the first scenario, the helicopter continues flying with the same autopilot controls until the recovery is applied, consisting of different magnitudes of left pedal inputs. In the second scenario, the main rotor collective is increased by a 20% stick input in 6.05 seconds from $t = 15.12\,s$ to $t = 21.17\,s$. Afterwards, the recovery is applied through different left pedal inputs while the main rotor collective is simultaneously decreased to the original value at $t = 15.12\,s$. Finally, the last scenario consists of the same simulation solution as the second scenario until the recoveries are applied, where the difference is that the main rotor collective is not decreased during the recovery and is maintained. For all recovery methods, if the yaw rate is reduced to zero degrees per second, a final phase with all the attitude controls and vertical speed control is activated in the Gensim autopilot to run some extra seconds of level flight.

In the first scenario, the helicopter flies with a blocked pedal input as it was already flying until $t = 19.93\,s$, 10.93 seconds after blocking the pedal when the yaw rate has reached 98.2 deg/s. Now, three magnitudes of the left pedal position are tested to reduce the yaw rate to zero. In Figure 4.41, the helicopter flight variables and controls are shown for the initial phase and the three tested recoveries. Pay attention to the fact that when the recoveries are applied, the autopilot only controls the roll and pitch attitudes. The first recovery was to use a 10% step input in 0.5 seconds on the left pedal, which is equivalent to a 3.26 degrees increase in the tail rotor collective; the case is shown in Figure 4.41 as red. The immediate observed reaction is the increase in the tail rotor thrust and, consequently, an increase in the anti-torque, so the yaw rate decreases. The main rotor collective is constant, so the main rotor torque changes only due to changes in the freestream condition of the main rotor. However, when a 10% left pedal input is applied, the yaw rate does not reach a zero value in a feasible amount of time since at $t = 37.72\,s$, 17.79 seconds after using the left pedal input, the helicopter still has a yaw rate of 28.11 deg/s. The yaw rate is increasing or reducing depending on the helicopter's heading and pitch due to the vertical stabiliser and fuselage creating different anti-torque as they are a function of the helicopter's sideslip and angle of attack. Additionally, the rest of the helicopter attitudes also react to the high yaw rate and the change in the aerodynamic forces from each component. For instance, the pitch attitude slightly changes within a 1 degree margin while the roll attitude changes within an 8 degree amplitude. The forward, lateral and vertical velocities oscillate at an absolute velocity of around 15 knots. Considering that the pilot is in a stressful situation and the helicopter is challenging to handle with a yaw rate, this amount of left pedal input is considered not to recover the yaw trim. Considering that the pilot is in a stressful situation and the helicopter is challenging to handle with a yaw rate, this amount of left pedal input

If the left pedal input is now a 24% step input in 0.5 seconds, corresponding to a tail rotor collective increase

of 7.82 degrees, the results shown in Figure 4.41 as green are considered. The yaw rate is reduced to zero for this step input in just 2.69 seconds. Then, the autopilot for all helicopter attitudes and the vertical speed to zero is activated for a final phase. Similarly, if the maximum left pedal is applied in 0.5 seconds, corresponding to 44.4% of left pedal or 14.4 degrees of tail rotor collective, the yaw rate is reduced to zero in 1.35 seconds. Then, a final phase of level flight follows. For the recovered cases, namely a maximum left pedal input and a 24% pedal input, the helicopter had made 1.01 and 1.18 revolutions, respectively.

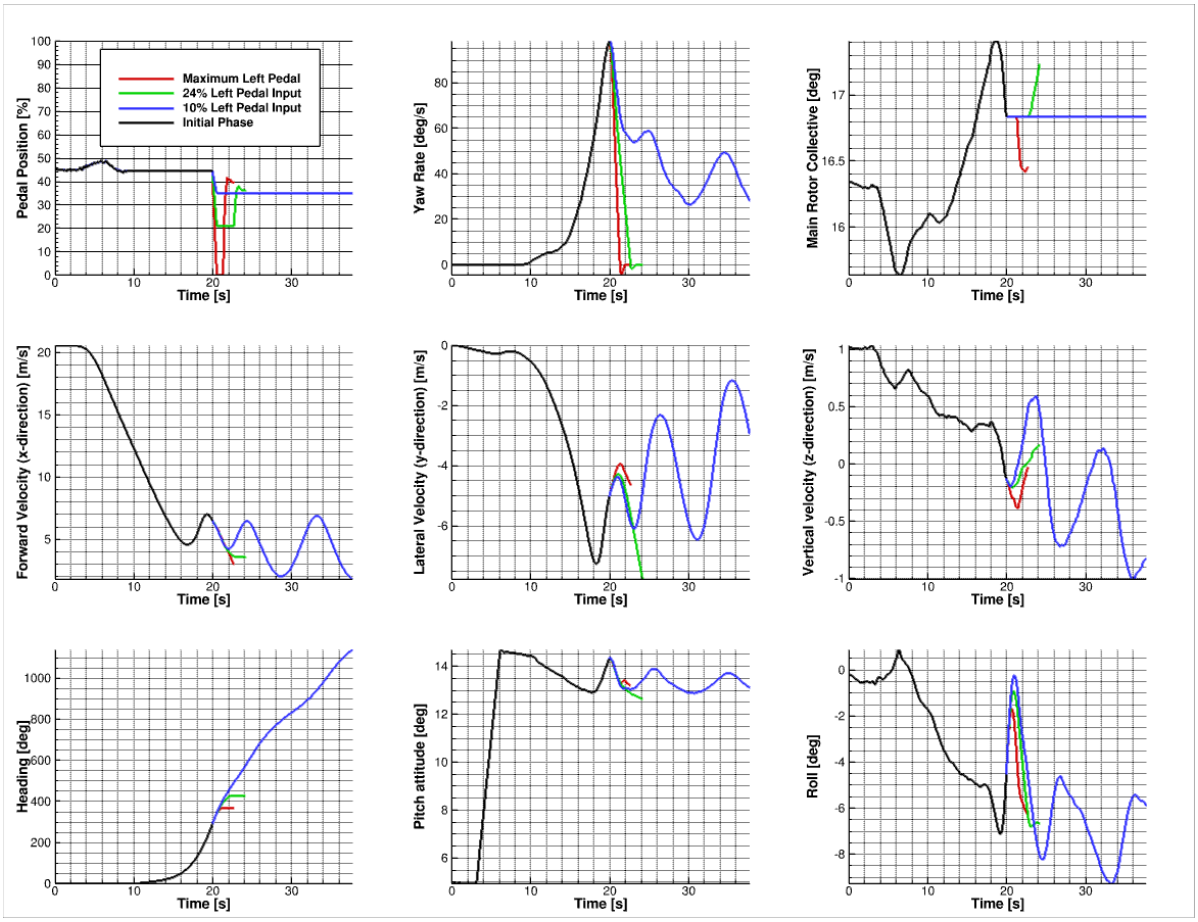

Figure 4.41: Evolution of helicopter variables during the unintended yaw simulation of an approach for landing. The pilot decreases the helicopter speed with a flare and recovers by applying pedal inputs. Three recoveries are tested.

The second scenario departs from the first scenario at $t = 15.12\,s$ by manually increasing the collective by a 20% collective stick increment in 6.05 seconds. This increases the collective stick from 73.5% to 93.5%, which or the main rotor collective from 16.6 degrees to 19.75 degrees. Afterwards, the magnitudes of three left pedal inputs are tested. When the recoveries are applied, the yaw rate has a maximum value of 120.5 deg/s. First, at $t = 21.1\,s$, a left pedal input of 10% is applied in 0.5 seconds while the main rotor collective is reduced back to 16.6 degrees simultaneously. The yaw rate for this amount of left pedal doesn't immediately respond to a decrease in the yaw rate. Instead, it slowly decreases until it almost reaches a zero yaw rate. More simulation time could not be simulated due to the lack of time; however, it is expected that a zero yaw rate will be reached nevertheless, as it takes 8.65 seconds to reach a yaw rate of 16.83 deg/s at the end of the simulation, which is considered to be too high for a feasible recovery. The subsequent recovery tested was a left pedal input of 24% applied in 0.5 seconds, and the main rotor collective was reduced back to 16.6 degrees in the same 0.5 seconds, resulting in the yaw rate being reduced to zero in 3.31 seconds. The reduction is practically instantaneous, and it takes around 0.4 seconds to achieve a negative yaw acceleration that reduces the yaw rate. When the maximum left pedal input is applied with the same reduction of the main rotor collective, the time to start the decrease in the yaw rate is 0.1 seconds, and the yaw rate reaches zero after 2.07 seconds. Notice that just before applying the recoveries, the helicopter reached a maximum vertical speed of -3 m/s or an ascent of 590 feet per minute due to the manual

increase in the main rotor collective. Then, this vertical speed is significantly reduced due to the reduction in the main rotor collective applied during the recovery. The forward speed continues to be reduced since the pitch attitude is maintained to high values, as observed also in Figure 4.42. The lateral velocity is diminished during the recoveries while the roll becomes more negative to compensate for the increase in tail rotor thrust. Since both pedal inputs can be recovered, a final phase of level flight is run to observe which values the controls take over. At the end of the 24% left pedal input recovery, the helicopter had made 2 full revolutions since the start, while for the maximum left pedal input recovery, it made 1.72 revolutions. A 10% left pedal input was not tested since it is expected to be recoverable

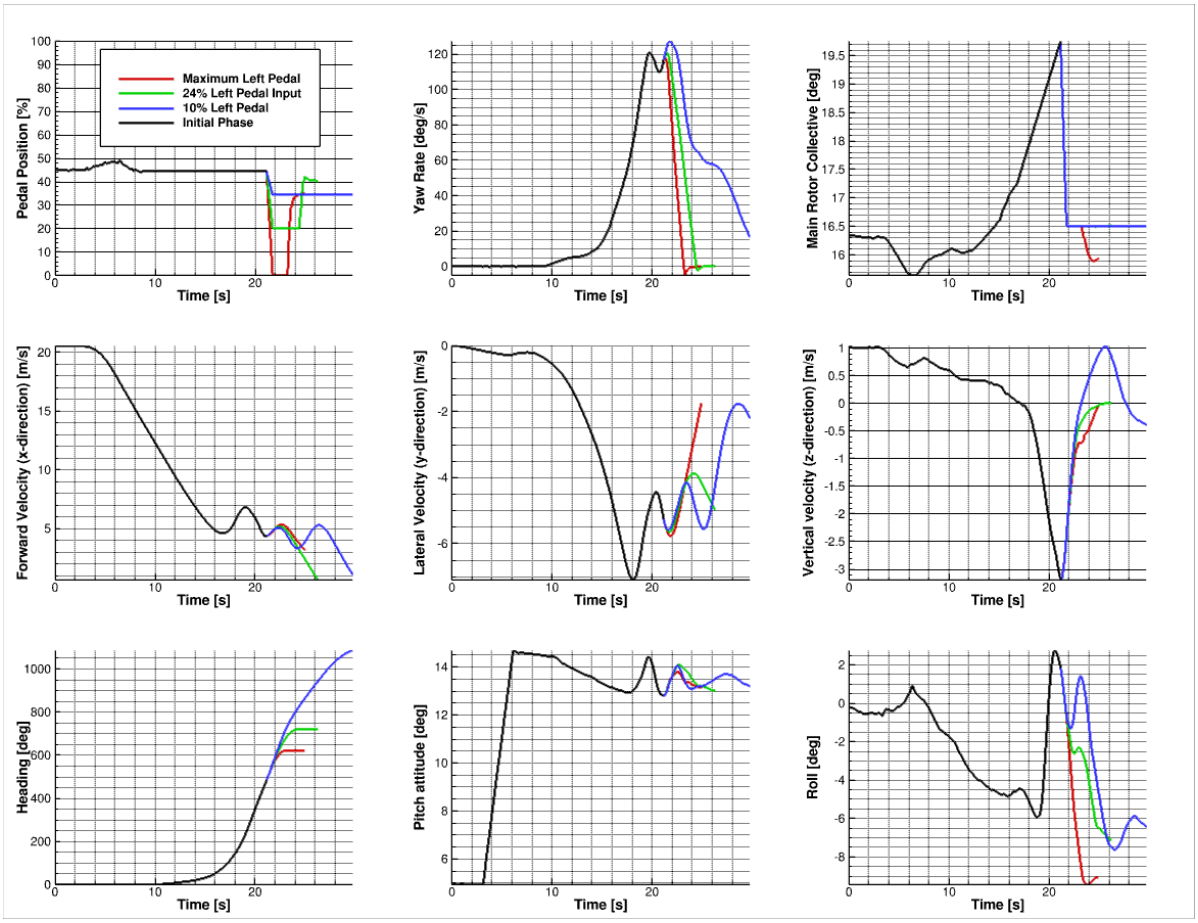

Figure 4.42: Evolution of helicopter variables during the unintended yaw simulation of an approach for landing. The pilot decreases the helicopter speed with a flare, increases the main rotor collective and then recovers by applying pedal inputs while decreasing the collective. Three recoveries are tested.

The last scenario is similar to the second scenario, except that the main rotor collective is not reduced when the pedal inputs are applied. The results are shown in Figure 4.43. For this case, applying a 10% left pedal input was insufficient to reduce the yaw rate. The yaw rate continued to increase due to the change in the helicopter heading. The forward and lateral speeds decreased in magnitude while the vertical speed grew. Since it was observed that a 10% left pedal input did not have any possibilities to recover the yaw trim, no more simulation data was stored and applying a 10% input was considered a failure to recover the yaw trim. When 24% of the left pedal is applied, the yaw rate is slightly reduced, but it reaches a periodically steady value of around 110 deg/s. The trend for the forward, lateral, and vertical velocities and helicopter attitudes was similar to applying a 10% left pedal input.

Ultimately, a maximum left pedal position is applied. This amount of left pedal effectively recovers the yaw rate, which reaches zero deg/s after 3.42 seconds of applying the pedal input. In this scenario, the maximum values reached for the vertical speed are around -6 m/s, equivalent to a rate of ascent of 1180 feet per minute. Hence, the helicopter climbs fast. After recovering, the helicopter has made 2 revolutions. Snapshots of the helicopter during the simulation are shown in Appendix C.

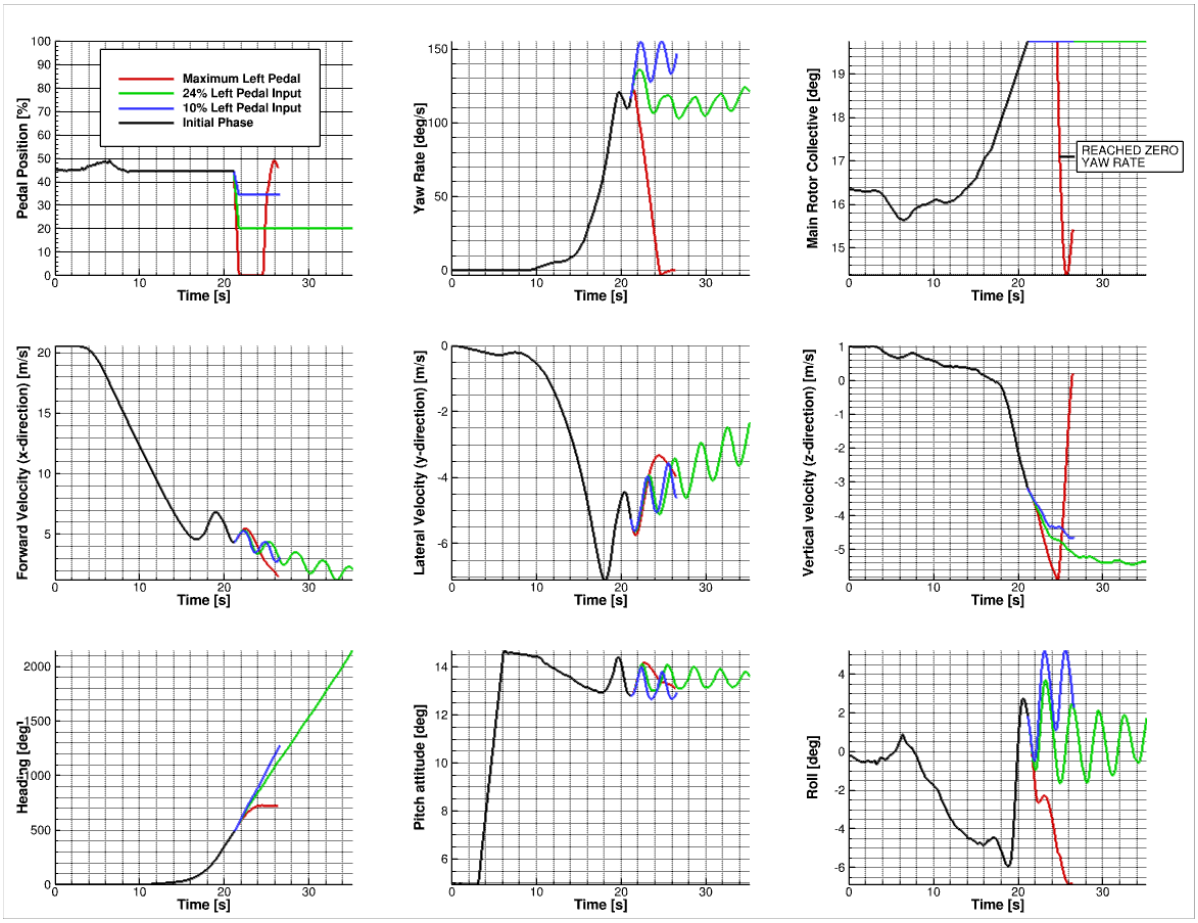

Figure 4.43: Evolution of helicopter variables during the unintended yaw simulation of an approach for landing. The pilot decreases the helicopter speed with a flare, increases the main rotor collective, and recovers by applying pedal inputs only. Three recoveries are tested.

4.4.1. Summary

Three scenarios have been considered to test recovery techniques for an unintended yaw case where, in the second and third scenarios, the main rotor collective was further increased around 6 seconds after the pedal blockage. A summary of the time needed to reduce the yaw rate to zero and the number of revolutions done after recovering for each investigated case are shown in Table 4.1. In general, applying a 10% of left pedal input is insufficient to recover the yaw trim effectively for two of the three evaluated cases. However, the time to recover for a successful case is too high to be accepted. For a 24% left pedal input, if only the pedal position is blocked, it takes less time to recover since the developed yaw rate is lower. If the main rotor collective is maintained at the high value, 24% of the left pedal input is insufficient. Finally, suppose the maximum left pedal is applied. In that case, the yaw trim can be obtained for all the evaluated cases, and it takes the least amount of time to recover if only the pedal is blocked, followed by the increase of collective when it is decreased during the recovery.

Table 4.1: Seconds to recover the yaw trim after unintended yaw for the three considered scenarios.

	Pedal block	**Pedal block + increase coll. + decrease coll.**	**Pedal block + increase coll. + maintain coll.**
10% left pedal input	>17.79 s	>8.65 s	∞
24% left pedal input	2.69 s	3.31 s	∞
Max. left pedal input	1.35 s	2.07 s	3.42 s

Table 4.2: Number of revolutions done after recovering the yaw trim for the three scenarios.

	Pedal block	**Pedal block + increase coll. + decrease coll.**	**Pedal block + increase coll. + maintain coll.**
10% left pedal input	>3.16 rev.	>3.01 rev.	∞
24% left pedal input	1.18 rev.	2 rev.	∞
Max. left pedal input	1.01 rev.	1.72 rev.	2 rev.

5

Conclusions & Future Work

This investigation has shown that unintended yaw is a phenomenon that needs a thoroughly detailed investigation of the helicopter yaw trim for typical flight conditions. The literature has already demonstrated that unintended yaw strongly involves several contributing effects, such as weathervane stability, main rotor wake interference, and tail rotor vortex ring state. The results from the thesis show the required pilot pedal input in trimmed flights at different wind velocities and azimuths for four main helicopter configurations: the original BK117-C2 helicopter model, which can be representative of a mid-weight helicopter with a classical tail rotor, the original helicopter model with the tail rotor rotating top forward, a modified helicopter model from the original configuration with the tail rotor at the tail boom height and lastly, the original helicopter with a low-weight and the tail rotor located at the tail boom height which is representative of light-weight helicopters. These results are supported by a detailed explanation of how rotor aerodynamics affects pedal demands. Then, optimum recovery techniques are evaluated to recover a realistic unintended yaw accident.

The answer to the first research question *"Is there a flight condition that causes uncontrollable unintended yaw?"* is given by the analysis of the trimmed flight simulations. Showing that there is no flight condition for all helicopter configurations where the tail rotor cannot create enough thrust to maintain the heading. Although enough tail rotor thrust can be provided, the influence of the wind azimuth was not intuitive for winds from the left (negative wind azimuths) where the pedal curve for trim flattens or even reverses. Additionally, the influence of the evaluated helicopter configurations showed that a tail rotor rotating top forward poses a detrimental configuration since the tail rotor thrust is reduced for the wind azimuths where the main rotor wake interacts with the tail rotor. Lowering the tail rotor at the tail boom height led to a more significant reduction of thrust on the sideward flight to the left, demanding more left pedal, attributed to a more substantial influence of VRS. Finally, the low-weight helicopter configuration showed an overall higher right pedal demand and an earlier influence of VRS due to lower tail rotor disk loading. Since no flight condition triggers unintended yaw, it can be concluded that unintended yaw starts due to wrong pedal inputs caused by the pilot.

Concerning the second research question *"Is a coupling between a flight mechanics code and an aerodynamics code needed to study unintended yaw?"*, the comparison of standalone Gensim simulations with the coupled Gensim simulations that receive feedback on the aerodynamic loads of the rotor thanks to the aerodynamics code showed that it is crucial to use the coupling of the flight mechanics code with the aerodynamics code. The main rotor performance improvement is substantial due to the better accuracy in the main rotor torque. Still, significant differences also appeared for regions where tail rotor VRS and main rotor wake interference were expected.

The third research question *"How do main rotor wake interactions and tail rotor vortex ring state affect tail rotor aerodynamics, and are they important for starting unintended yaw?"* was answered with a detailed assessment of the rotor aerodynamics. The results show that the main rotor wake interactions increase the local induced velocities at the tail rotor blades, leading to a higher thrust in the case of the top aft rotating rotor while a reduction of thrust for top forward rotation. Nevertheless, this only appeared significant for the original tail rotor configuration since the main rotor wake was observed to influence half of the tail rotor plane. In contrast, the lower tail rotor location showed a small benefit for top aft rotors since the tail rotor was immersed in the main

rotor wake. The main rotor super-vortices influenced the overall induced velocities at the tail rotor plane, but they were insignificant. The analysis of VRS appearing at the tail rotor when flying in wind azimuths close to -90º showed that the VRS was very unsteady and disturbed by the main rotor blade tip vortices. Therefore, this stopped the fully developed VRS at the tail rotor. The direct effect of the disturbed VRS at the tail roto was to reduce the effective blade's angle of attack, which resulted in a reduction in thrust. The disturbed VRS appeared for wind azimuths ranging from -60º to -120º, and it was most intense for wind velocities of 15 to 20 knots. It is concluded that the main rotor wake interference and the now-known disturbed tail rotor vortex ring state directly affect the tail rotor thrust and, consequently, the pedal position for trim. These effects alone don't trigger unintended yaw since the pilot can maintain the heading. Nevertheless, they pose an added difficulty, which influences the handling qualities of the helicopter.

The fourth research question *"How do the physical effects related to unintended yaw affect the handling characteristics?"* is answered from the trimmed flight results. The physical effects related to unintended yaw are mainly the disturbed VRS, main rotor wake interference and weathervane stability. The handling qualities of the helicopter are affected by the disturbed VRS since the required pedal for trim is flattened or reversed, causing a non-intuitive behaviour that could be difficult to manoeuvre for an inexperienced pilot who could apply the wrong pedal inputs. On the other hand, the central rotor wake interference does not present any added difficulties in the handling qualities for a top aft rotating tail rotor since the pedal position is shifted to an overall more right pedal. However, for a top forward tail rotor, the left pedal range is reduced, resulting in more critical conditions. Finally, weathervane stability is a well-known difficulty where significant pedal inputs are required to yaw the helicopter when flying backwards, increasing the handling difficulties.

Lastly, the research question *"Is unintended yaw recoverable and what pilot control inputs are needed"* could be answered through time-domain simulations of a realistic unintended yaw accident where the yaw control was lost. The results conclude that the unintended yaw is always recoverable if a fast maximum opposite pedal to the yawing direction is applied. Pedal inputs lower than the maximum range pedal inputs did not always result in a complete and fast enough recovery of the yaw rate. Notice also that although lowering the main rotor collective helps decrease the yaw rate, it can lead to confusion for pilots to have multiple inputs to be applied. Therefore, since the maximum opposite pedal always succeeds in recovering the yaw rate to zero even in the most detrimental situations, it is concluded that the pilot controls to be applied in case of developed unintended yaw are maximum pedal opposite to the direction of yaw rotation.

Future Work

Even though sufficient output has been provided in the present thesis to redefine the causes of unintended yaw and the recovery methods, future investigations can still improve the characterisation of such phenomenon. These include the investigation of helicopters with Fenestron, where the tail rotor aerodynamics can be affected due to the closed tail rotor blades. On top of that, an investigation focusing on the pedal fluctuations depending on the wind velocity and azimuth that could affect the handling qualities of the helicopter can be investigated as a study itself.

From the numerical perspective, to investigate the yaw capabilities of a helicopter with a Fenestron, an aerodynamics code that can deal with the flow separation at the Fenestron shroud should be implemented. Additionally, introducing the tight coupling between a flight mechanics code and UPM will provide higher capabilities of capturing high-frequency oscillations higher than the main rotor frequency since the loose coupling acts like a low-pass filter.

References

[1] AAIB. “SA341G Gazelle 1, G-HAVA”. In: *AAIB Bulletin* (1998).

[2] AAIB. “Westland Gazelle HT Mk3 G-BXZE”. In: *AAIB Bulletin* (2002).

[3] “AAIU Report 2004-021 on Bell 206B G-AYMW accident in Newgrange”. In: *Co. Meath* (2004).

[4] Federal Aviation Administration. “Unanticipated Right Yaw in Helicopters”. In: *Advisory Circular* 90-95 (1995).

[5] S.R. Ahmed and V.T. Vidjaja. “Unsteady Panel Method Calculation of Pressure Distribution on BO105 Model Rotor Blades”. In: *Journal of the American Helicopter Society* 43.1 (1998), pp. 47–56.

[6] D.T. Balch and J. Lombardi. “Experimental Study of Main Rotor Tip Geometry and Tail Rotor interactions in Hover”. In: *NASA* CR177336 (1985).

[7] D.T. Balch, A. Saccullo, and T.W. Sheehy. “Experimental Study of Main Rotor / Tail Rotor/ Airframe Interaction in Hover”. In: *Journal of the american helicopter society* 30.2 (1985), pp. 49–56.

[8] A. Bottai. *Computational fluid dynamics / flight dynamics simulations of an autonomous helicopter using actuator disk couplings for main and tail rotors*. The Pennsylvania State University, 2018.

[9] A. Brand et al. “The Nature of Vortex Ring State”. In: *Journal of the American Helicopter Society* (2011).

[10] CAA. “Helicopter Tail Rotor Failures”. In: *CAA Bulletin* (2003).

[11] Y. Cao, S. Lv, and G. Li. “A coupled free-wake/panel method for rotor/fuselage/empennage aerodynamic interaction and helicopter trims”. In: *Journal of Aerospace Engineering* 0.0 (2014), pp. 1–10.

[12] Carla Cavalcante et al. “Application of Fuzzy Control to Helicopter Navigation”. In: *Brazil-Japan Joint Symposium on Fuzzy Systems* 1 (1994).

[13] F. Cuzieux, P. Basset, and A. Desopper. “Modeling of Loss of Tail Rotor Effectiveness Conducting to Unanticipated Yaw”. In: *28th International Congress of the Aeronautical Sciences* (2012).

[14] A. Dequin. “The myth of losing tail rotor effectiveness”. In: *45th European Rotorcraft Forum* (2019).

[15] Lieutenant Commander ADS Ellin. “An In-Flight Investigation of Lynx AH MK5 Main Rotor/Tail Rotor Interactions”. In: *19th European Rotorcraft Forum* (1993).

[16] D. Ferullo. “An explanation of unanticipated yaw phenomenon on Helicopters”. In: *Vertical Flight Society’s 78th Annual Forum* (2022).

[17] T.M. Fletcher and R.E. Brown. “Helicopter Tail Rotor Thrust and Main Rotor Wake Coupling in Crosswind Flight”. In: *Journal of Aircraft* 47.6 (2010).

[18] T.M. Fletcher and R.E. Brown. “Main Rotor–Tail Rotor Interaction and Its Implications for Helicopter Directional Control”. In: *Journal of American Helicopter Society* (2007).

[19] J. P. Giesing. “Nonlinear two-dimensional unsteady potential flow with lift”. In: *Journal of Aircraft* 5.2 (1968), pp. 135–143.

[20] Harry H.H. and S. Katzoff. “Induced Velocities Near a Lifting Rotor with Nonuniform Disk Loading”. In: *NACA TR 1319* (1981).

[21] Airbus Helicopters. “Fenestron versus Conventional Tail Rotor (CTR) for helicopters equipped with a main rotor rotating clockwise when seen from above”. In: *Airbus Safety Information Notice* 3539-I-00 (2020).

[22] Airbus Helicopters. “GENERAL Ground Rescue Booklet”. In: *Airbus Safety Information Notice* 2971-S-00 (2015).

[23] Airbus Helicopters. “Unanticipated right yaw (main rotor rotating counter clockwise), commonly referred to as LTE”. In: *Airbus Safety Information Notice* 3298-S-00 (2019).

[24] J.L. Hess and A.M.O. Smith. “Calculation of potential flow about arbitrary bodies”. In: *Progress in Aerospace Sciences* 8 (1967), pp. 1–138.

[25] Captain M.J.T Hewetson. “Tail Rotor Breakaway”. In: *US Army Aviation Digest* (1980), pp. 40–41.

[26] “How to crash by the book”. In: *US Army Aviation Digest* (1977), pp. 43–45.

[27] P. Kunze and T. Ries. “Quasi-Steady Aeromechanic Helicopter Simulations Using Mid-Fidelity Aerodynamics”. In: *Vertical Flight Society’s 78th Annual Forum & Technology Display* (2022).

[28] R.P. Menger, T.L. Wood, and J.T. Beieger. “Effects of Aerodynamic Interaction Between Main Rotor and Tail Rotor on Helicopter Hover Performance and Noise”. In: *NASA* CR 166477 (1983).

[29] “Mishap review: loss of tail rotor effectiveness”. In: *Flightfax* 10.26 (1982), pp. 1–2.

[30] Davide Montagnani et al. “Mid-fidelity analysis of unsteady interactional aerodyanmics of complex VTOL configurations”. In: *45th European Rotorcraft Forum* (2019).

[31] NTSB. “Loss of Tail Rotor Effectiveness in Helicopters”. In: *Safety Alert SA-062* (2017).

[32] “OH-58 tail rotor spin accidents increasing”. In: *Flightfax* 10.41 (1982), pp. 1–2.

[33] RAAF. “Bell 206B-1 Directional Control in Low Airspeed Flight”. In: *ARDU-TI-721* (1981).

[34] A. Ragazzi et al. “AW169 Loss of Tail Rotor Effectiveness Simulation”. In: *43rd European Rotorcraft Forum* (2017).

[35] K.R. Reddy and T.T Truong. “Effect of Main Rotor Wake Interference on Tail Rotor Aerodynamic Characteristics”. In: *11th Australasian Fluid Mechanics Conference* (1992).

[36] N. Roh, D. Park, and S. Oh. “Investigation on Loss of Tail-rotor Effectiveness of Helicopter with Ducted Fan Tail Rotor”. In: *44th European Rotorcraft Forum* (2018).

[37] V. Srinivas and I. Chopra. “Prediction of yaw control effectiveness and tail rotor loads”. In: *19th European Rotorcraft Forum* (1993).

[38] J. Stanislawski. “Simulation investigation of aerodynamic effectiveness reduction of helicopter tail rotor”. In: *Institute of Aviation* 242.1 (2016), pp. 36–56.

[39] J. M. Summa. “Potential Flow About Three-Dimensional Streamlined Lifting Configurations, with Application to Wings and Rotors”. In: *Stanford University* (1974).

[40] “Tail Rotor Stall”. In: *US Army Aviation Digest* (1978), pp. 43–45.

[41] C. Wang et al. “Main Rotor Wake Interference Effects on Tail Rotor Thrust in Crosswind”. In: *International Journal of Aerospace Engineering* (2021), pp. 1–13.

[42] W. Wiesner and G. Kohler. “Tail Rotor Performance in Presence of Main Rotor, Ground and Winds”. In: *American Helicopter Society, 29th Annual Forum Proceedings* (1973).

[43] Wikipedia. *Swashplate*. 2024. URL: `https://commons.wikimedia.org/wiki/File:Helicopter-swashplate-tilted.png` (visited on 05/10/2024).

[44] Wikipedia. *Tail Rotor*. 2024. URL: `https://en.wikipedia.org/wiki/Tail_rotor` (visited on 05/10/2024).

[45] G.S. Winckelmans and A. Leonard. “Contributions to Vortex Particle Methods for the Computation of Three-Dimensional Incompressible Unsteady Flows”. In: *Journal of Computational Physics* 109.2 (1993), pp. 247–273.

[46] J. Yin. “Prediction - and its Validation - of the Acoustics of Multiblade Rotors in Forward Flight Utilising Pressure Data from a 3-D Free Wake Unsteady Panel Method”. In: *20th European Rotorcraft Forum* (1994).

[47] J. Yin and S.R. Ahmed. “Helicopter Main-Rotor/Tail-Rotor Interaction”. In: *Journal of the American Helicopter Society* 45.4 (2000), pp. 293–302.

[48] J. Yin and S.R. Ahmed. “Treatment of Unsteady Rotor Aerodynamics”. In: *DLR* (1994).

[49] P. Zanella. *A methodology to improve the proactive mitigation of helicopter accidents related to loss of tail rotor effectiveness*. Georgia Institue of Technology, 2021.

A

Tail Rotor Vortex Ring State: Further Data

Streamlines for the investigation of isolated freestream velocity effect.

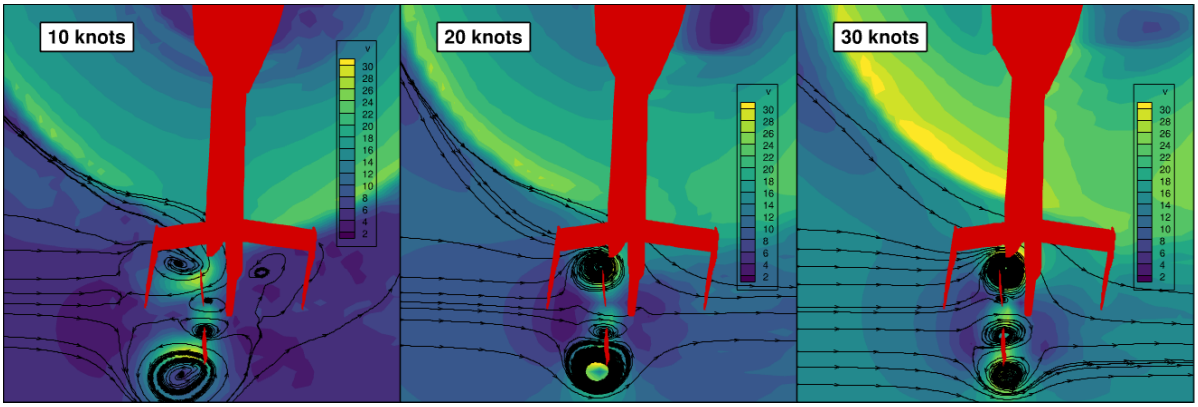

Figure A.1: Streamlines of the averaged flow field for 10, 20 and 30 knots.

The tail rotor loads for the investigation of isolated freestream velocity effect.

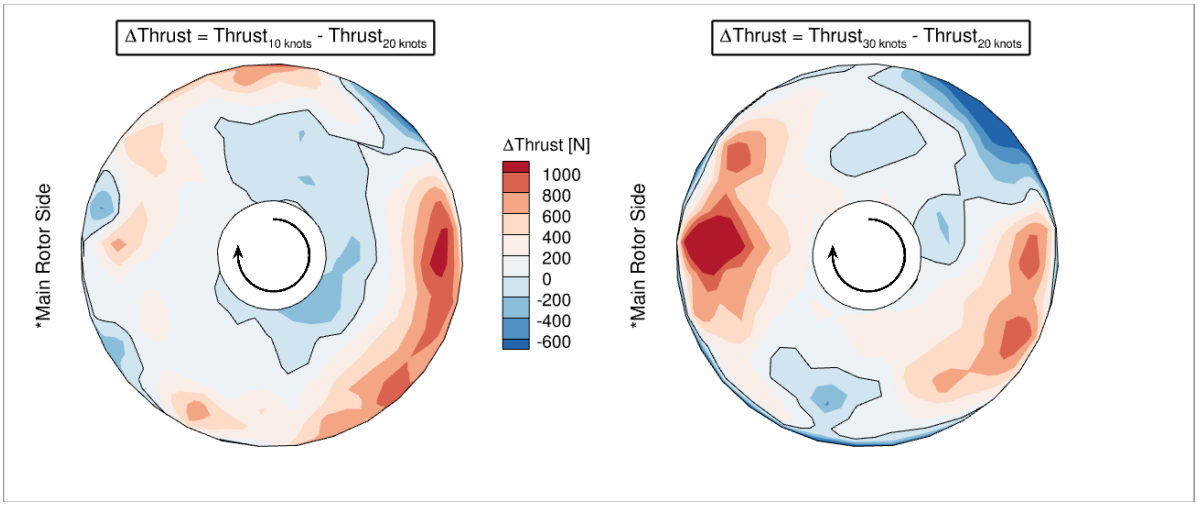

Figure A.2: Tail rotor loads for 10, 20 and 30 knots.

The relative change in the effective velocities at the tail rotor plane for the evaluated velocities with the same helicopter and blade motion.

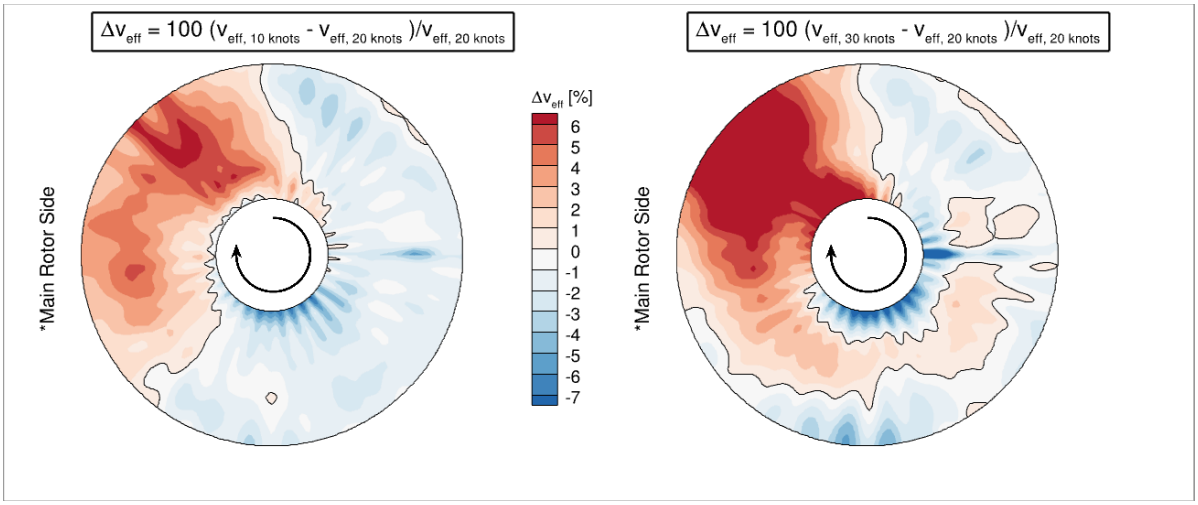

Figure A.3: Relative change in effective velocities between 10, 20 and 30 knots.

Flow field streamlines for the case without main rotor computation.

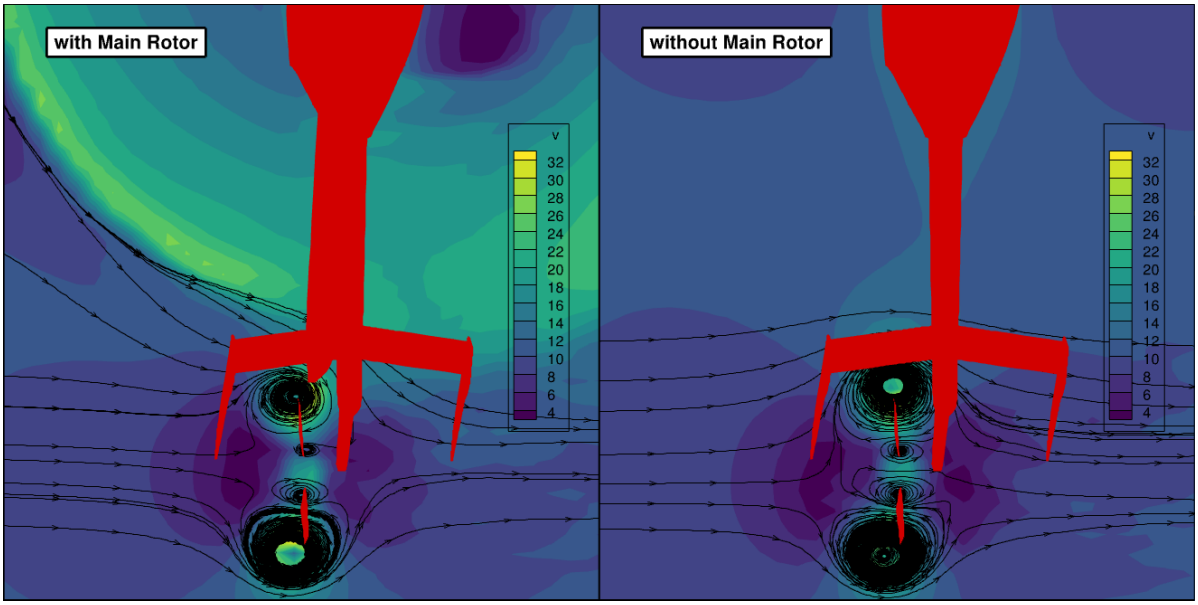

Figure A.4: 2D Streamlines at the tail rotor plane with an without main rotor.

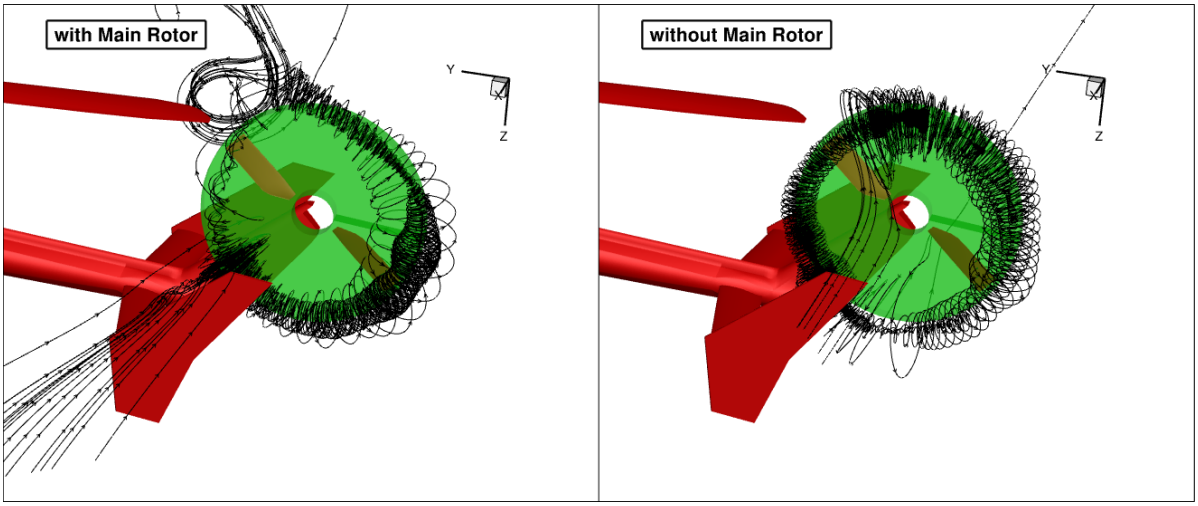

Figure A.5: 3D Streamlines at the tail rotor plane with an without main rotor.

B

Main Rotor Wake Interference: Further Data

The relative change in loads and effective velocity between top aft and top forward at tail rotor plane for 30 knots forward flight.

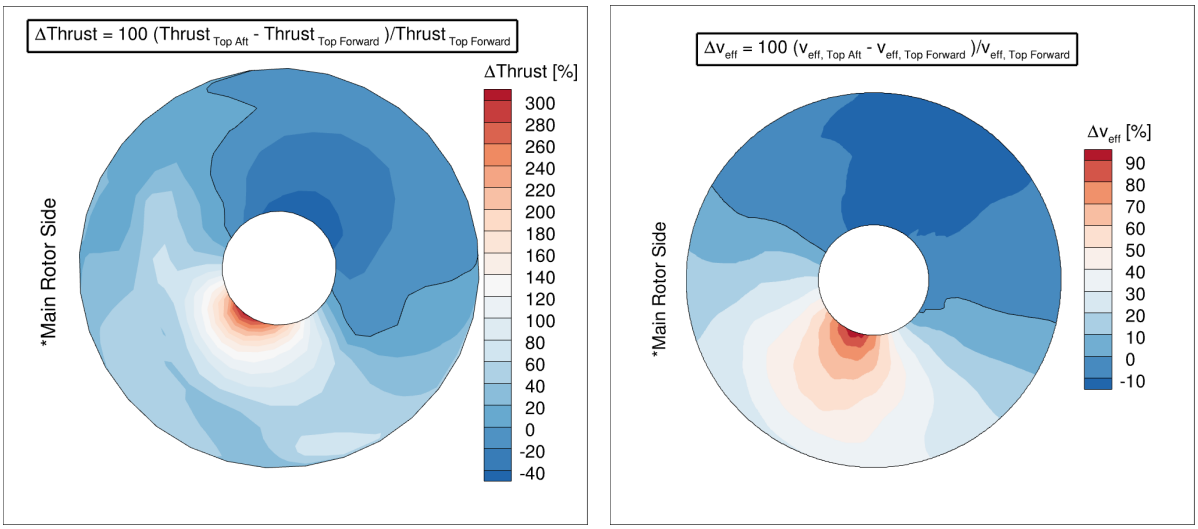

(a) Thrust.

(b) Effective velocity.

Figure B.1: Relative difference in loads and effective velocity between top aft and top forward configurations. 30 knots forward flight.

The relative difference in loads between top aft and top forward for quartering flights with a wind azimuth of 50° and -50° are shown.

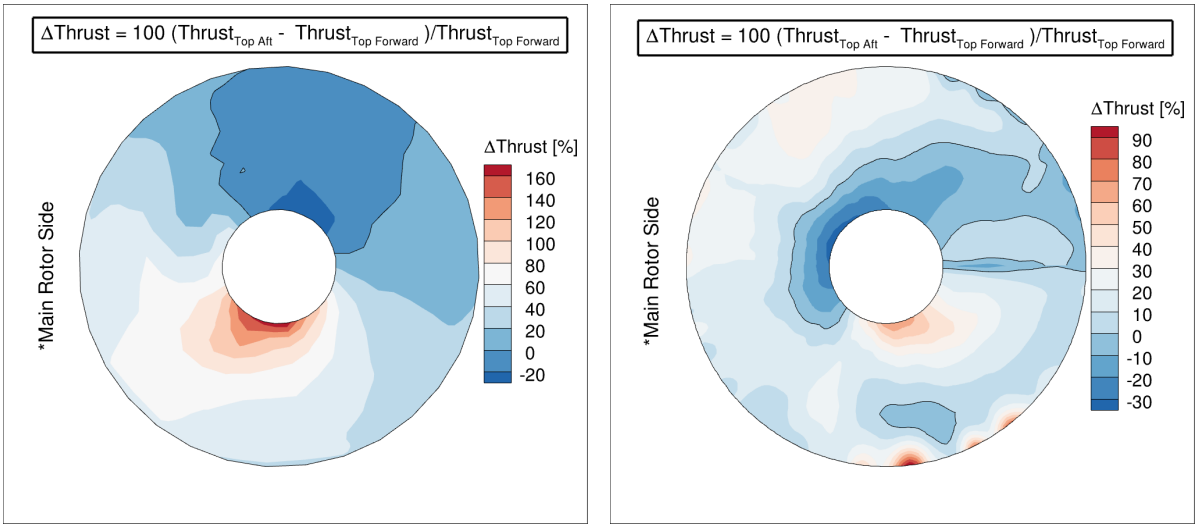

(a) Wind azimuth 50°.

(b) Wind azimuth -50°.

Figure B.2: Relative difference in loads between top aft and top forward configurations. Quartering flights.

C

Recovery Methods: Further Data

Frames every one second for the time domain simulation of a dynamic approach to landing when the pedal has been frozen, the main rotor collective increased and maximum left pedal is applied.

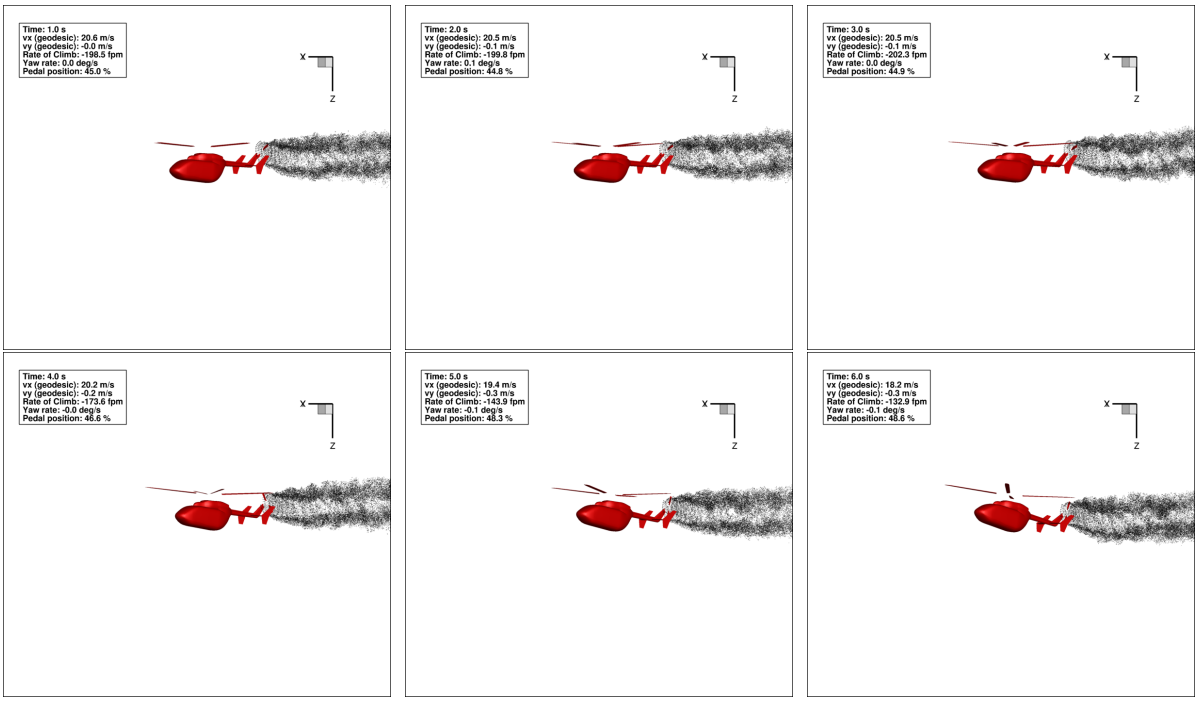

Figure C.1: Instantaneous images for the time domain simulation of a dynamic approach for landing. From $t = 1\,s$ to $t = 6\,s$.

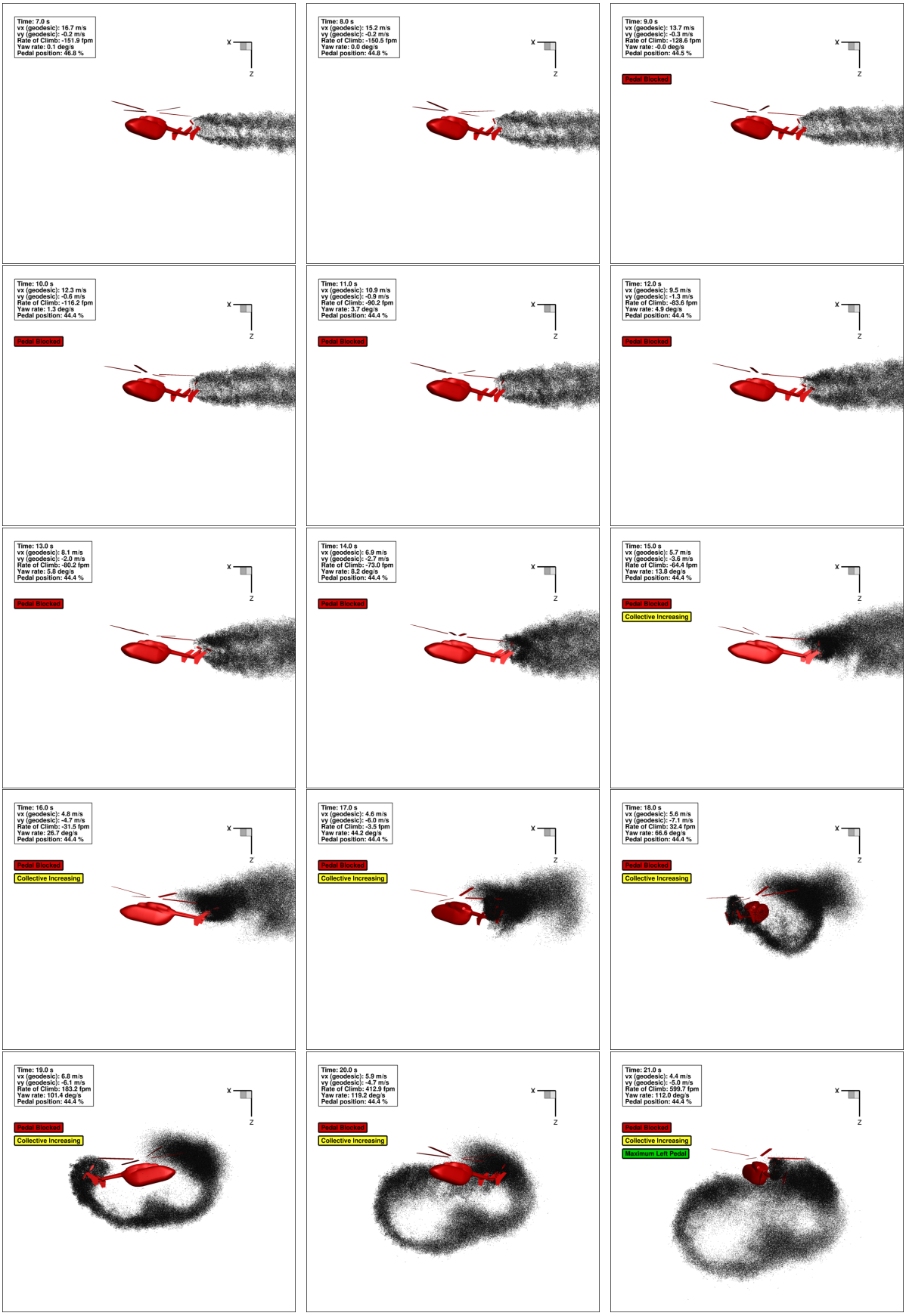

Figure C.2: Instantaneous images for the time domain simulation of a dynamic approach for landing. From $t = 7\,s$ to $t = 21\,s$.

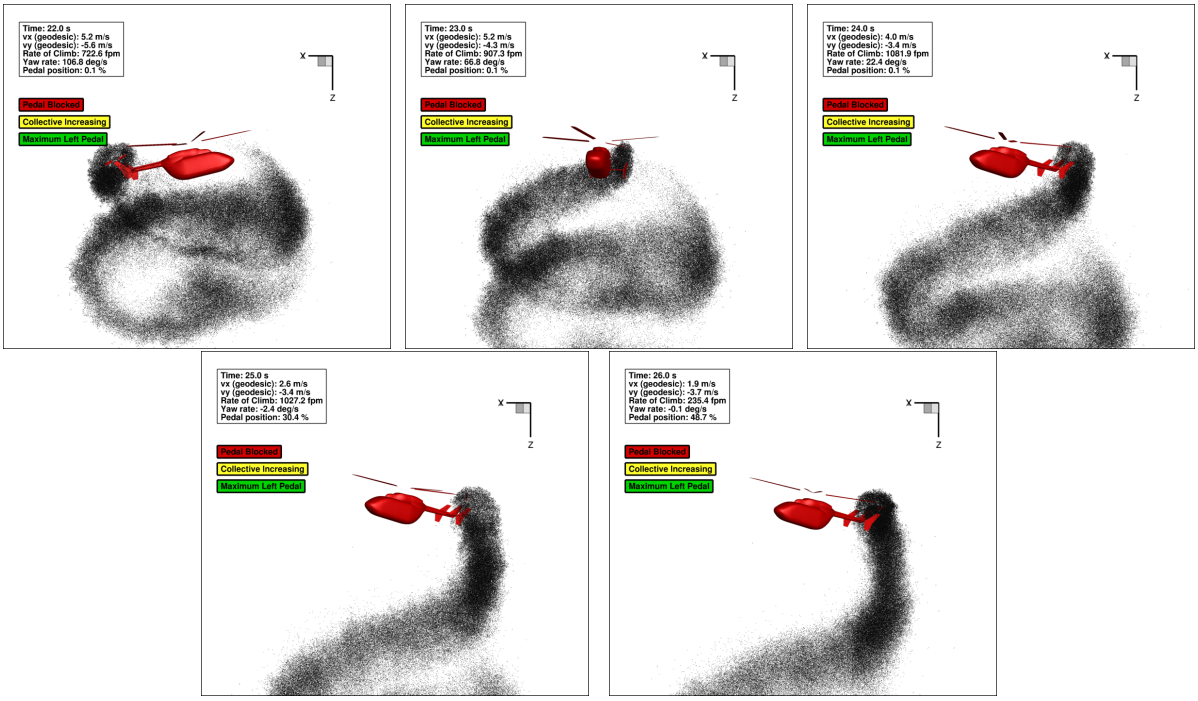

Figure C.3: Instantaneous images for the time domain simulation of a dynamic approach for landing. From $t = 22\,s$ to $t = 26\,s$.